ANTIMALARIAL ACTIVITY, TOXICITY, PHARMACOKINETICS AND
METABOLIC DRUG INTERACTION OF *PLUMBAGO INDICA* LINN.

BY

MISS WIRIYAPORN SUMSAKUL

A DISSERTATION SUBMITTED IN PARTIAL FULFILLMENT OF
THE REQUIREMENTS FOR THE DEGREE OF THE
DOCTOR OF PHILOSOPHY
(BIOMEDICAL SCIENCES)

GRADUATE PROGRAM IN BIOMEDICAL SCIENCES
FACULTY OF ALLIED HEALTH SCIENCES
THAMMASAT UNIVERSITY
ACADEMIC YEAR 2015

ANTIMALARIAL ACTIVITY, TOXICITY, PHARMACOKINETICS AND

METABOLIC DRUG INTERACTION OF *PLUMBAGO INDICA* LINN.

BY

MISS WIRIYAPORN SUMSAKUL

A DISSERTATION SUBMITTED IN PARTIAL FULFILLMENT OF

THE REQUIREMENTS FOR THE DEGREE OF THE

DOCTOR OF PHILOSOPHY

(BIOMEDICAL SCIENCES)

GRADUATE PROGRAM IN BIOMEDICAL SCIENCES

FACULTY OF ALLIED HEALTH SCIENCES

THAMMASAT UNIVERSITY

ACADEMIC YEAR 2015

THAMMASAT UNIVERSITY

FACULTY OF ALLIED HEALTH SCIENCES

DISSERTATION

BY

Miss WIRIYAPORN SUMSAKUL

ENTITLED

ANTIMALARIAL ACTIVITY, TOXICITY, PHARMACOKINETICS AND METABOLIC DRUG

INTERACTION OF *PLUMBAGO INDICA* LINN.

was approved as partial fulfillment of the requirements for the degree of the

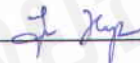Doctor of Philosophy (Biomedical Sciences)

on December 21, 2015

Chairman

_____

(Prof. Juntra Karbwang-Laothavorn, M.D., Ph.D.)

Member and Advisor

_____

(Prof. Kesara Na-Bangchang, Ph.D.)

Member
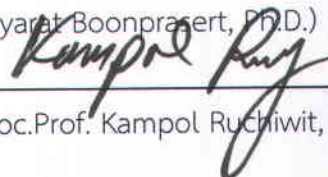
_____

(Assist.Prof. Jiraporn Kuesap, Ph.D.)

Member

_____

(Tullayakorn Plengsuriyakarn, Ph.D.)

Member

_____

(Kanyarat Boonprasert, Ph.D.)

Dean

_____

(Assoc.Prof. Kampol Ruchiwit, Ph.D.)

Dissertation Title	Antimalarial Activity, Toxicity, Pharmacokinetics and Metabolic Drug Interaction of *Plumbago indica* Linn.
Author	Miss Wiriyaporn Sumsakul
Degree	Doctor of Philosophy (Biomedical Sciences)
Department/Faculty/University	Graduate Program in Biomedical Sciences Faculty of Allied Health Sciences Thammasat University
Dissertation Advisor	Prof. Kesara Na-Bangchang, Ph.D.
Dissertation Co-Advisor	Prof. Vithoon Viyanant, Ph.D.
Dissertation Co-Advisor	Prof. Kazuhisa Sekimizu, Ph.D
Dissertation Co-Advisor	Prof. Wichittra Tassaneeyakul, Ph.D.
Dissertation Co-Advisor	Assoc.Prof. Korbtham Sathirakul, Ph.D.
Academic Years	2015

ABSTRACT

Malaria is widespread in tropical and subtropical regions. Throughout the history of mankind, this highly infectious disease has been one of the major causes of human illness and death. *Plasmodium falciparum* is the most virulent and widespread infectious malarial species in tropical and subtropical countries due to the resistance of the parasite to most of the available antimalarial drugs. As antimalarial drug resistance compromises the effective treatment of the disease, there is a pressing need for ongoing drug discovery research. Natural products including medicinal plants may offer relatively cheap alternative treatment opportunities for malaria patients. The crude ethanolic extract of *Plumbago indica* Linn. has been shown to possess good to moderate antimalarial activity (class III antimalarial activity) in our previous *in vitro* screening. Among the 32 plants

investigated, *Plumbago indica* Linn. showed the most promising activity against both K1 chloroquineresistant (IC_{50} 3 µg/ml) and 3D7 chloroquine-sensitive (IC_{50} 6.2 µg/ml) clones, with highest selectivity (SI = 44.7 and 21.6, respectively). Plumbagin is the major active constituent in several plants including *Plumbago indica* Linn. (root). This compound has been shown to exhibit a wide spectrum of pharmacological activities such as activities against malaria, leishmania and trypanosome parasites, as well as against virus, cancers, and bacteria.

Plumbagin exhibited promising antimalarial activity with *in vitro* IC_{50} (concentration that inhibits enzyme activity by 50%) against 3D7 chloroquine-sensitive *Plasmodium falciparum* and K1 chloroquine-resistant *Plasmodium falciparum* clones of 580 (270-640) and 370 (270-490) nM, respectively. *In vivo* antimalarial activity was investigated in *Plasmodium berghei* infected mouse model. Chloroquine exhibited the most potent antimalarial activity in mice infected with *Plasmodium berghei* ANKA strain with respect to its activity on the reduction of parasitaemia on day 4 and the prolongation of survival time. Plumbagin at the dose of 25 mg/kg body weight given for 4 days produced moderate antimalarial activity with regards to its inhibitory activity on the reduction of parasitaemia and the prolongation of survival time.

Toxicity testing in ICR mice indicated maximum oral dose at the dose levels up to 100 (single oral dose) and 25 (daily doses for 28 days) mg/kg body weight for acute and subacute toxicity, respectively whereas toxicity testing in wistar rats indicated maximum oral dose at the dose levels up to 150 (single oral dose) and 25 (daily doses for 28 days) mg/kg body weight for acute and subacute toxicity, respectively. Fifty percent lethal dose (LD_{50}) of plumbagin in wistar rats was 250 mg/kg body weight.

Permeation (P_{app}) of plumbagin (2-8 µM) for the apical to basolateral and basolateral to apical directions were $10.29\text{-}15.96\times10^{-6}$ and $7.40\text{-}9.02\times10^{-6}$ cm/s, respectively, with the efflux ratios of 0.57-0.73. Plumbagin was not either a substrate

or inhibitor of P-glycoprotein (p-gp). It did not interfere with the P-glycoprotein-mediated R123 transport across Caco-2 cell monolayer, as well as the function of P-glycoprotein and the expression of MDR-1 (multidrug resistance 1) mRNA. Results suggest moderate permeability of plumbagin across the Caco-2 cell monolayer in both directions. The transport mechanism is likely to be a passive transport. The propensity to inhibit CYP-mediated hepatic metabolism (CYP1A2, CYP2C19, CYP2D6 and CYP3A4) of the five Thai medicinal plants with promising activities against malaria (Table 1) using human liver microsomes were investigated. Results showed that all plants exhibited varying inhibitory potencies on various CYP isoforms. With regard to the inhibitory activity of each plant extract on the four CYP isoforms, PI and DM showed potent inhibitory activities on most CYP isoforms (CYP2C19, CYP2D6, and CYP3A4, respectively) while DL showed potent inhibitory activities on the two CYP isoforms (CYP1A2 and CYP3A4 respectively). Moreover, plumbagin showed significant inhibitory effects on all cytochrome P450 (CYP) isoforms under investigation, but with the most potent activity on CYP2C19-mediated omeprazole hydroxylation. The IC_{50} values (mean±SD) of plumbagin and nootkatone (selective inhibitor) for CYP2C19 were 0.78±0.01 and 27.31±0.66 µM, respectively. The inhibitory activities on CYP1A2-mediated phenacetin O-deethylation and CYP3A4-mediated nifedipine oxidation were moderate. The IC_{50} values of plumbagin and α-naphthoflavone (selective inhibitor) for CYP1A2 were 1.39±0.01 and 0.02±0.36 µM, respectively. The corresponding IC_{50} values of plumbagin and ketoconazole (selective inhibitor) for CYP3A4 were 2.37±0.10 and 0.18±0.06 µM, respectively. Furthermore, Plumbagin did not induce hepatic drug metabolizing enzymes, especially CYP1A2 and CYP3A11 of treated mice with plumbagin (6.25, 12.50 and 25.00 mg/kg body weight) for 28 days, and that plumbagin exhibited a little inhibitory effect on CYP1A2 but did not reach the level of significance.

The pharmacokinetic study in wistar rats showed that the average (±) half-life ($T_{1/2}$) and time to reach maximum blood concentration (T_{max}) of plumbagin

were 9.98±1.63 and 5.00±0.00 h, respectively after oral administration. Maximum blood concentration (C_{max}) was 0.46±0.08 (µg/ml). The mean residence time (MRT) of plumbagin was 13.67±1.62 h. In addition, the area under the time curve (AUC_{0-inf}) was 6.72±0.74 (µg•h/ml) whereas (AUC_{0-48h}) was 6.47±0.62 (µg•h/ml). On the other hand, systemic clearance (CL) and volume of distribution (Vd) of plumbagin were 7.51±0.84 (l/h) and 0.11±0.01 (l), respectively. Comparison between blood kinetics of healthy mice and *P. berghei*-infected mice following intravenous injection of ^{99m}Tc-plumbagin complex demonstrated the mean residence time (MRT) of the labelled complex in healthy mice (3.16 h) was significantly longer than *P. berghei*-infected mice (2.21 h) ($p<0.001$). In addition, the area under the time curve (AUC_{0-inf}) was significantly higher in healthy (13.54 %ID/g*h) compared with *P. berghei*-infected (7.85 %ID/g*h) mice ($p<0.001$). On the other hand, systemic clearance (CL) and volume of distribution (Vd) of ^{99m}Tc-plumbagin were significantly higher in *P. berghei*-infected (12.76 l/h *vs* 41.95 ml) compared with healthy (7.39 l/h *vs* 29.56 ml) mice ($p<0.001$). Plumbagin was rapidly cleared from blood circulation and major routes of excretion were renal, hepatobiliary and pulmonary routes. Malaria disease state influenced the pharmacokinetics and disposition of plumbagin in animal model.

Results suggest that clinical relevance of the interference of human drug metabolizing enzymes should be aware of for further development scheme of plumbagin as antimalarial drug when used in combination with other antimalarial drugs which are metabolized by these CYP isoforms. Preparation of modified formulation is required to improve its systemic bioavailability. Increase in the dose of plumbagin, together with improvement of its oral bioavailability may be required if the compound will be selected as a candidate compound for treatment of malaria.

Keywords: Plumbagin, Antimalarial, *Plasmodium falciparum, Plasmodium berghei*, Permeability, Transport, Efflux transporters, Caco-2 cell, P-glycoprotein, Pharmacokinetics, Metabolic drug interaction.

ACKNOWLEDGEMENTS

TABLE OF CONTENTS

TABLE OF CONTENTS (Cont.)

TABLE OF CONTENTS (Cont.)

TABLE OF CONTENTS (Cont.)

TABLE OF CONTENTS (Cont.)

TABLE OF CONTENTS (Cont.)

TABLE OF CONTENTS (Cont.)

TABLE OF CONTENTS (Cont.)

LIST OF TABLES

LIST OF TABLES (Cont.)

LIST OF TABLES (Cont.)

LIST OF TABLES (Cont.)

LIST OF FIGURES

LIST OF FIGURES (Cont.)

LIST OF FIGURES (Cont.)

LIST OF ABBREVIATIONS

Symbols/Abbreviations	Terms
°C	Degree of Celsius
%	Percentage
α	Alpha
<	Less than
>	More than
µl	Microlitre
µM	Micromolar
$2^{-\Delta\Delta Ct}$	Two power by minus delta delta ct
3D	Three-dimensional
5-FU	5-fluorouracil
$\times g$	G force
10X	10 time of volume
ACT	Artemisinin combination therapy
ART	Artemisinin
AS	Artemisinin and derivative
AMA1	Apical membrane antigen 1
Asn	Asparagine
ATP	Adenosine-5'-triphosphate
AUMC	Under the first moment curve
AUC	Area under the concentration–time curve
β	Beta
BC	Before Christ
BCRP	Breast cancer resistance protein
BSA	Bovine serum albumin
B_{max}	Values for receptor number

LIST OF ABBREVIATIONS (Cont.)

Symbols/Abbreviations	Terms
B_{max}/K_d	Binding potential
Bw	Body weight
CAR	Central African Republic
cm^2	Area of cetrimetre square
CO_2	Carbondioxide gas
CQ	Chloroquine
CL	Clearance
C_{nom}	Nominal mass concentration
C_{obs}	Observed mass concentration
C_{max}	Maximal tissue radiotracer concentrations
CT	Computed tomography
CV	Coefficient of variation
C_{18}	Carbon 18 atom
CRC	Cancer Research Campaign
CYP	Cytochrome P450
DDT	Drug-Drug interaction
DHA	Dihydroartemisinin
DHFR	Dihydrofolate reductase
DHPS	Dihydropteroate synthase
DL	*Dracaena loureiri* Gagnepv
DM	*Dioscorea membranacea* Pierre
DMSO	Dimethyl sulfoxide
DNA	Deoxyribonucleic acid
E. coli	*Escherichia coli*
EDTA	Ethylenediamine tetraacetic acid
e.g.	For example

LIST OF ABBREVIATIONS (Cont.)

Symbols/Abbreviations	Terms
et al.	*et all*
EST	Expressed sequence tags
ET	Emission tomography
ESI	Enzyme substrate inhibitor
ESI	Negative-ion mode
F	Blood flow
^{18}F	Fluorine-18
g	Gram
GAF	Gametocyte activating factors
GM	*Garcinia mangostana* Linn
GPI	Glucose phosphate isomerase
h	Hour
HEPES	2-[4-(2-hydroxyethyl)-1-piperazinyl] ethanesulfonic acid
HBSS	Hanks' Balance Salt Solution
HLM	Human liver microsomes
HPLC	High performance liquid chromatography
H_2O	Water
i.p.	Intraperitoneal inoculation
i.h.	Intra-hemolymph injection
IC_{50}	Drug concentration that produces 50% inhibitory effect on parasite growth
ICR	Outbred strain of mice
i.d.	Internal diameter
i.v.	Intravenous injection
kb	Kilobase

LIST OF ABBREVIATIONS (Cont.)

Symbols/Abbreviations	Terms
kg	Kilogram
keV	Kiloelectronvolt
K_m	Michaelis-menten constant
K_d	Affinity
K_i	Inhibitor constant
l	Liter(s)
LC/MS/MS	Liquid chromatography-tandem mass spectrometry
LD_{50}	Fifty percent lethal dose
MF	*Myristica fragrans* Houtt
M.W.	Molecular weight
Max	Maximum
Min	Minimum
mg/ml	Milligram per milliliter
ml	Mililitre
mM	Millimolar
MCT	Monocarboxylate transporter protein
MDCK	Madin-Darby Canine Kidney Epithelial Cells
MDR1	Multidrug resistance 1
MSP1	Merozoite surface protein-1
MRSA	Methicillin-resistant *Staphylococcus aureus*
MSSA	Methicillin-resistant *Staphylococcus aureus*
MSP4/5	Merozoite surface protein-4/5

LIST OF ABBREVIATIONS (Cont.)

Symbols/Abbreviations	Terms
Mz	Merozoite
MRI	Magnetic resonance imaging
mCi/mmol	Millicurie per millimol
MRM	Multiple reaction monitoring
MRT	Mean residence time
MTT	3-(4,5-dimethylthiazolyl-2)-2,5-diphenyltetrazolium bromide
n	Number
NaCl	Sodium chloride
NADPH	Nicotinamide adenine dinucleotide phosphate tetrasodium salt
no.	Number
NMR	Nuclear magnetic resonance
nM	Nanomolar
NSS	Normal saline solution
N_2	Nitrogen
OD	Optical density
OECD420	Guidelines for the testing of chemicals in acute oral toxicity in repeated dose 28-
OECD407	Guidelines for the testing of chemicals in acute oral toxicity
O_2	Oxygen
OATP	Organic anion transporting polypeptide
OCT	Organic cation transporter
OCTN	Carnitine/organic cation transporter
P_{app}	Permeation

LIST OF ABBREVIATIONS (Cont.)

Symbols/Abbreviations	Terms
PBS	Phosphate buffered saline
pH	Negative logarithm of hydrogen ion activity
PI	*Plumbago indica* Linn
PL	Plumbagin
Pmol	Picomol
P. berghei	*Plasmodium berghei*
P. chabaudi	*Plasmodium chabaudi*
P. falciparum	*Plasmodium faciparum*
p-gp	P-glycoprotein
P. knowlesi	*Plasmodium knowlesi*
P. malariae	*Plasmodium malariae*
P. ovale	*Plasmodium ovale*
p.o.	Oral administration
P. vivax	*Plasmodium vivax*
P. vinckei	*Plasmodium vinckei*
P. yoelii	*Plasmodium yoelii*
PIR's	*Plasmodium* interspersed repeats
pfmdr1	*Plasmodium faciparum* multidrug resistance 1 gene
pfcrt	*Plasmodium Falciparum* chloroquine resistance transporter gene
P25	Protein number 25
P28	Protein number 28
P48/45	Protein number 45/48
P47	Protein number 47

LIST OF ABBREVIATIONS (Cont.)

Symbols/Abbreviations	Terms
P230	Protein number 230
PET	Positron emission tomography
PEPT	Peptide transporter protein
PMAT	Plasma membrane monoamine
PfEMP1	*Plasmodium falciparum* erythrocyte membrane protein 1
QN	Quinine
RBC	Red blood cell
ROIs	Regions of interest
RSD	Relative standard deviation
RhopH3	Rhoptry H3 protein
S. aureus	*Staphylococcus aureus*
[S]	Substrate concentration
sec	Second
SEM	The standard error of the mean
SD	Standard deviation
SEA	South-East Asia
SP	Sulfadoxinepyrimethamine
SDH	Succinate dehydrogenase
SNR	Signal-to-noise ratio
SPECT	Single photon emission computed
STEVOR	STEVOR expressed on the merozoite surface and to be associated with the plasma membrane of mature gametocyte-infected erythrocytes
SUV	Standardized uptake value

LIST OF ABBREVIATIONS (Cont.)

Symbols/Abbreviations	Terms
SUB2	Subtilisin-like protease 2
SYBR Green	Syber Green
U	Unit
UK	United Kingdom
USA	United States of America
TACs	Time-versus-radioactivity curves
^{9m}Tc	Technetium-99m
T_{max}	Time to reach C_{max}
$T_{1/2}$	Half-life
Tyr	Tyrosine
U/ml	Unit per milliliter
Vd	Volume of distribution
VEGF	Vascular endothelial growth factor
V_{max}	The maximum initial velocity or rate of a reaction
vs	Versus
WHO	World Health Organization
w/w	Weight per weight
w/v	Weight per volumn

CHAPTER 1

INTRODUCTION

Malaria is widespread in tropical and subtropical regions. Throughout the history of mankind, this highly infectious disease has been one of the major causes of human illness and death in the world with an estimated 350-500 million clinical cases and a corresponding mortality rate of 2-3 million deaths each year.[1] Malaria is caused by Plasmodium parasites and transmitted by the female Anopheles mosquito acting as a host and a vector of the parasite.[2] *Plasmodium falciparum* is the most virulent and widespread infectious malarial species in tropical and subtropical countries due to the resistance of the parasite to most of the available antimalarial drugs.[3] Chemotherapy with effective antimalarial drugs remains the mainstay for malaria control in the absence of a suitable vaccine treatment. However, multidrug resistance *P. falciparum* has been a major problem in controlling this disease in several endemic areas of the world. In a race to combat the increasing multidrug resistance *P. falciparum,* artemisinin-based combination therapy (ACT) has been recommended by the World Health Organization (WHO) as the first-line treatment for acute uncomplicated multidrug resistance *P. falciparum* malaria in all the malaria endemic areas of the world.[4] As antimalarial drug resistance compromises the effective treatment of the disease, there is a pressing need for ongoing drug discovery research that will provide effective, safe, and affordable antimalarial agents. Natural products including medicinal plants may offer relatively cheap alternative treatment opportunities for malaria patients.[5,6] Two antimalarial drugs currently widely used for malaria control originally came from indigenous medicinal plants; quinine is isolated from the Peruvian Cinchona's bark and artemisinins are obtained from the Chinese plant *Artemisia annua* Linn. Medicinal plants have been used in traditional health care systems since pre-historic time and remain the most important health care source for the vast majority of the population around the world. The use of alternative or herbal remedies, both as single therapies and in combination have increased steadily in recent years, with approximately 5-20% of

the general public use.[7] Nevertheless, the mechanisms of their action are generally unknown and there is no evidence to support their efficacy and toxicity. Due to the crucial role that plant-derived compounds have played in drug discovery and development for the treatment of several diseases, the isolation of new bioactive compounds from medicinal plants based on traditional use or ethnomedical data appears to be a very promising approach. Although there is widespread use of traditional herbal remedies in the management of malaria, scientific understanding of the plants is largely unexplored and therefore, it is a neccessary to collect ethnobotanical information on antimalarial plants which is essential for further evaluation of the efficacy and safety of the plants as antimalarial remedies.

Plumbagin (5-hydroxy-2-methyl-1,4-naphthoquinone) is a major constituent of *Plumbago indica* Linn. It is a natural product isolated from several plants in the families of Plumbaginaceae, Droseraceae, Ancestrocladaceae, and Dioncophyllaceae. It is a naphthoquinone that occurs in plant roots as a colorless combined form that can be processed to plumbagin by acid treatment.[8] This compound has been shown to display a wide spectrum of biological and pharmacological activities such as activities against malaria, leishmania and trypanosome parasites, as well as against virus, cancers, and bacteria.[9] The ethanolic extract of *Plumbago zeylanica* has been reported to exhibit *in vitro* antimalarial activity against chloroquine-sensitive clone of *P. falciparum* (3D7) with an IC_{50} (concentration that inhibits parasite growth by 50%) of 17 μg/ml.[10] The activity against *P. falciparum* enzyme succinate dehydrogenanse (SDH) including parasite growth has been shown to be inhibited to 50% by plumbagin at inhibitory concentrations of 5 and 0.27 mM, respectively.[11] Recently, It has been demonstrated that the ethanolic extract of *Plumbago indica* Linn exhibits promising antimalarial activity.[12]

The cytochrome P450 enzymes (CYP) represent a large family of proteins involved in the metabolism of drugs and other xenobiotics as well as endogenous compounds. They are abundant in human liver. They play crucial roles in the metabolism of drugs and thus have a significant impact on the occurrence of drug-

drug interactions which could lead to untoward adverse effects or toxicity. The CYP1A2, CYP2A6, CYP2C9, CYP2C19, CYP2D6 and CYP3A4 isoforms are responsible for the metabolism and disposition of more than 90% of the therapeutics currently available on the market.[13] There are several mechanisms by which drug interactions can occur. Many interactions occurs secondary to effects on drug-metabolizing enzymes or drug transporters. Drug-metabolizing enzymes are known to alter drug absorption and metabolism. Drug transporters are likely to affect drug absorption, distribution and elimination. The inhibitory effect on the CYP enzymes may result in enhanced concentration of therapeutics drug in plasma and/or tissue, leading to increased efficacy or toxicity of the drug, On the other hand, an inductive effect may cause sub-therapeutic plasma drug or treatment failure.[14] Several investigations have already shown that extracts from medicinal plants can exert inhibitory effects towards CYP, particularly CYP2D6.[15-17] Data on CYP induction by *in vitro* methodology are limited. It has been shown that St. John's wort has an inhibitory effect on all three CYP *in vitro*[18], but this herb is also a potent inducer of CYP3A4 both *in vitro* and *in vivo*, when taken over a period of time.[19,20] On the contrary, one report found no effect at all in man of St. John's wort on either CYP3A4 or CYP2D6.[19] Drug-drug interactions that involve absorption commonly result from drug transporter. Drug transporters play a significant role in the absorption, distribution and elimination of many drugs or xenobiotics. Thus, modulation of transporter activity represents another mechanism by which these drugs can interact with one another as well as with other classes of agents. The P-glycoprotein (p-gp), the most prominent drug transporter, is a member of the ATP-binding cassette transporter family. The inhibitory effect of natural compounds on p-gp function suggests that they may potentially give rise to p-gp-mediated drug interactions. The constituents in medical plants or herbal formulations may interfere with human liver drug metabolizing enzyme particularly CYP or drug transporters. This interaction may result in toxicity when co-administered these plants with therapeutic drug. The aim of the present study were to investigate the *in vitro* absorption and propensity for

metabolic drug interactions including *in vivo* toxicity, antimalarial activity and pharmacokinetics of *Plumbago indica* Linn. and its active constituent plumbagin.

Table 1.1 Five medicinal plants under investigation (plant parts, voucher numbers, traditional uses in medicine, extraction yields, biomarker compounds used and amounts for standardization.

Plant	Plant part used	Voucher number	Traditional use in medicine	Extraction yields (%)	Biomarker compounds Used and amounts (%w/w)	References
Dioscorea membranacea Pierre. (DM)	Rhizome	SKP 062041305	Treatment of lymphopathy, dermopathy, venereal diseases, leprosy, cancers	4.25	Dioscorealide B (6.14%)	[21-23]
Dracaena loureiri Gagnep. (DL)	Stem, Bark	SKP 065041201	Antipyretic, analgesic, anti-inflammatory	17.87	Loureirin B (0.4%)	[24,25]
Myristica fragrans Houtt. (MF)	Seed	SKP 121130601	Antidiarrheal , analgesic (uterus)	13.67	Myristicin (2.7%)	[25,26]
Plumbago indica Linn. (PI)	Root	SKP 148160901	Antirheumatism	10.60	Plumbagin (0.38%)	[24,27]
Garcinia mangostana Linn. (GM)	Pericarp	SKP 207411234	Anti-infective (skin infections, wound)	10.55	α-Mangostin (32.90%)	[28]

CHAPTER 2

OBJECTIVES

The objectives of the dissertation were to investigate the *in vitro* absorption and propensity for metabolic drug interactions including *in vivo* toxicity, antimalarial activity and pharmacokinetics of *Plumbago indica* Linn. and its active constituent plumbagin. Specific objectives include:

(1)   To assess antimalarial activity of plumbagin *in vitro* and in animal models;

(2)   To investigate permeability of plumbagin in caco-2 cell monolayers and their effects on the p-glycoprotein (p-gp);

(3)   To investigate the propensity to inhibit CYP-mediated hepatic metabolism (CYP1A2, CYP2C19, CYP2D6 and CYP3A4) of the five Thai medicinal plants with promising activities against malaria (Table 1.1) using human liver microsomes *in vitro*;

(4)   To investigate the *in vitro* inhibition and *in vivo* induction CYP-mediated hepatic metabolism of plumbagin;

(5)   To evaluate the toxicity and pharmacokinetics of plumbagin in wistar rats model; and

(6)   To investigate blood kinetics and tissue distribution of radiolabeled plumbagin in healthy and *Plasmodium berghei*-infected mice by using application of SPECT/CT imaging system and radiochemical analysis.

CHAPTER 3

REVIEW OF LITERATURES

3.1 Malaria and current situation

Malaria is caused by a eukaryotic protist of the phylum Apicomplexa, order Haemosporodia, family Plasmodiidae and genus Plasmodium. Four species of Plasmodium commonly infect humans including *P. malariae*, *P. ovale*, *P. vivax* and *P. falciparum*. In recent years, human cases of lethal or febrile malaria have also occurred with *P. knowlesi*, a parasite usually found in macaques, in certain forested areas of Southeast Asia.[29-32] In human and other mammalian, Plasmodium species are transmitted by anopheline mosquitoes. *P. falciparum* is responsible for most malaria deaths, especially in Africa. *P. falciparum* infection can develop suddenly and produce several life-threatening complications. With prompt, effective treatment, however, it is almost always curable. *P. vivax*, the most geographically widespread of the species, produces less severe symptoms. Relapses, however, can occur for up to 3 years, and chronic disease is debilitating. Once common in temperate climates, *P. vivax* is now found mostly in the tropics, especially throughout Asia. *P. malariae* infections not only produce typical malaria symptoms but also can persist in the blood for very long periods, possibly decades, without ever producing symptoms. A person with asymptomatic (no symptoms) *P. malariae*, however, can infect others, either through blood donation or mosquito bites. *P. malariae* has been wiped out from temperate climates, but it persists in Africa. *P. ovale* is rare, can cause relapses, and generally occurs in West Africa. The malaria parasite exhibits a life cycle with typical apicomplexan features. There are three distinct invasive stages: sporozoite, merozoite and ookinete. All are characterized by apical organelles and can invade or pass through host cells. Two distinct types of merogony are observed. The first, called exoerythrocytic schizogony, occurs in the liver and is initiated by the sporozoite. The resulting merozoites then invade erythrocytes and undergo repeated rounds of merogony called erythrocytic

schizogony. Some of the merozoites produced from the erythrocytic schizogony will undergo gamogony. Plasmodium gamogony is described in two phases: gametocytogenesis occuring in the bloodstream of the vertebrate host, and gametogenesis taking place in the mosquito gut. The gametes fuse to become a zygote which first develops into an ookinete and then becomes an oocyst where sporogony takes place.[33]

3.1.1 Malaria situation in worldwide

The World Health Organization (WHO) estimates that 300-500 million people are afflicted each year.[34] The World Malaria Report 2011 summarizes information received from 106 malaria-endemic countries and a range of other sources. It analyses prevention and control measures according to a comprehensive set of indicators, and highlights continued progress towards global malaria targets. This year's report builds primarily on data received from countries for the year 2010. The report shows clear progress in the fight against malaria and a decline in estimated malaria cases and deaths. For the first time, the report contains individual profiles for 99 countries with ongoing malaria transmission.[35]

In Southeast Asian, malaria is a major public health problem of which out of 11 countries of the region 10 countries are malaria endemic. WHO estimates that globally 33.96 million DALYs lost due to malaria in which SEA region contributes around 1.34 million.[36] Malaria is an enormous health and development problem in the SEA region as 1,322 million people are at risk of malaria. The social, cultural and economic dimensions in terms of disproportionate impact on the poor, the associated loss of wages and productivity both at the micro and macro levels are enormous. The disease is deeply rooted in the poor communities affecting national development and takes away major share of the health budgets. An estimated 1,322 million people or 76% of the total population of SEA region are at risk of malaria. Out of which around 29% population at moderate to high risk of malaria, 71% are at low risk of malaria, whereas remaining 24% of population is free from malaria. About 93% of the population of moderate to high risk of malaria in SEA region are living in Bangladesh, India, Indonesia, Myanmar, Thailand and Timor Leste, and contributing

more than 95% of confirmed malaria cases and deaths in the region. Among the population living in malaria endemic areas, infants, young children and pregnant women have been identified as high risk groups. Other groups of people which constitute high malaria risk are mobile population particularly those engaged in forest-related economy, gem-mining, fishing, industrial and engaged in road construction work. In some countries, ethnic minorities, refugees, displaced persons, tourists and pilgrims also constitute high risk group.[36]

Chloroquine resistant *P. falciparum* is reported from all endemic countries (except DPR Korea); nearly 400 million people live in areas with risk of contracting drug resistant malaria sulfadoxin-pyrimethamine resistance is also reported from all endemic countries except Sri Lanka and DPR Korea with an estimated 140 million population at risk. Deteriorating epidemiological indices are associated with drug resistance and operational problems. Multidrug resistant *P. falciparum* is highly prevalent on the Thai-Cambodia and Thai-Myanmar border areas. Even responses to ACTs have reduced in Thai-Combodia border. Frequent epidemics are being observed by Member Countries.[36]

3.1.2 Malaria situation in Thailand

Malaria has been a leading cause of morbidity and mortality in Thailand for many decades. Around 32 million people are at risk of malaria. All the four types of malaria are prevalent in the country. The border areas with Myanmar and Cambodia are worst affected. Non-immune migrant workers occupied with gem mining in forests, logging, agriculture and construction are the most vulnerable and most affected. High mobility of migrant and cross-border population also encourages the spread of multi-drug resistant of *P. falciparum* malaria from the Thai-Cambodia border to the Thai-Myanmar border, which poses more difficulties. Malaria epidemics occurred periodically in high risk areas, especially along the international borders of Thailand and Myanmar and Thailand and Cambodia. The intensive malaria control program in Thailand during the past five decades has resulted in considerable reduction in malaria incidence. Confirmed cases declined from 81,692 cases in 2000 to 32,126 cases in 2011 showing a decrease of 60.7% whereas the deaths have gone

down from 625 to 80 registering a decrease of 87.2%. *P. falciparum* proportions were around 50% of the confirmed cases.[37]

3.2 Clinical manifestation of malaria

Infection with malaria parasites may result in a wide variety of symptoms, ranging from absent or very mild symptoms to severe disease and even death. Malaria disease can be categorized as uncomplicated or severe (complicated). In general, malaria is a curable disease if diagnosed and treated promptly and correctly. All the clinical symptoms associated with malaria are caused by the asexual erythrocytic or blood stage parasites. When the parasite develops in the erythrocyte, numerous known and unknown waste substances such as hemozoin pigment and other toxic factors accumulate in the infected red blood cell. These are dumped into the bloodstream when the infected cells lyse and release invasive merozoites. The hemozoin and other toxic factors such as (GPI) stimulate macrophages and other cells to produce cytokines and other soluble factors which act to produce fever and rigors and probably influence other severe pathophysiology associated with malaria. *P. falciparum*-infected erythrocytes, particularly those with mature trophozoites, adhere to the vascular endothelium of venular blood vessel walls and do not freely circulate in the blood. When this sequestration of infected erythrocytes occurs in the vessels of the brain it is believed to be a factor in causing the severe disease syndrome known as cerebral malaria, which is associated with high mortality.[38,39]

Following the infective bite by the Anopheles mosquito, a period of time (the incubation period) goes by before the first symptoms appear. The incubation period in most cases varies from 7 to 30 days. The shorter periods are observed most frequently with *P. falciparum* and the longer ones with *P. malariae*. Antimalarial drugs taken for prophylaxis by travelers can delay the appearance of malaria symptoms by weeks or months, long after the traveler has left the malaria-endemic area (This can happen particularly with *P. vivax* and *P. ovale*, both of which can produce dormant liver stage parasites; the liver stages may reactivate and cause

disease months after the infective mosquito bite). Such long delays between exposure and development of symptoms can result in misdiagnosis or delayed diagnosis because of reduced clinical suspicion by the health-care provider. Returned travelers should always remind their health-care providers of any travel in areas where malaria occurs during the past 12 months.[40]

Uncomplicated Malaria: The classical (but rarely observed) malaria attack lasts 6-10 h. It consists of:[40]

- A cold stage (sensation of cold, shivering)

- A hot stage (fever, headaches, vomiting; seizures in young children)

- A sweating stage (sweats, return to normal temperature, tiredness)

- Classically the attacks occur every second day with the tertian parasites (*P. falciparum, P. vivax* and *P. ovale*) and every third day with the quartan parasite (*P. malariae*)

- More commonly, the patient presents with a combination of the following symptoms: fever, chills, sweats, headaches, nausea, vomiting, body aches and general malaise

3.3 Chemotherapy of malaria

Malaria is an important cause of death and illness in children and adults, especially in tropical countries. Malaria control requires an integrate approach, including prevention (primarily vector control) and prompt treatment with effective antimalarials. The treatment of malaria depends on the severity of the infection, the patient's age, the degree of background immunity, the pattern of susceptibility to antimalarial drugs, the cost and availability of such drugs. For this reason, recommendations vary according to geographic region and should be under constant review. The three so-called benign malarias *P. vivax, P. malariae* and *P. ovale* should all be treated with chloroquine. High-grade resistance to chloroquine in *P. vivax* has been reported from Oceania, but elsewhere the parasite remains generally sensitive and responds rapidly. Chloroquine is usually well tolerated, although it

commonly produces pruritus in dark skinned patients, and in the treatment of acute malaria it may cause nausea, dysphoria and very rarely, a transient neuropsychiatric syndrome or cerebellar dysfunction. The conventional drugs used in malarial chemotherapy include, chloroquine, quinine, sulfadoxine/pyramethamine and primaquine. Newer drugs in use include artemisine and its derivatives (such as dihydroartemisinine, artesunate, artemether), halofantrine, atovaquone, artemisinine combinations (such as artemether/lumenfantrine, artesunate/mefloquine) and malaria vaccines. These newer drugs were developed based on some short comings of the conventional drugs such as drug resistance and unbearable side effects.[41-44]

3.4 Current status of drug resistant malaria

Resistance to antimalarial drugs is a major threat to the control and elimination of malaria. The greatest problem with antimalarial drug resistance is with *P. falciparum.* All geographical areas are affected, with the exception of Central America, and the worst affected is mainland South-East Asia, where parasites with reduced susceptibility to all the available antimalarial medicines are now prevalent. Resistance to antimalarial drugs has been described for two of the four species of malaria parasite that naturally infect humans, *P. falciparum* and *P. vivax*. *P. falciparum* has developed resistance to nearly all antimalarials in current use, although the geographical distribution of resistance to any single antimalarial drug varies greatly. *P. vivax* infection acquired in some areas has been shown to be resistant to chloroquine and/or primaquine. Chloroquine-resistant *P. falciparum* malaria has been described everywhere that *P. falciparum* malaria is transmitted except for malarious areas of Central America (north-west of the Panama Canal), the island of Hispaniola, and limited areas of the Middle East and Central Asia. In contrast, resistance to antifolate drugs and atovaquone arises frequently and it can be induced readily in both *P. falciparum* and *P. vivax*.[45] Sulfadoxine/pyrimethamine (SP) resistance occurs frequently in South-East Asia and South America. SP resistance is becoming more prevalent in Africa as that drug is increasingly being relied upon as

a replacement for chloroquine. Mefloquine resistance is frequent in some areas of South-East Asia and has been reported in the Amazon region of South America and sporadically in Africa. Cross-resistance between halofantrine and mefloquine is suggested by reduced response to halofantrine when used to treat mefloquine failures. Genetically encoded resistance to the artemisinin derivatives in *P. falciparum* has emerged recently in South-East Asia and is now affecting therapeutic responses to ACTs.[46-48] Piperaquine resistance has begun to emerge in Cambodia. Resistance also occurs in *P. vivax*; high-level resistance to chloroquine is prevalent in Indonesia and Papua New Guinea, and lower levels of resistance have been reported in several other areas of Asia and the Americas.[49] Antifolate resistance is also common in *P. vivax*. There are very few reports of resistance in *P. malariae* or *P. ovale*.[42,50]

3.5 Antimalarial drug development

The emergence and spread of multidrug-resistant *P. falciparum* has become especially problematic in undermining malaria control programs in most endemic regions of the world. Nevertheless, antimalarial chemotherapy remains as the mainstay for controlling malaria in the absence of a suitable vaccine treatment. Since antimalarial drug resistance compromises the effective treatment of the disease, there is a pressing need for ongoing drug discovery research that will provide effective and affordable antimalarial agents that are also simple to administer. Many different approaches to the identification of new antimalarial are described below (**Table 3.1**).

Table 3.1 Approaches to antimalarial drug discovery and development.[51]

Approach	Examples
Optimize therapy with existing agents	Amodiaquine/sulfadoxine/pyrimethamine
	Amodiaquine/artesunate
	Artesunate/sulfadoxine/pyrimethamine
	Artesunate/mefloquine
	Artemether/lumefantrine
	Chlorproguanil/dapsone
	Chlorproguanil/dapsone/artesunate
	Atovaquone/proguanil
Develop analogs of existing agents	New aminoquinolines
	New endoperoxides
	New folate antagonists
Natural products	New natural products
Compounds active against other diseases	Folate antagonists
	Antibiotics
	Atovaquone
	Iron chelators
Drug resistance reversers	Verapamil, desipramine, trifluoperazine
	Chlorpheniramine

3.6 Traditional plant used for the treatment of malaria

Plant-derived compounds offer a third approach to chemotherapy. Importantly, this approach can benefit from knowledge of medicinal plants among natives of malaria regions, where the appreciation of the use of plant products to treat febrile illnesses has grown over many generations. Therefore, as a great improvement over random screening, a plant product with specific clinical activity

can be the starting point for a medicinal chemistry effort. Natural products are the sources of the two most important drugs currently available to treat severe falciparum malaria, quinine and derivatives of artemisinin. In the case of artemisinin, relatively simple chemical modifications of the natural product parent compound have led to a series of highly potent antimalarials that are playing an increasingly important role in the treatment of malaria. However, the cost of these compounds may be limiting, and so efforts to design fully synthetic endoperoxides that are less expensive to produce are an important priority.[52,53] Extensive evaluations of natural products as potential new therapies for many human diseases are underway.[54] It is important that such trials include the evaluation of the antimalarial activity of plant extracts and potential drugs purified from these extracts. As with both the quinolines and artemisinins, it is likely that antimalarial natural products will be the parent compounds for the semi-synthetic or fully synthetic production of new drugs.[51]

Due to the crucial role that plant-derived compounds have played in drug discovery and development for the treatment of several diseases, the isolation of new bioactive compounds from medicinal plants based on traditional use or ethnomedical data appears to be a very promising approach. The limitation of availability or affordability of pharmaceutical medicines in many tropical countries, about 80% of the rural population in Africa depends on traditional herbal remedies.[55] Although there is widespread use of traditional herbal remedies in the management of malaria, scientific understanding of the plants is, however, largely unexplored and therefore, there is a need to collect ethnobotanical information on antimalarial plants which is essential for further evaluation of the efficacy and safety of the plants as antimalarial remedies.

3.7 Plumbagin

Plumbagin (5-hydroxy-2-methyl 1,4-naphthoquinone) is a major constituent of *Plumbago indica* Linn. It is a natural product found in many plants

(**Figure 3.1**). A yellow naphthoquinone pigment, it occurs in plant roots as a colorless combined form that can be processed to plumbagin by acid treatment. Plumbagin is found in the plants of the Plumbaginaceae, Droseraceae, Ancestrocladaceae and Dioncophyllaceae families.[8] Plumbagin has been used in the Indian medicine since the period of Charaka, from 750 BC, as an antiatherogenic, cardiotonic, hepatoprotective and neuroprotective agent. The active principle, plumbagin, was first isolated in 1829.[56] According to the Botanical Dermatology Database, the following species have been reported to yield plumbagin[57]:

- Ceratostigma
- Limonium
- *Limonium carolinianum* (sea lavender)
- Plumbagella
- Plumbago (leadwort)
- *Plumbago capensis* (cape leadwort)
- *Plumbago coerulea*
- *Plumbago europaea*
- *Plumbago rosea*
- *Plumbago pulchella*
- *Plumbago scandens*
- *Plumbago zeylanica* (Ceylon leadwort)
- Statice
- *Statice limonium* (English sea lavender)
- *Plumbago indica* Linn.

Plumbagin is also contained in members of the Droseraceae (Sundew) family. This family of insectivorous plants comprises some 105 species in four genera. *Drosera L.*, the largest genus, is usually found in acid bogs. The following Drosera species have been reported to contain plumbagin:

- *D. anglica* Hudson.

- *D. auriculata* Backh.

- *D. binata* Labill.

- *D. capensis* L.

- *D. cistiflora* L.

- *D. intermedia* Hayne.

- *D. longifolia* L.

- *D. peltata* Smith.

- *D. rotundifolia* (round-leaved sundew)

- *D. whitakeri* Planchon.

- *D. ramentacea* Burchell.

Other genera in the Droseraceae family are *Aldrovanda vesiculosa* L., a free floating aquatic plant, *Dionaea muscipula* Ellis, also known as Venus' Fly Trap, and *Drosophyllum lusitanicum* Link, commonly called Portugese.

Pure plumbagin is used primarily in research designed to exploit its properties as a superoxide generator, an antibiotic and an antineoplastic agent. Between 1976 and 1999, 32 patents involving plumbagin were obtained in the United States. Many of these patents involve polymer scale prevention agents. Impure extracts of plumbagin from Plumbagineae and Droseraceae have long traditions of use in folk medicines. *Plumbago zeylamica* L., *Plumbago rosea* L., and *Plumbago europaea* L. have been used in China and other Asian countries for the treatment of cancer, rheumatoid arthritis, dysmenorrhea and contusion of extremities. The round-leaved sundew has been used in North America to remove warts, corns, keratoses and freckles. The crushed leaves of *Drosera burnammii* Vahl are considered to be a powerful rubefacient in Hindu medicine. *Plumbago europaea,* or leadwort, has long been used in France to relieve toothache.[58] The antibacterial properties of plumbagin are well documented in traditional medicine. The stem barks of *Pera benesis,* containing plumbagin as the most active compound, are employed by the Chimane Indians in the Bolivian Amazon as treatment of cutaneous leishmaniasis. Sundew reportedly has great benefit in treating bronchitis and

whooping cough.[58,59] *Plumbago zeylanica* is grown as a perennial herb in the plains of Bengal and southern India. Extracts of the root have been reported to be a powerful poison which, when given internally or applied to the ostium uteri, causes abortion.[60,61]

Plumbagin is the major compound of *Plumbago indica* Linn. *Plumbago indica* Linn has shown a good antimalarial activity *in vitro* screening in previous study.[12] This compound has been shown to display a wide spectrum of biological and pharmacological activities such as antimalarial, leihsmanicidal, trypanocidal, antiviral, antitumoral, microbiological, and insecticidal activities.[9] Ethanolic extract of *Plumbagozey lanica* has been reported to exhibit *in vitro* antimalarial activity against chloroquine-susceptible clone of *P. falciparum* (3D7) with an IC_{50} (concentration that inhibits parasite growth by 50%) of 17 μg/ml.[10] The activity of *P. falciparum* enzyme, the succinate dehydrogenase (SDH), has been demonstrated to be inhibited by 50% by plumbagin at an inhibitory concentration of 5 mM, and also inhibited the growth of the parasite with an IC_{50} of 0.27 mM.[11]
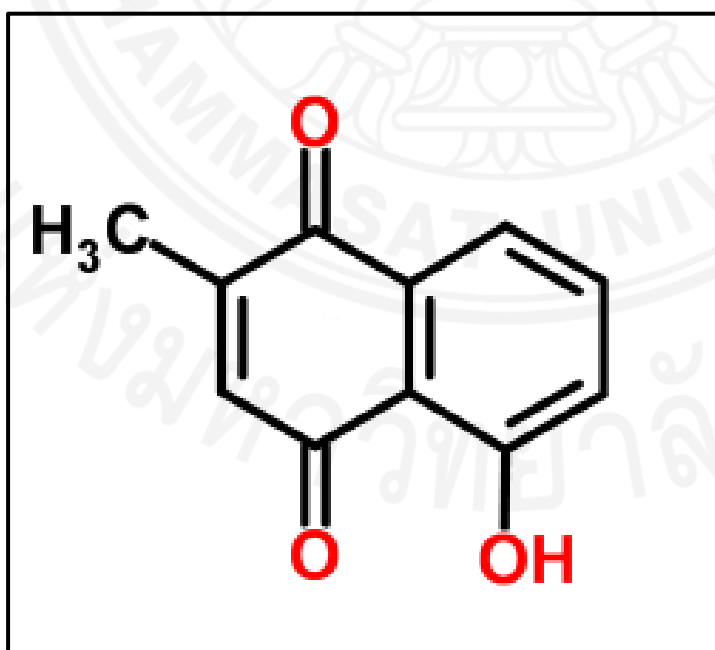
Figure 3.1 Structure of plumbagin.[62]

Plumbagin has been shown to produce many toxic side effects including diarrhea, skin rashes, increases in white blood cell and neutrophil counts, increases in serum phosphatase and acid phosphatase levels, and hepatic toxicity.[63]

Acute oral toxicity of plumbagin has been investigated in wistar rats and mice. It showed no toxicity following a single oral dose of 65 and 40 mg/kg in wistar rat and mice, respectively in both control and experiment groups.[61]

3.8 Drug metabolism and transport

Metabolism is the mechanism of elimination of foreign and undesirable compounds from the body and the control of levels of desirable compounds such as vitamins in the body (**Figure 3.2**). Drug metabolism is the biochemical modification of pharmaceutical substances, usually through specialized enzymatic systems. This is a form of xenobiotic metabolism. Metabolism often converts lipophilic chemical compounds into more readily excreted hydrophilic products.[64] Drug metabolism can result in toxication or detoxication the activation or deactivation of the chemical. While both occur, the major metabolites of most drugs are detoxication products. Drugs are almost all xenobiotics. Other commonly used organic chemicals are also xenobiotics, and are metabolized by the same enzymes as drugs. This provides the opportunity for drug-drug and drug-chemical interactions or reactions. The major site of metabolism in the body is the liver but metabolizing enzymes are also expressed in extrahepatic tissues such as in the gut epithelium, lungs and kidneys. Metabolism in liver occurs in two stages: Phase I pathways in liver microsomes where the drug is functionalized and Phase II pathways in liver cells where the parent or the metabolite from Phase I gets conjugated. Liver microsomes are in the endoplasmic reticulum of liver cells or hepatocytes. Phase I reactions in microsomes are catalyzed by a group of enzymes known as the cytochrome P450 system that plays a significant role in drug metabolism. The common chemical reactions involved in Phase I are aromatic hydroxylation, aliphatic hydroxylation, oxidative N-dealkylation, oxidative O-dealkylation, S-oxidation,

reduction and hydrolysis. Most often this simple functionalization could be sufficient to make a drug more soluble, facilitating elimination through the kidneys. Further conjugation in Phase II occurs by glucuronidation, sulfation, amino acid conjugation, acetylation, methylation or glutathione conjugation to facilitate elimination.[65] Drug metabolism can lead to inactivation of an active compound, activation of an inactive compound, *i.e.*, prodrug, formation of an active metabolite from an active compound or toxification of an active or inactive compound. Thus, changes in the activity of a drug metabolizing enzyme can have different consequences depending on the properties of the compound. Moreover, a decrease in the enzyme activity leads to increased plasma concentrations of the substrate drug, which usually means increased effects and toxicity, and vice versa, an increase in enzyme activity leads to decreased plasma concentrations of the substrate, which most often reduces the effectiveness of the drug. Alterations in enzyme activity are most relevant in the case of drugs with a narrow therapeutic window.

Movement of molecules across biological membranes into and out of cells can occur by passive diffusion or by active transport via influx and efflux transporters, respectively. Drug transporters are expressed in many tissues such as the intestine, liver, kidney and brain. It plays key roles in drug absorption, distribution, and excretion. The information on the functional characteristics of drug transporters provides important information to allow improvements in drug delivery or drug design by targeting specific transporter proteins. The expression system of transporters is an efficient tool for screening the activity of individual transport processes. The changes in pharmacokinetics due to genetic polymorphisms and drug-drug interactions involving transporters can often have a direct and adverse effect on the therapeutic safety and efficacy of many important drugs.[66]
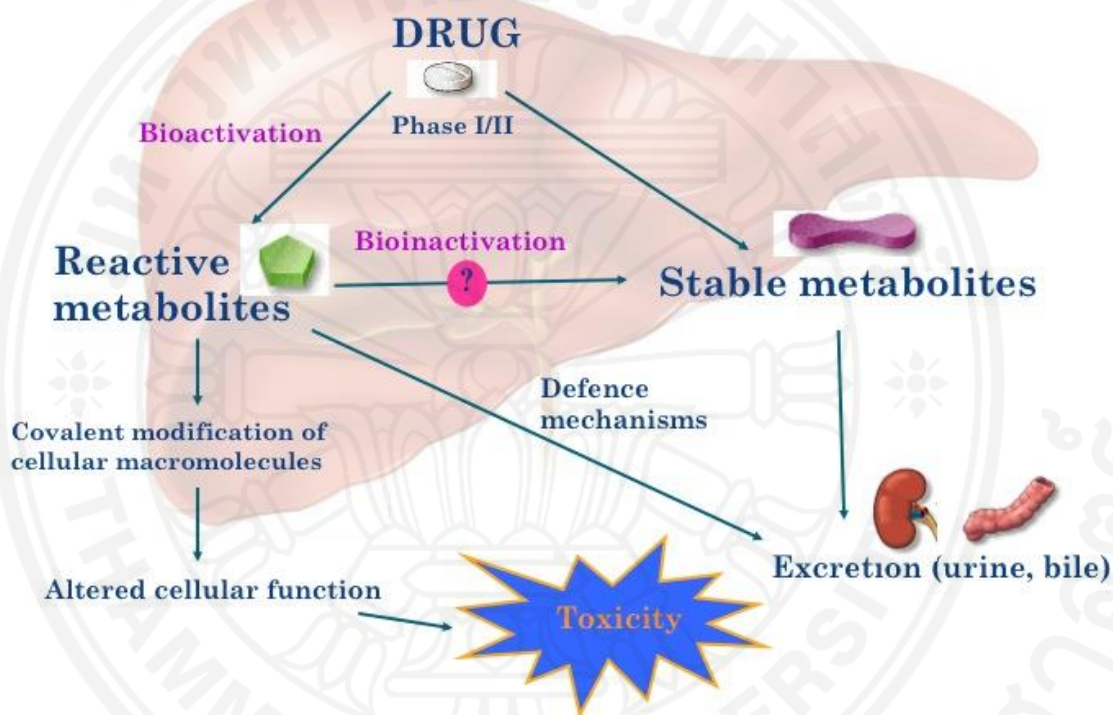
Figure 3.2 Relationship between drug metabolism and toxicity: when reactive metabolites are not detoxified, interference with macromolecules (functional proteins, phospholipids and DNA) can occur. If cellular repair is not sufficient, these interactions can result in drug toxicity.[67]

Cytochrome P450 (CYP) enzyme system, a very large group of enzymes encoded by the P450 gene superfamily, is one of the widely studied topics in drug development. CYP are membrane bound proteins with an approximate molecular weight of 50 kd, and contain a heme moiety. CYP and other mixed function oxygenases are mainly found in the endoplasmic reticulum of the liver. The monooxygenase function of CYP involves a number of steps but the end reaction is the transfer of one oxygen atom to the substrate (R) that has a site for oxidation as shown below.[68]

$$NADPH + H^+ + O_2 + R\text{-}H \xrightarrow{\text{CYP450}} NADP^+ + H_2O + R\text{-}OH$$

There are about 30 human cytochrome P450 enzymes, out of which only six, CYP1A2, CYP2C9, CYP2C19, CYP2D6, CYP2E1 and CYP3A4 are the major metabolizing enzymes (**Table 3.2**). CYP3A is the most abundant and most clinically important isozyme in humans. It metabolizes nearly 50% of the clinically available drugs.[69] Some drugs can be inducers or inhibitors of specific isozymes but not necessarily substrates. CYP enzymes are distributed throughout the body, especially at locations which come into contact with the environment such as the intestine, skin and nasal epithelium. The liver and intestines are the most important locations for drug metabolism. A survey of liver CYP enzymes which are responsible for metabolic transformations of drugs is given in **Table 3.2**.[70]

Table 3.2 Human liver microsome CYP enzymes.[70]

CYP	Relative content (%)	Variability	Estimate fraction of drugs metabolized by the P450	Marker activity
1A1	1	100	< 1 %	None
1A2	12	40	4 %	Caffeine
2A6	4	30	<1%	None
2B6	1	50	<1%	None
2C9/10/19	20	20	11 %	diclofenac (2C9), (S)-mephenytoin (2C19)
2D6	4	1000	30 %	sparteine, debrisoquine, dextromethorphan
2E1	6	20	2%	Chlorzoxazone
3A4	30	60	52%	nifedipine, erythromycin, alprazolam, dextrometorphan

3.9 Pharmacokinetic drug interaction

Elimination of a drug may occur through metabolism to one or more active or inactive metabolites, excretion of the parent drug by renal or biliary routes, or by a combination of excretory and metabolic elimination pathways. If elimination occurs primarily through metabolism, identification of the principal metabolic route may have important safety implications. Some drugs and dietary xenobiotics have the ability to influence the metabolism of concomitantly administered drugs by acting as inhibitors or inducers of drug-metabolizing enzymes. Thus, drug interactions may have the potential to result in substantial increases or decreases in the blood and tissue concentrations of the drug under investigation or certain of its metabolites. The clinical significance of the interactions resulting from inhibition or induction will be dependent on the relative pharmacodynamics activity and toxicity of the parent drug and its metabolites. In situations where a drug interaction results in variations in the relative levels of a parent drug and metabolite that are approximately equipotent in terms of efficacy and safety considerations, inhibition and induction may be of little therapeutic consequence. Probe substrates that use in *in vitro* experiments are conducted to determine whether a drug inhibits a specific CYP enzyme involve incubation of the drug with probe substrates for the CYP enzymes. There are two scientific criteria for selection of a probe substrate, the substrate should be selective (predominantly metabolized by a single enzyme in pooled human liver microsomes or recombinant CYP) and should have a simple metabolic scheme (ideally no sequential metabolism). There are also some practical criteria-commercial availability of substrate and metabolite(s); assays that are sensitive, rapid, simple and a reasonable incubation time. Preferred substrates listed in **Table 3.3** meet a majority of the criteria listed above. Acceptable substrates of FDA meet some of the criteria, and are considered acceptable by the scientific community.[70]

Table 3.3 Preferred and acceptable chemical substrates for *in vitro* drugs metabolism experiments.[70]

CYP	Substrate Preferred	Km (μM)	Substrate Acceptable	Km (μM)
1A2	phenacetin-O-deethylation	1.7-152	7-ethoxyresorufin-O-deethylation	0.18-0.21
			theophylline-N-demethylation	280-1230
			caffeine-3-N-demethylation	220-1565
			tacrine 1-hydroxylation	2.8, 16
2A6	coumarin-7-hydroxylation	0.30-2.3		
	nicotine C-oxidation	13-162		
2B6	efavirenz hydroxylase	17-23	propofol hydroxylati on	3.7-94
	bupropion-hydroxylation	67-168	S-mephenytoin-N-demethylation	1910
2C8	Taxol 6-hydroxylation	5.4-19	amodiaquine N-deethylation	2.4,
			rosiglitazone para-hydroxylation	4.3-7.7
2C9	tolbutamide methyl-hydroxylation	67-838	flurbiprofen 4'-hydroxylation	6-42
	S-warfarin 7-hydroxylation	1.5-4.5	phenytoin-4-hydroxylation	11.5-117
	diclofenac 4'-hydroxylation	3.4-52		
2C19	S-mephenytoin 4'-hydroxylation	13-35	omeprazole 5-hydroxylation	17-26
			fluoxetine O-dealkylation	3.7-104
2D6	(±)-bufuralol 1'-hydroxylation	9-15	debrisoquine 4-hydroxylation	5.6
	dextromethorphan O-demethylation	0.44-8.5		
2E1	chlorzoxazone 6-hydroxylation	39-157	p-nitrophenol 3-hydroxylation	3.3
			lauric acid 11-hydroxylation	130
			aniline 4-hydroxylation	6.3-24
3A4/5*	midazolam 1-hydroxylation	1-14	erythromycin N-demethylation	33 – 88
			dextromethorphan N-demethylation	133-710
			triazolam 4-hydroxylation	234
	testosterone 6 b -hydroxylation	52-94	terfenadine C-hydroxylation	15
			nifedipine oxidation	5.1- 47

* Recommend use of two structurally unrelated CYP3A4/5 substrates for evaluation of *in vitro* CYP3A inhibition. If the drug inhibits at least one CYP3A substrate *in vitro*, then *in vivo* evaluation is warranted.

3.9.1 Induction of CYP enzymes

Nature has created the ability to induce metabolism in order to eliminate a xenobiotic faster from the body during long-term exposure. Usually, enzyme induction leads to lower drug efficacy due to the enhanced elimination of an active compound.[71] But in some cases, nature works against itself, and induction can lead to increased efficacy or even toxicity of metabolite. It is thought that induction of a metabolizing enzyme leads to an increased amount of the enzyme, not to changes in the activity of existing enzymes.[72] Induction usually takes place at the transcription site. Inducers of drug metabolism can enhance protein synthesis or they can stabilize the RNA, both of which lead to increased formation of the active protein. In some cases, the inducer can stabilize the protein, thus prolonging its lifespan. As induction is such a complex process, it takes time, and induction can usually be seen only days or even weeks after the exposure to the inducer has begun.[72] Common inducers include polycyclic aromatic hydrocarbons, antiepileptic drugs, corticosteroids and rifampicin.[71,72] Among others, CYP1A, CYP2C and CYP3A enzyme families are susceptible to induction.[73] This activation is mediated by nuclear receptors, which include the constitutive androstane receptor (CAR), the pregnane X receptor (PXR) and the aromatic hydrocarbon receptor (AhR).

Enzyme inducers increase specific enzyme levels by modulating the gene expression. Some drugs induce CYP enzymes that are not involved in their metabolism. For example, omeprazole induces human CYP1A2 but is metabolized by CYP2C19 and CYP3A4.[74] Administration of omeprazole can lower the effect of a drug normally metabolized by CYP1A2, *e.g.*, acetaminophen. Primary human hepatocyte cultures and hepatocyte cell lines (*e.g.* HepG2 human hepatoma cell line) have sometimes proved useful for the study of induction phenomena.[75] Artifacts are common, however, as cultured hepatocytes typically undergo a time-dependent loss of CYP expression and may also exhibit a diminished capacity for induction. The predictive value of hepatocyte cell lines is often limited by substantial phenotypic differences between these cells and the tissues from which they were derived. Enzyme induction can be measured by assaying for the activity

of specific isoforms, immune-detection of isoform protein, or quantification of mRNA. The use of known inducers as positive control agents is necessary to verify the sensitivity of these systems. In evaluating the potential for a drug to induce a specific CYP enzyme, the experiment should include an acceptable enzyme inducer as a control, such as those listed in **Table 3.4.**

Table 3.4 Chemical inducers for *in vitro* drugs metabolism experiments.[70]

CYP	*In Vitro* Inducer as Positive Controls	Recommended Concentration (µM) of the Positive Controls	Reported Fold Induction In Enzyme Activities
1A2	omeprazole	25-100	14-24
	lansoprazole	10	10
2B6	phenobarbital	500-1000	5-10
2C8	rifampin	10	2-4
2C9	rifampin	10	3.7
2C19	rifampin	10	20
2D6	none identified		
3A4	rifampin	10-50	4-31

3.9.2 Inhibition of CYP enzymes

CYP inhibition is an important consideration for the development of novel therapeutic agents. Knowledge of the potential for a drug to decrease CYP activity at an early stage of drug discovery and development reduces the risk of failure in the clinic. Liver microsomes are a widely used model system for assessing inhibition of CYP enzymes, because they contain a full complement of CYP. Incubations with liver microsomes have been shown to retain the most important part of liver function like CYP-mediated metabolism of drugs. The type of CYP

inhibition can be either reversible or irreversible (mechanism-based inhibition). Reversible inhibition is the most common type of enzyme inhibition and can be further divided into competitive, noncompetitive, uncompetitive, and mixed-type inhibition.[76,77] Irreversible inhibition requires biotransformation of the inhibitor, while reversible inhibition can take place directly, without metabolism. Enzyme inhibition can lead to higher systemic levels of a drug causing enhanced efficacy or toxicity. This should be considered when multiple drugs are simultaneously prescribed and/or when over-the-counter drugs or neutraceuticals are concomitantly administered with prescription drugs. Most chemical inhibitors are not absolutely specific for an individual CYP enzyme, but a valuable attribute of chemical inhibitors is their commercial availability. Although not all inclusive, the chemical inhibitors listed in **Table 3.5** can be used to identify individual CYP enzymes responsible for a drug metabolism and determine the relative contribution of an individual CYP enzyme.

Reversible inhibition: For the competitive inhibition, enzyme can bind either substrate or inhibitor, but not both. Inhibitor binds in same site as substrate change in active site so, substrate can't bind. Competitive inhibitor increases apparent K_m, but doesn't affect V_{max}.[78] **For the non-competitive inhibition**, enzyme can bind both substrate and inhibitor simultaneously, but ESI complex can't make product. Inhibitor must dissociate in order for catalysis to occur. Therefore, inhibitor binding decreases V_{max} but has no effect on K_m. **For the uncompetitive inhibition**, inhibitor binds only to ES complexes at locations other than the catalytic site. Substrate binding modifies enzyme structure, making inhibitor-binding site available. Inhibition cannot be reversed by substrate. The effect of the three forms of inhibition on the Lineweaver-Burk and Eadie-Hofstee plots is illustrated in **Figure 3.3**.[79]
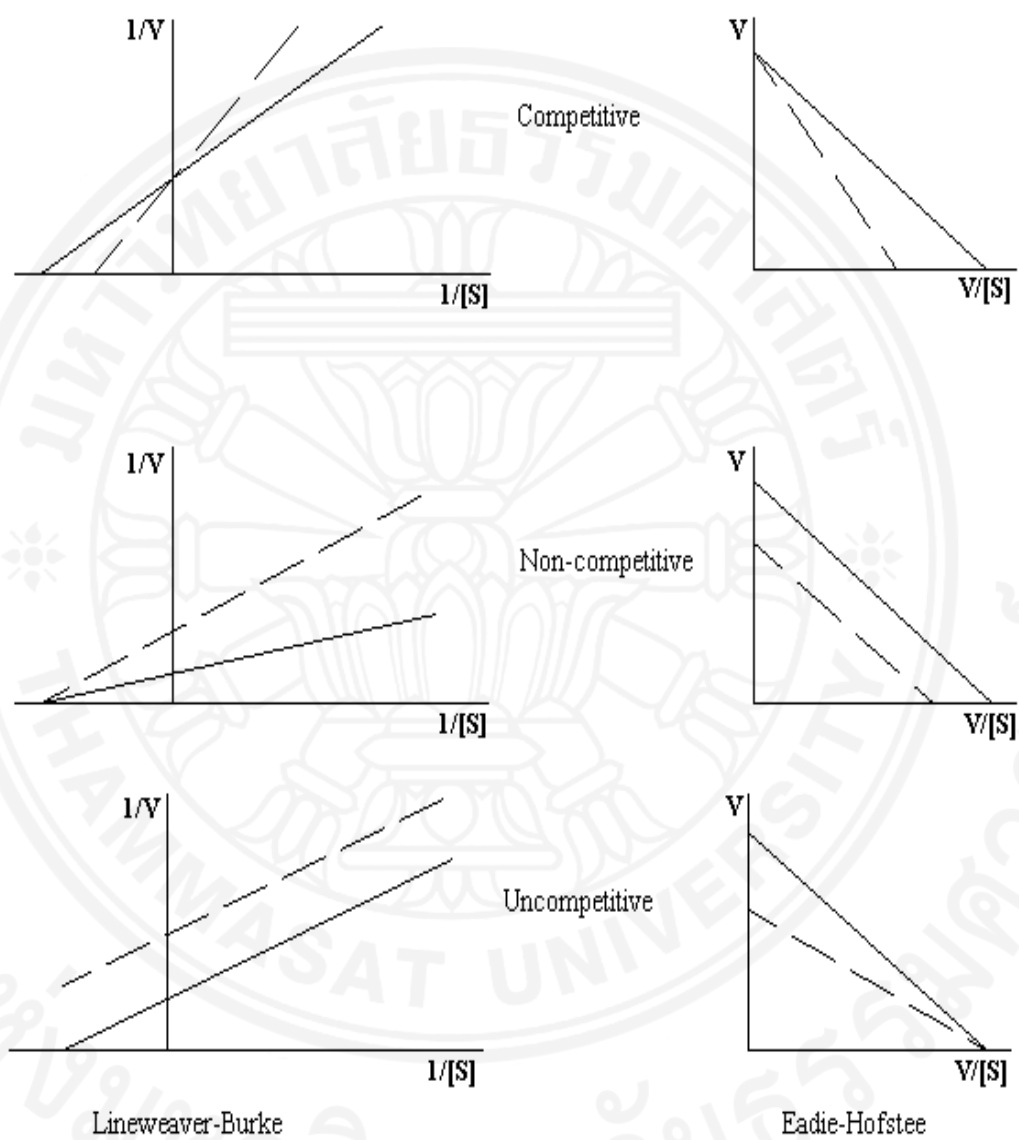
Figure 3.3 The effect of inhibitors on the Lineweaver-Burk and Eadie-Hofstee plots.[80]

Table 3.5 Chemical inhibitors for *in vitro* drugs metabolism experiments.[70]

CYP	Inhibitor Preferred	Ki (µM)	Inhibitor Acceptable	Ki (µM)
1A2	furafylline	0.6-0.73	α-naphthoflavone	0.01
2A6	tranylcypromine	0.02-0.2	pilocarpine	4
	methoxsalen	0.01-0.2	tryptamine	1.7
2B6			3-isopropenyl-3-methyl diamantane	2.2
			2-isopropenyl-2-methyl adamantane	5.3
			sertraline	3.2
			phencyclidine	10
			triethylenethiophosphoramide (thiotepa)	4.8
			clopidogrel	0.5
			ticlopidine	0.2
2C8	montelukast		trimethoprim	32
	quercetin	1.1	gemfibrozil	69-75
			rosiglitazone	5.6
			pioglitazone	1.7
2C9	sulfaphenazole	0.3	fluconazole	7
			fluvoxamine	6.4-19
			fluoxetine	18-41
2C19			ticlopidine	1.2
			nootkatone	0.5
2D6	quinidine	0.027-0.4		
2E1			diethyldithiocarbamate	9.8-34
			clomethiazole	12
			diallyldisulfide	150
3A4/5	ketoconazole	0.0037- 0.18	azamulin	
	itraconazole	0.27, 2.3	troleandomycin	17
			verapamil	10, 24

3.9.3 Michaelis-Menten model

The Michaelis-Menten model is the one of the simplest and best-known approaches to enzyme kinetics. It takes the form of an equation relating reaction velocity to substrate concentration for a system where a substrate S binds reversibly to an enzyme E to form an enzyme-substrate complex ES, which then reacts irreversibly to generate a product P and to regenerate the free enzyme E. This system can be represented schematically as follows[79]:

$$E + S \underset{K_1}{\overset{K_1}{\rightleftharpoons}} ES \xrightarrow{K_2} E + P$$
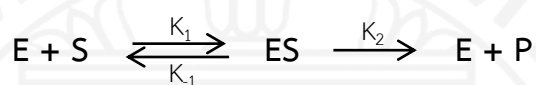
The Michaelis-Menten equation for this system is :

$$V = \frac{V_{max}[S]}{K_m + [S]}$$

where, V_{max} represents the maximum velocity achieved by the system, at maximum (saturating) substrate concentrations. K_m (the Michaelis constant; sometimes represented as KS instead) is the substrate concentration at which the reaction velocity is 50% of the V_{max}. [S] is the concentration of the substrate S.

The plot of the Michaelis-Menten equation's predicted reaction velocity as a function of substrate concentration is presented in **Figure 3.4,** with the significance of the kinetic parameters V_{max} and K_m graphically depicted.
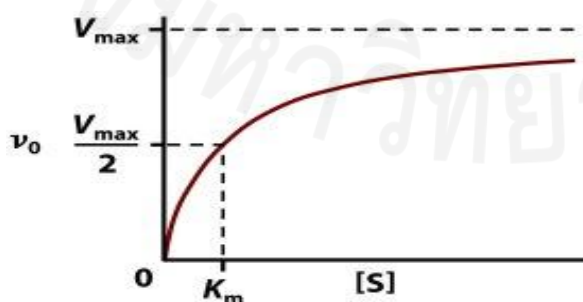
Figure 3.4 Michaelis-Menten plot showed effect of substrate concentration against velocity.[81]

Linear plot of Michaelis-Menten

The plot of v versus [S] is not linear; although initially linear at low [S], it bends over to saturate at high [S]. Before the modern era of nonlinear curve-fitting on computers, this nonlinearity could make it difficult to estimate K_m and V_{max} accurately.[79] Therefore, several researchers developed linearization of the Michaelis-Menten equation, such as the Lineweaver-Burk plot, the Eadie-Hofstee diagram and the Hanes-Woolf plot. All of these linear representations can be useful for visualizing data, but none should be used to determine kinetic parameters, as computer software is readily available that allows for more accurate determination by nonlinear regression methods.

The Lineweaver-Burk plot

The Lineweaver-Burk plot or double reciprocal plot is a common way of illustrating kinetic data. This is produced by taking the reciprocal of both sides of the Michaelis-Menten equation.[79] This is a linear form of the Michaelis-Menten equation and produces a straight line with the equation: $y = mx + c$ with a y-intercept equivalent to $1/V_{max}$ and an x-intercept of the graph representing $-1/K_m$. The Lineweaver-Burk Plots of Inhibited Enzymes are shown in **Figure 3.5**.

Advantage of Lineweaver-Burk plot were used for determining the type of enzyme inhibition, the Lineweaver-Burk plot can distinguish competitive, non-competitive and uncompetitive inhibitors. Competitive inhibitors have the same y-intercept as uninhibited enzyme (since V_{max} is unaffected by competitive inhibitors the inverse of V_{max} also doesn't change) but there are different slopes and x-intercepts between the two data sets. Non-competitive inhibition produces plots with the same x-intercept as uninhibited enzyme (K_m is unaffected) but different slopes and y-intercepts. Uncompetitive inhibition causes different intercepts on both the y- and x-axes but the same slope.[82]

Disadvantage of Lineweaver-Burk plot was classically used but it is prone to error, as the y-axis takes the reciprocal of the rate of reaction thus increasing any small errors in measurement. Also, most points on the plot are found far to the right of the y-axis (due to limiting solubility not allowing for large values of

[S] and hence no small values for 1/[S], calling for a large extrapolation back to obtain x- and y-intercepts.[82]
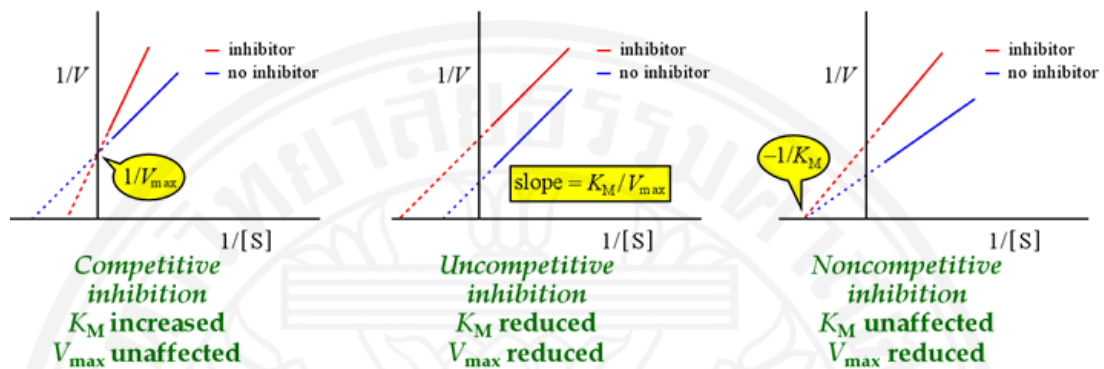
Figure 3.5 Lineweaver-Burk plots of inhibited enzymes.[83]

The Eadie-Hofstee diagram

The Eadie-Hofstee diagram is a graphical representation of enzyme kinetics in which reaction rate is plotted as a function of the ratio between rate and substrate concentration[79] :

$$V = -K_m \frac{V}{[S]} + V_{max}$$

where v represents reaction rate, K_m is the Michaelis-Menten constant, [S] is the substrate concentration, and V_{max} is the maximum reaction rate. It can be derived from the Michaelis-Menten equation as follows[79] :

$$V = \frac{V_{max}[S]}{K_m + [S]}$$

A plot of v against V/[S] will hence yield Vmax as the y-intercept, V_{max}/K_m as the x-intercept, and K_m as the negative slope. Like other techniques that linearize the Michaelis-Menten equation, the Eadie-Hofstee plot was used historically for rapid identification of important kinetic terms like K_m and V_{max}, but has been

superseded by nonlinear regression methods that are significantly more accurate and no longer computationally inaccessible. It is also more robust against error-prone data than the Lineweaver-Burk plot, particularly because it gives equal weight to data points in any range of substrate concentration or reaction rate. One drawback from the Eadie-Hofstee approach is that neither ordinate nor abscissa represents independent variables: both are dependent on reaction rate. Thus any experimental error will be present in both axes. Also, experimental error or uncertainty will propagate unevenly and become larger over the abscissa thereby giving more weight to smaller values of V/[S]. Therefore, the typical measure of goodness of fit for linear regression, the correlation coefficient R, is not applicable. The Michaelis-Menten kinetics according to Eadie–Hofstee diagram was shown in **Figure 3.6**.
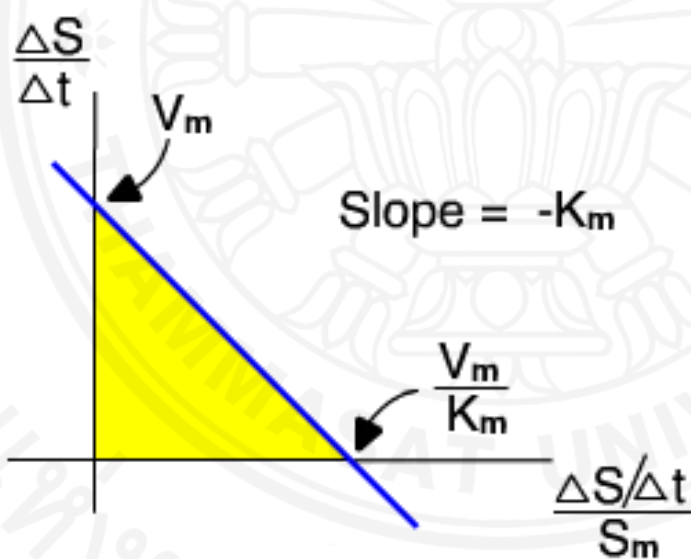
Figure 3.6 The Michaelis-Menten kinetics according to Eadie-Hofstee diagram.[84]

The Hanes-Woolf plot

The Hanes-Woolf plot is a graphical representation of enzyme kinetics in which the ratio of the initial substrate concentration [S] to the reaction velocity V is plotted against [S]. It is based on the rearrangement of the Michaelis-Menten equation shown below[79] :

$$\frac{[S]}{V} = \frac{[S]}{V_{max}} + \frac{K_m}{V_{max}}$$

where K_m is the Michaelis–Menten constant and V_{max} is the maximum reaction velocity. It was first described by Barnet Woolf. Charles Samuel Hanes subsequently pointed out that the use of linear regression to determine kinetic parameters from this type of linear transformation is flawed, because it generates the best fit between observed and calculated values of 1/V, rather than V. The equation can be derived from the Michaelis-Menten equation as follows :

$$V = \frac{V_{max}[S]}{K_m + [S]}$$

The Hanes-Woolf plot is clear from the equation, perfect data will yield a straight line of slope $1/V_{max}$, a y-intercept of K_m/V_{max} and an x-intercept of K_m. Like other techniques that linearize the Michaelis-Menten equation, the Hanes-Woolf plot was used historically for rapid determination of the important kinetic parameters K_m, V_{max} and V_{max}/K_m, but it has been superseded by nonlinear regression methods that are significantly more accurate and no longer computationally inaccessible. It remains useful, however, as a means to present data graphically. One drawback of the Hanes-Woolf approach is that neither ordinate nor abscissa represents independent variables: both are dependent on substrate concentration. As a result, the typical measure of goodness of fit, the correlation coefficient R, is not applicable. The Michaelis-Menten kinetics according to the Hanes-Woolf plot was shown in **Figure 3.7**.[82]
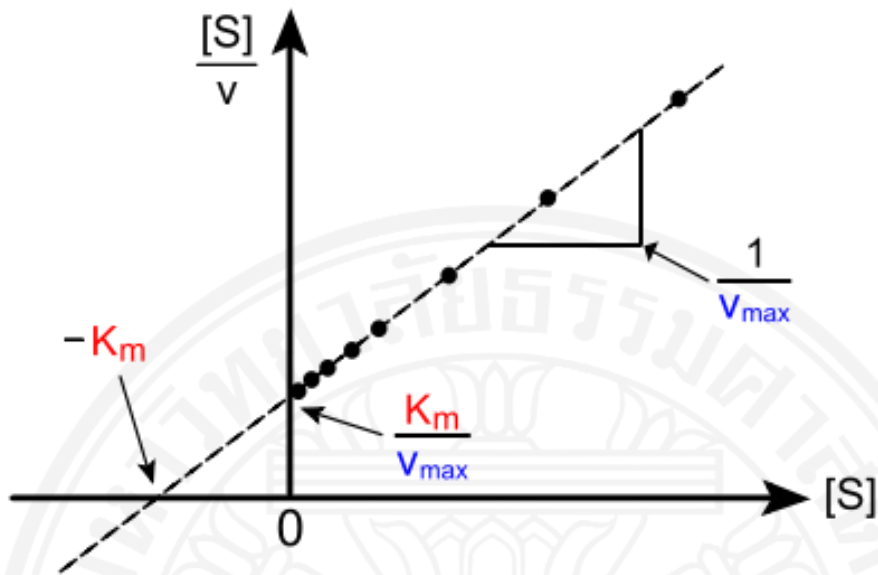
Figure 3.7 The Michaelis-Menten kinetics according to the Hanes-Woolf plot.[85]

3.10 Drug transporters and P-glycoprotein

Membrane transporters can be major determinants of the pharmacokinetics, safety and efficacy profiles of drugs. Transporters are the gatekeepers for cells and organelles, controlling uptake and efflux of crucial compounds such as sugars, amino acids, nucleotides, inorganic ions and drugs. Transporter expression in the intestine and liver, the two major sites affecting how much of a drug will get into the systemic circulation after an oral dose, suggests that factors affecting their function will be important determinants of oral drug pharmacokinetics. Intestinal drug transporters are of increasing interest as evidence emerges about the importance of transporters in affecting pharmacokinetics.[86] The diagram of major drug transporters proteins expressed at the intestinal was shown in **Figure 3.8**.
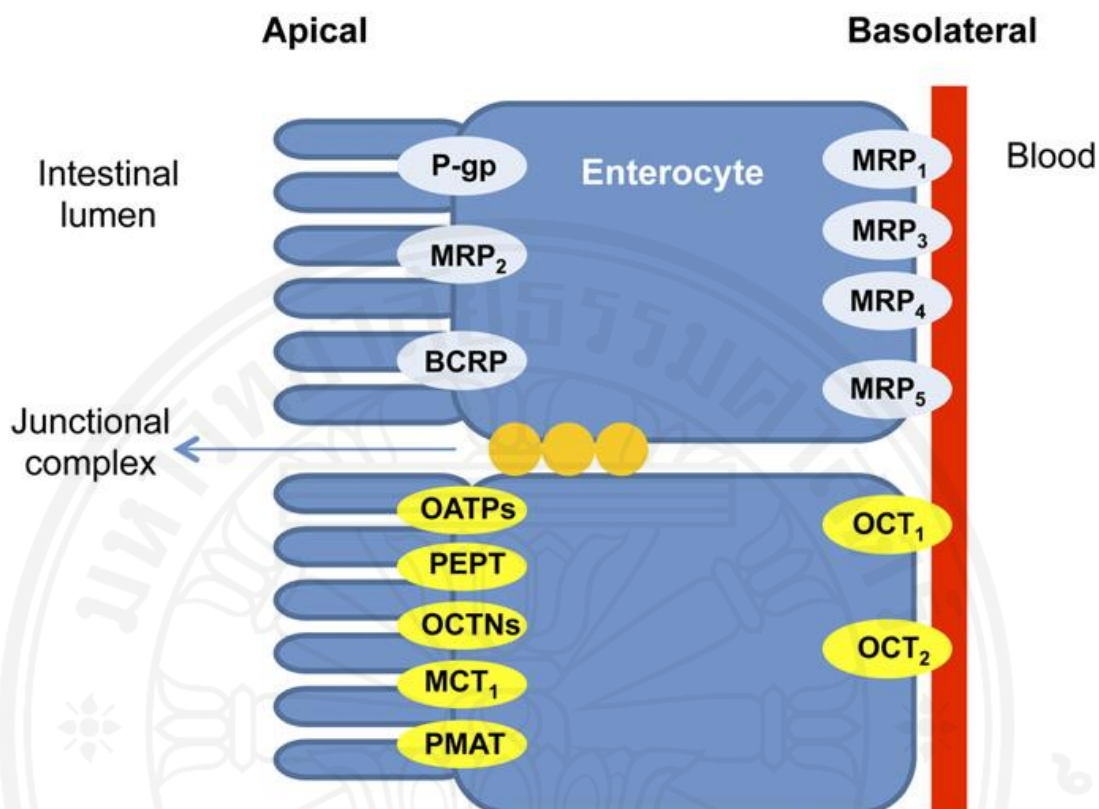
Figure 3.8 Diagram of major drug transporters proteins expressed at the intestinal epithelia including intestinal uptake (yellow) and efflux (light blue) transporters. Multidrug resistance protein (MDR1, P-glycoprotein), multidrug resistance associated protein (MRP), breast cancer resistance protein (BCRP), monocarboxylate transporter protein (MCT), peptide transporter protein (PEPT), organic anion transporting polypeptide (OATP), organic cation transporter (OCT), carnitine/organic cation transporter, (OCTN), and plasma membrane monoamine transporter (PMAT).[86]

Drug transporters may control the access of a drug to metabolizing enzymes. Lipophilic drugs can easily pass through biological membranes, but many hydrophilic drugs need to be transported.[87] Drug molecules may pass through membranes via passive diffusion or via transporter processes. Membrane transport can be divided into facilitated and active mechanisms. Facilitated transport is performed through transporters that allow the passage of solutes (*e.g.*, glucose, amino acids and urea) across membranes down their electrochemical gradients and without energy expense. Active transport in contrast utilizes diverse energy-coupling mechanisms and is performed by active transport systems that create ion gradients across membranes. These latter mechanisms are classified as either primary, secondary or tertiary active transporters. Secondary and tertiary active transporters are driven by an exchange of intracellular ions while the driving force for primary transporters, like ATP-binding cassette transporters, is ATP hydrolysis.[88] Various transporters expressed in the small intestine are involved in the absorption of nutrients or endogenous compounds. Primary active efflux transporters, such as P-glycoprotein (p-gp) encoded by multidrug resistance gene (MDR1/ABCB1), multidrug resistance associated protein 2 (MRP2/ABCC2) or the breast cancer resistance protein (BCRP/ABCG2) are expressed on the brush border membrane of enterocytes and excrete their substrates into the lumen, resulting in a potential limitation of net absorption (**Figure 3.9**). P-gp contributes to the absorption of many drugs because of its broad substrate specificity.[88] Due to the broad substrate specificity of drug transporters, drug-drug interactions involving these transporters are very likely. Recently, both inhibition and induction of transporters have been implicated as one mechanism responsible for certain drug-drug interactions. Humans possess one gene (originally named MDR1 but today also denoted as ABCB1) encoding drug transporting p-gp whereas rodents have two (MDR1a and MDR1b). The combined tissue distribution of these two genes in rodents roughly coincides with that of the single MDR1 in humans, indicating that mdr1a and MDR1b together fulfill the same function as the human MDR1.[89]
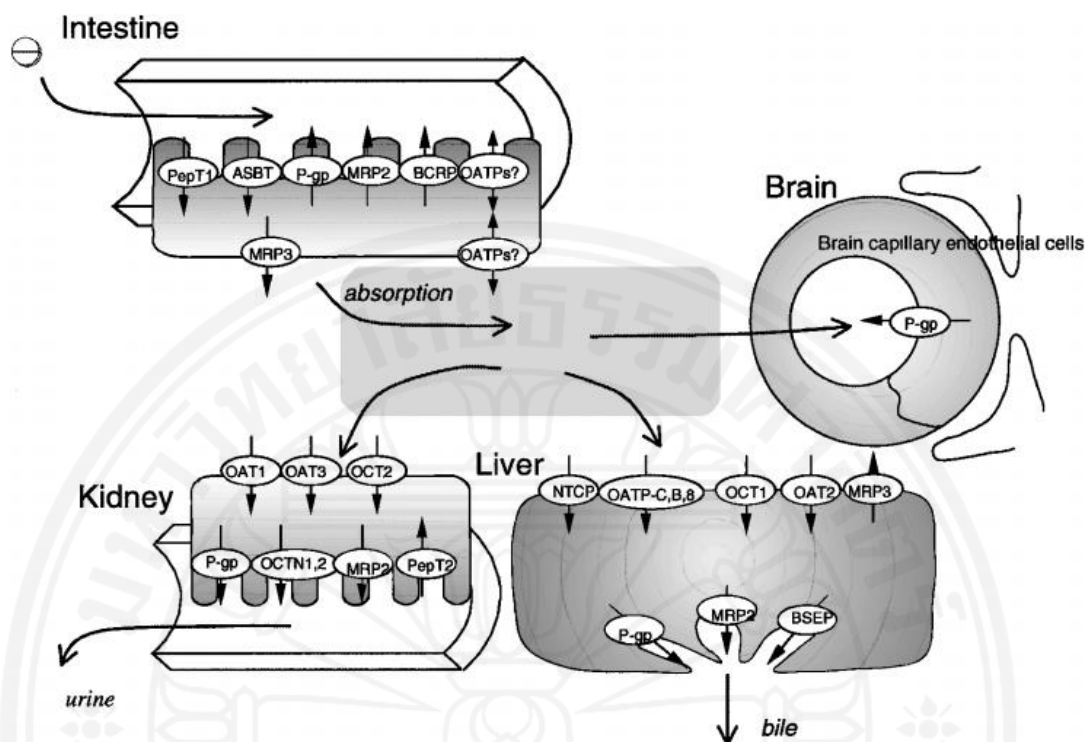
Figure 3.9 Major drug transporters in humans.[88]

The human p-gp is composed of polypeptide approximately 170 kDa molecular weight having 1280 long amino acid glycoprotein and comprising of two analogous fractions of same length in one line, both comprising of six trans-membrane domains and with a flexible linker polypeptide region separates two ATP binding regions (**Figure 3.10**).[90] The 12 transmembrane segments fold together to form a barrel-like structure that traverses the plasma membrane. The two ATP-binding sites are located at the cytoplasmic site, and hydrolysis of ATP provides the energy necessary for drug transport.[90] The exact mechanism of drug transport has not been elucidated yet, but increasing amounts of evidence suggest that p-gp recognizes its substrates in the plasma membrane.[91] p-gp is able to recognize and transport an impressive array of substrates ranging in size from approximately 250 Da (cimetidine) to more than 1850 Da (gramicidin D).[90] These substrates include a wide variety of chemotherapeutic agents of natural origin such as anthracyclines (doxorubicin), vinca alkaloids (vinblastine), epipodophyllotoxins (etoposide), and

taxanes (paclitaxel). P-gp substrates may act as competitive inhibitors of p-gp, *e.g.* the drugs cyclosporine A and verapamil[92], which have been used as p-gp inhibitors since the early eighties. An understanding of the physiological regulation of these transporters is a key to designing strategies for the improvement of therapeutic efficacy of drugs which are their substrates.[93]
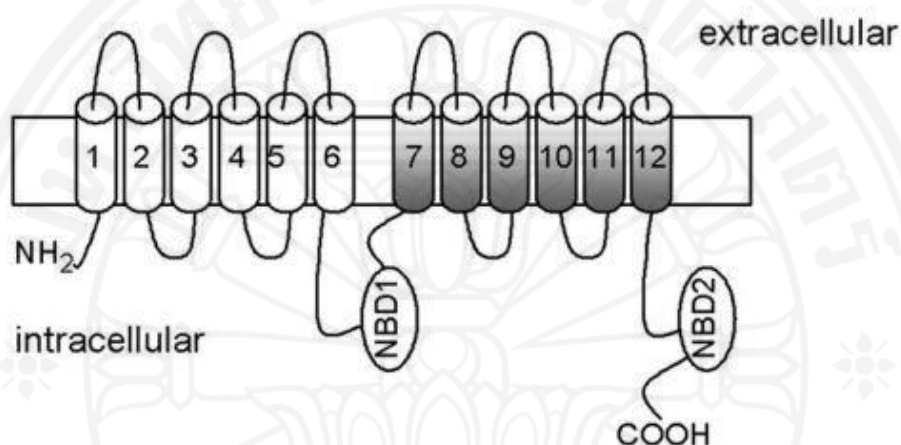
Figure 3.10 Structure of P-glycoprotein efflux pump[94]

Permeability and transportation of the candidate drug compounds across biological membranes are key limiting steps in the absorption of drugs through intestinal lumen to blood circulation. Caco-2 cell monolayer model has been applied successfully as a tool during lead optimization phase in drug discovery, for investigating the transportation of new molecular entities across the biological membranes by various mechanisms, *i.e.*, passive paracellular, transcellular permeability and carrier mediated-process.[95-98] The US FDA recommends Caco-2 cell monolayer model for measuring permeability of drug candidates as part of the bioequivalence waiver process in pre-clinical drug development.[70] Caco-2 cell is an immortalized cell line, originally obtained from a heterogeneous human epithelial colorectal adenocarcinoma cell. It differentiates spontaneously in culture and exhibits structural, morphological (polarized columnar cells on the apical side), and

functional characteristics of mature small intestinal enterocytes with the expression of various drug metabolizing enzymes[99,100] including the efflux transporter P-glycoprotein (multidrug resistance-1 protein: MDR1). P-glycoprotein is located on the brush border membrane of intestinal and colon (apical) cells, as well as endothelial cells of the blood brain barrier, and basolateral membrane of liver cells.[101,102] The expression of the MDR1 in the Caco-2 cells correlates well with expression in normal human jejunum.[103]

3.10.1 *In vitro* evaluation of P-glycoprotein (p-gp, MDR1) substrates and/or inhibitors

There are several *in vitro* methods that can evaluate whether a drug candidate is a substrate or inhibitor of the p-gp efflux transporter. The most commonly used methods are listed in **Table 3.6**. Bi-directional transport methodology is the preferred functional assay used to identify drugs as substrates and/or inhibitors of p-gp. These experiments require the use of known p-gp substrates and inhibitors. The Criteria for preferred *in vitro* p-gp probe substrates including (1) selective for the p-gp transporter, (2) exhibits low to moderate passive membrane permeability (2-30 x 10^{-6} cm/sec), (3) no significant metabolism of the substrate occurs (optional), (4) commercially available (optional), (5) may be used as an *in vivo* p-gp probe substrate (optional).[104] Unfortunately, a p-gp substrate that meets all of the above criteria has not been identified, due to overlapping substrate selectivity between transporter/transporter and transporter/metabolizing enzymes. Acceptable p-gp substrates that meet the majority of the above mentioned criteria are shown in **Table 3.7**. These p-gp substrates serve as positive controls to ensure the cell systems have functional p-gp expression when used for transport experiments.[70]

Table 3.6 *In vitro* methods for identifying whether a drug is a p-gp substrate and/or inhibitor.[104]

Assay Type	Tissues	Parameters	Comments
Bi-Directional Transport	- Caco-2 cells - MDCK-MDR1 cells - LLC-PK1-MDR1cells	- Net drug flux ratio of B to A and A to B	- Directly measure efflux across cell barrier - Evaluation of p-gp transport and inhibition - Allow for localization/ identification of the transporters within the apical or basolateral side of the membrane
Uptake/efflux	- Tumor cells - cDNA transfected cells - oocytes injected with cRNA of transporters	- Inhibition of uptake or efflux ofluorescent probe (Calcein-AM, rhodamine-123)	- Cannot distinguish substrate from Inhibitor - Tends to fail to identify substrate and/or inhibitor with low permeability
ATPase	- Membrane vesicles from tissues or cells expressing p-gp, reconstituted p-gp	- ATPase stimulation assay	- Same comments as uptake/efflux

Table 3.7 Acceptable p-gp substrates.[70]

Drug	Conc. Used (μM)	Ratio**		
		Caco-2	MDR1-MDCK***	MDR1-LLCPK***
Digoxin	0.01-10	4-14	4	4
Loperamide	1-10	2-5		3.4
Quinidine	0.05	3		5
Vinblastine [a]	0.004-10	2-18	> 9 [b]	3
Talinolol	30	26		

* Note that this is not an exhaustive list

** $P_{app, B-A}$ / $P_{app, A-B}$; P_{app} = apparent permeability

*** Data for MDR1-MDCK and MDR1-LLCPK are the ratio observed in transfected cells relative to the ratio observed in respective wild-type cells.

[a] Vinblastine is also a substrate for MRP2 that is constitutively expressed in Caco-2, and wild type MDCK and LL-CPK1 cells.

[b] Data are derived from net B to A flux in the absence of GF120918, a potent p-gp inhibitor, relative to that observed in the presence of GF120918.

3.11 Rodent malaria parasites as models for human malaria

In assessment of antimalarial activities are usually use four rodent Plasmodium species such as *P. berghei*, *P. yoelii*, *P. chabaudi* and *P. vinckei*. They are unlike the human pathogens; there has been no evolutionary adaptation of parasite and laboratory mouse. For this reason, and because the rodent parasites differ in virulence and in the fine details of immune elimination from the host, it has been argued that mouse models are not very relevant to the human disease. However, it is likely that the principles by which erythrocytic stage parasites can be recognized by the immune system and the possible pathological consequences of infection are similar in mice and humans. Clearly, the more similar the models are among themselves, the more likely it is that they will reflect human malaria infections the major rodent parasites that have been used to investigate mechanisms of pathogenesis (including cerebral malaria) and immunity, and also for design of therapeutic drugs. Mouse malaria infections are useful models with which to study the interactions between the host and the erythrocytic stage of the parasite that is an important prerequisite for improving chemotherapy and also for vaccine design. Some of the models such as *P. berghei* (ANKA), *P. vinckei*, and *P. chabaudi chabaudi* that are also allow investigations of malarial disease and immunologically related pathology. In order to gain a better insight into *in vivo* interactions, various murine model systems have been developed. Four rodent Plasmodium species infect inbred mouse strains with varying degrees of morbidity and mortality.[105] Some of these parasites are uniformly lethal in all strains of mice and some are lethal in only some strains of mice (**Table 3.8**) such as *P. berghei* and *P. vinckei* and some strains of *P. yoelii* and *P. chabaudi* cause lethal infections in mice, whereas infections with *P. yoelii*, *P. chabaudi chabaudi*, *P. chabaudi adami,* and *P. vinckei petterei* are cleared after the initial acute parasitemia or after a subsequent low grade chronic parasitemia. The outbred albino mouse inoculated with *P. berghei* is generally considered to be a valid model for the primary and largescale screening of drugs for eventual use against human malaria (**Table 3.9**). Although none of these models

exactly reflects the infection in humans, they provide valuable insight into the mechanisms of immunity and immunopathogenesis in human malaria. *In vivo* antimalarial activity is commonly determined by the peters' 4-day suppressive test against *P. berghei* strain.[106] In recent research, Willcox *et al*. (2004) showed cut-off pointspercent inhibition *in vivo* of antimalarial extracts which can be categorized level of activity (**Table 3.10**).[107]

Rodent malaria parasites are used in many research institutes for studies aiming at the development of new drugs or a vaccine against malaria. The advantages of using laboratory rodents are obvious and include having access to well-characterized animals (*e.g.* inbred lines of mice), which are cheap and easily maintained. This model makes it possible to envisage studies that would otherwise be difficult, including the study of genetic factors in susceptibility or the use of specifically immunologically-deprived hosts. In addition, it is possible to work with clones of well-characterized malaria parasites and experiment with a range of different inoculation protocols.

The advantages of studying human malaria parasites, rodent parasites are recognised as valuable model parasites for the investigation of the developmental biology of malaria parasites, parasite-host interactions, vaccine development and drug testing.[108]

The basic biology of rodent and human parasites is similar.

- The genome organisation and genetics is conserved between rodent and human parasites
- Housekeeping genes and biochemical processes are conserved between rodent and human parasites
- The molecular basis of drug-sensitivity and resistance show similar characteristics in rodent and human parasites
- The structure and function of vaccine candidate target antigens are conserved between rodent and human parasites
- The manipulation of the complete lifecycle of rodent parasites, including mosquito infections is simple and safe

- *In vitro* culture techniques for large-scale production and manipulation of different life cycle stages are available. For example, *in vitro* cultures of liver and mosquito stages provide tools to investigate the less accessible parts of the life cycle of the human parasites

- Methodologies for genetic modification are available

- Rodent parasites allow *in vivo* investigations of parasite-host interactions and in vivo drug testing

- Rodent hosts with extensively characterised genetic backgrounds and transgenic lines are valuable and available tools for immunological studies

Although of rodent malaria parasites have many species, only four have been adapted to laboratory mice and have been extensively used as models:

- *P. berghei*

- *P. yoelii*

- *P. vinckei*

- *P. chabaudi*

These four species include 10 subspecies (each with their characteristic isoenzyme forms) and over 70 different laboratory strains. All these parasites have a 24 h erythrocytic schizogony; two have a predilection for reticulocytes (*P. berghei* and *P. yoelii*), while the other two develop in adult erythrocytes.[108]

Plasmodium berghei

P. berghei is an excellent model for research on the developmental biology of malaria parasites, because of the availability of[108]

- Technologies for *in vitro* cultivation and large scale production and purification of the different life cycle stages

- Knowledge on the genome sequence and organization

- Methodologies for genetic modification of the parasite

- Well characterised clones and genetically modified mutant lines, including transgenic parasites expressing reporter genes such as Green Fluorescent Protein and Luciferase

- The wide availability of susceptible, genetically defined or knockout mouse strains

- An extensive range of well-characterized clones of *P. berghei*, some with important biological phenotypes, *e.g.,* an inability to produce mature sexual-stage parasites

- The facility to make and analyze *in vivo*-defined gene knockouts in this parasite species currently surpasses that in other Plasmodium species (*e.g., P. falciparum* and *P. knowlesi*)

- The parasite can be transmitted through major vector species from Africa, India, and South America

- Infections can readily be synchronized

- All the life cycle stages can be grown *in vitro*, thus permitting direct comparison of *in vivo* and *in vitro* data

- The genome is now being analyzed and expressed sequence tags (EST) and gene sequence survey (GSS) databases are under construction

The other rodent parasites are invaluable in different areas of malaria research. For example, *P. chabaudi* is recognised as a useful model for investigations of mechanisms of drug resistance and antigenic variation. This parasite shows antigenic variation during long lasting, non-lethal, infections in laboratory rodents. In contrast, *P. berghei* infections are usually rapidly lethal to laboratory rodents which hamper studies on the *in vivo* generation and selection of antigenic variants. Another example is *P. yoelii*, which is extensively used in studies on the biology of liver stage and blood stage antigens and their role in immunity and vaccine development.[108]

P. berghei is one of the many species of malaria parasites that infect mammals other than humans. *P. berghei* is one of the four species that have been described in murine rodents of West Africa. The rodent parasites are not of direct practical concern to man or his domestic animals. The interest of rodent malaria parasites is that they are practical models for the experimental study of mammalian malaria. These parasites have proved to be analogous to the malarias of man and other primates in most essential aspects of structure, physiology and life cycle.[108,109]
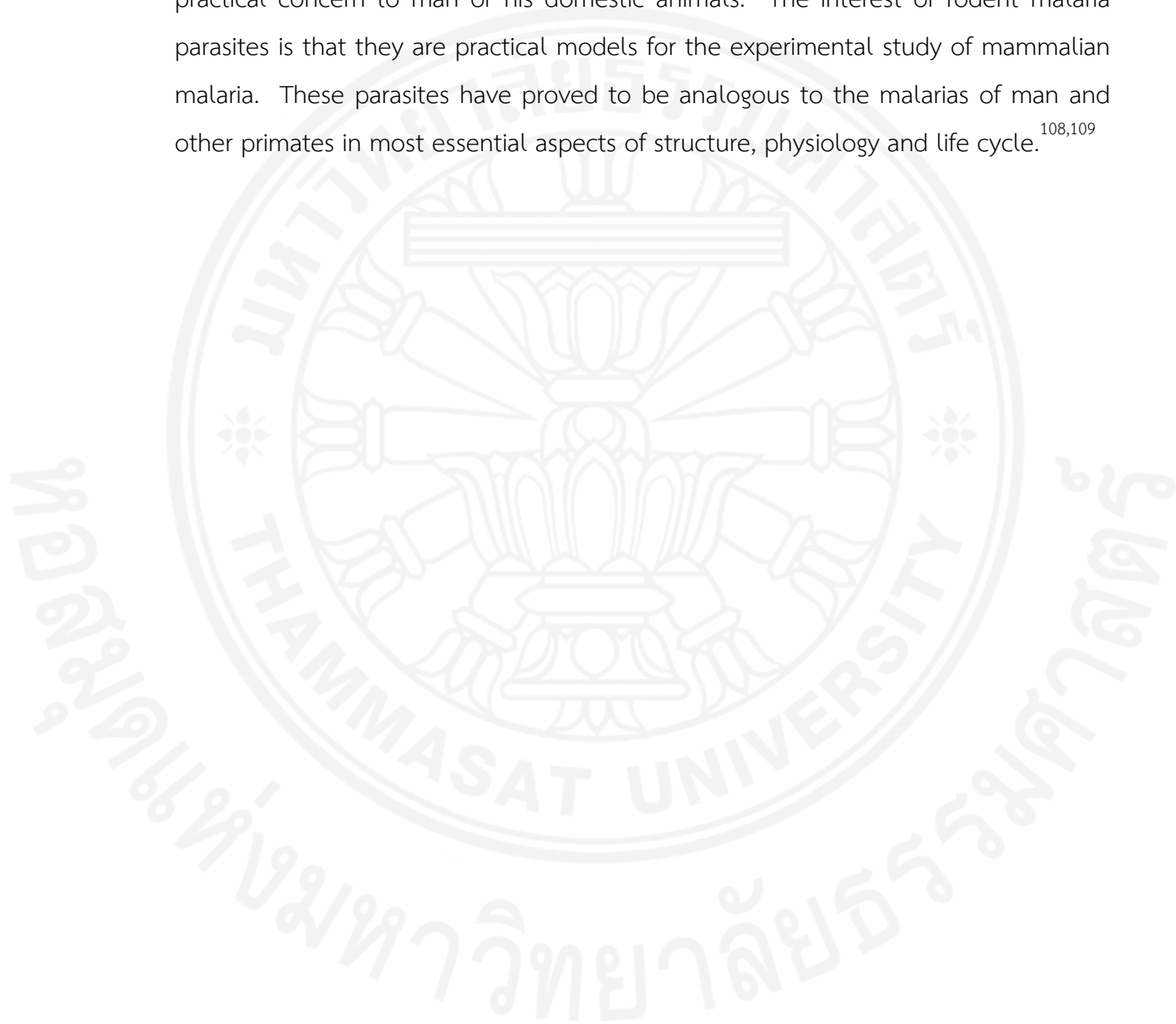
Table 3.8 Lists of the major rodent parasites that have been used to investigate mechanisms of pathogenesis (including cerebral malaria) and immunity, and also for design of therapeutic drugs.[110]

Plasmodium	Strains/ clones	Mouse strain	RBC infected	Lethal infection	Experimental study
berghei	ANKA	CBA/T6	Mature RBC and reticulocytes	Yes: d 6-8	Pathogenesis CM
		BALB/c			
		C57BL/6			
		DBA/2J	Mature RBC and reticulocytes	Yes: d 15-22	Resolving CM model
	K173	CBA/T6	Mature RBC and reticulocytes	Yes: d 15-22	Non CM control for CM study
		BALB/c			
		DBA/2J			
		C57BL/6	Mature RBC and reticulocytes	Yes: d 6-8	Pathogenesis CM
yoelii	17X	Swiss	Reticulocyte	Yes: d 7-9	Pathogenesis CM
		BALB/c			
		CBA/Ca	Reticulocyte	No	Immune mechanisms Pathogenesis
		BALB/c,			
	YM (lethal)	CBA/T6,	Mature RBC and reticulocytes	Yes: d 7-8	Vaccine
		BALB/c			
		C57BL/6			
		DBA/2J			
		Swiss			
vinkei vinkei		BALB/c	Mature RBC and reticulocytes	Yes: d 8	Chemotherapy Immune mechanisms Pathogenesis
chabaudi chabaudi	AS	C57BL/6	Mature RBC	No: peak d 8-10	Immune mechanisms Pathogenesis
		NIH,			
		CBA/Ca			
		BALB/c			
		A/J DBA/2J	Mature RBC	Yes; d 9	
chabaudi adami	CB	CBA/Ca	Mature RBC or all	Yes: in 20-50%, after d 8	Immune mechanisms
	556 KA	BALB/c	Mature RBC	No: peak d 7-11	Immune mechanisms Pathogenesis
vinckei petteri		C3H			
		C57BL/6			
		C57BL/6	Mature RBC	No: peak d 10	Chemotherapy
		BABL/c			Immune mechanisms

Table 3.9 Characteristics of rodent malaria infections.[111]

| | *Plasmodium species* | | | |
	P. berghei	*P. yoelii*	*P. chabaudi*	*P.vinckei*
First isolated	1948 (Zaire)	1965 (CAR)	1965 (CAR)	1952 (Zaire)
Cycle	Asynchronous	Asynchronous	Synchronous	Synchronous
Periodicity	22-25 h	22-25 h	24 h	24 h
Host cells	Reticulocytes	Reticulocytes	Mature RBC	Mature RBC
Merozoite per schizont	12 to 18	12 to 18	6 to 8	6 to 12
Primary use	Drug screening	Liver stage biology and vaccine studies antigenic variation	Mechanisms of drug resistance	

Table 3.10 The inhibitory activity proposed for *in vivo* activity of antimalarial extracts at a fixed dose of 250 mg/kg/day.[107]

% Inhibition	Level of activity
100-90	Very good
90-50	Good to moderate
50-10	Moderate to weak
0	In active

3.12 The Single-Photon Emission Computed Tomography/Computed Tomography (SPECT/CT) systems

A Single Photon Emission Computed Tomography/Computed Tomography (SPECT/CT) scan is a technology used in nuclear medicine by injection with a radiopharmaceutical which will emit gamma rays that demonstrate how well blood is flowing to tissues and organs in the body. It has enabled the evaluation of disease processes based on functional and metabolic information of organs and cells. Integration of X ray computed tomography (CT) into SPECT has recently emerged as a brilliant diagnostic tool in medical imaging, where anatomical details may delineate functional and metabolic information. Combined SPECT/CT imaging provides sequentially functional information from SPECT and the anatomic information from CT, obtained during a single examination. CT data are also used for rapid and optimal attenuation correction of the single photon emission data.[112,113] It is a sensitive technique that can be used to measure drug pharmacokinetics and pharmacodynamics noninvasively in target tissues that uses a special gamma camera picks up signals from the tracer as it moves around body. The tracer's signals are converted into images by a computer to form a three-dimensional (3D).[114,115] Furthermore, SPECT/CT scan also shows how organs and tissues are working.[116] This is different than magnetic resonance imaging (MRI) and computed tomography (CT), which show the structure of and blood flow to and from organs. There is a great need in medicine for methods to non-invasively image the interior of the human or animal body.[117] Emission tomography (ET) is the generic term for all methods that are based on the detection of radiation emitted from radioactive material within the body. The two main representatives of ET are single photon emission computed tomography (SPECT) and positron emission tomography (PET). SPECT is a method which works with virtually every emitting substance. As shown in **Figure 3.11**, it uses a collimator in front of a detector to determine the direction of an incoming photon. This leads to a cone on which the decay must have taken place (**Figure 3.11b**). By

rotating the detector and using appropriate algorithms, it is possible to reconstruct the three dimensional distribution of the radioactive emitter.
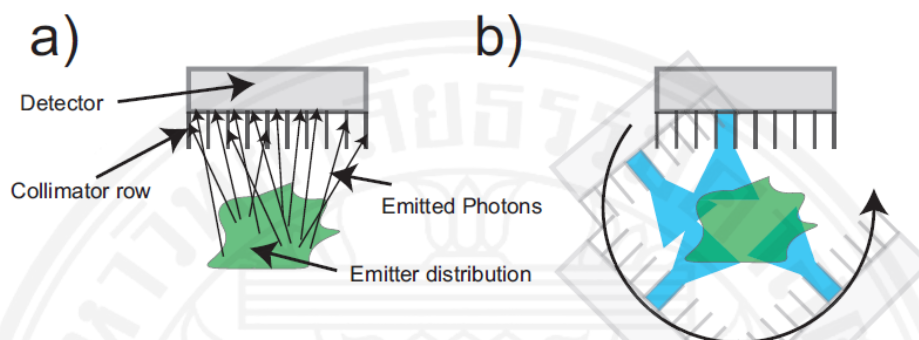
Figure 3.11 The principle of single photon computed emission tomography (SPECT).[117]

PET and SPECT technologies, when compared to each other, have many differences; for instance PET radiopharmaceuticals emit positrons (two rays simultaneously), whereas SPECT radiopharmaceuticals emit gamma radiations, as PET has two electrons. At the same time, PET requires a higher number of cameras to capture them, thereby increasing the cost. Besides, PET radiopharmaceuticals require a cyclotron for production, escalating the cost further. On the other hand, the quality of image generated through PET is far better than that through SPECT.[118] Comparison of molecular imaging technologies between high resolution SPECT and PET are showed in **Table 3.11**.

Table 3.11 Comparison of molecular imaging technologies between high resolution
SPECT and PET.[118]

SPECT	PET
Emits gamma radiations	Emits position
Lower resolution	Higher resolution
Less captal intensive scanner	Costlier scanner
Longer lived radioisotopes	Limited halflife of radiopharmaceuticals

The radioisotopes most widely used in SPECT to label tracers are
technetium-99m, iodine-131, iridium-192, phosphorus-32, samarium-153, chromium-
51, Yttrium-90 and molybdenum-99 (**Table 3.12**). These radioactive forms of natural
elements and will pass safely through the body. Technetium-99m (^{99m}Tc) is the
radioisotope most widely used in medicine. It can benefit for diagnose various heart,
lung, liver, kidney and thyroid conditions and some cancers. It is an isotope of the
artificially produced element technetium and it has almost ideal characteristics for a
nuclear medicine scan. ^{99m}Tc was similar to iodine and concentrates in the thyroid,
salivary glands, brain, blood pool, urinary bladder and stomach and may be used to
scan any of these organs. The stomach receives the majority of the dose and
contains ~25% of the administered dose after 4 h. Physical half-life of Technetium-
99m was 6 h.[119] Because the plasma half-life of plumbagin is 1.8 h to 2.8 h, it is
theoretically quite compatible with the physical half-life of 6 h of Technetium-
99m.[120]

Table 3.12 A list of radioisotope most widely used and their half-lives.[121]

Radioisotope	Half-life	Use
Chromium-51	27.7 days	Used to label red blood cells and quantify gastro-intestinal protein loss.
Iodine-131	8.02 days	Used to diagnose and treat various diseases associated with the human thyroid.
Iridium-192	73.83 days	Supplied in wire form for use as an internal radiotherapy source for certain cancers, including those of the head and breast.
Molybdenum-99	66 hours	Used as the 'parent' in a generator to produce technetium-99m, the most widely used radioisotope in nuclear medicine
Phosphorus-32	14.28 days	Used in the treatment of excess red blood cells
Samarium-153	46.7 hours	Used to reduce the pain associated with bony metastases of primary tumours
Technetium-99m	6.01 hours	Used to image the brain, thyroid, lungs, liver, spleen, kidney, gall bladder, skeleton, blood pool, bone marrow, heart blood pool, salivary and lacrimal glands, and to detect infection.
Yttrium-90	64 hours	Used for liver cancer therapy

CHAPTER 4

MATERIALS AND METHODS

4.1 Antimalarial activity of plumbagin *in vitro* and in animal models

The aim of this part was to investigate *in vitro* antimalarial activity of plumbagin against both chloroquine-resistant K1 and chloroquine-sensitive 3D7 clones of *P. falciparum*, toxicity (acute and subacute) and including antimalarial activity in mice model

4.1.1 Chemicals and reagents

Plumbagin (purity 98.2%) was obtained from Apin chemicals Co. Ltd. (Oxford, UK). Tween-80, sodium bicarbonate and chloroquine diphosphate were obtained from Sigma-Aldrich (St. Louis, MO, USA). RPMI 1640 powder containing L-glutamine, streptomycin/penicillin, and HEPES were obtained from Gibco BRL Life Technologies (Grand Island, NY, USA). Gentamicin was obtained from Invitrogen Life Technologies Inc. (Carlsbad, CA, USA).

4.1.2 *In vitro* experiment

4.1.2.1 Culture medium

The stock culture medium was prepared by dissolving 10.43 g of RPMI 1640 powder containing L-glutamine and 2.0 g of sodium bicarbonate in 1 liter of distilled water. The medium was sterilized by filtering through a 0.2 μm acrylic filter (Corning, NY, USA). After that, the medium was incubated at 37°C for 24 h in order to check for contamination. In case of the contamination, the medium was an increase of the turbidity and a color change from pink to yellow. The stock medium was stored at 4°C until use.

Complete culture medium was prepared by adding 5 ml of a 1 M pre-sterilized HEPES and 20 ml of pooled human B or AB serum into 200 ml of the stock medium. Contamination was rechecked by incubating the medium at 37°C for 24 h. Unused complete medium was discarded after one week to avoid the effect of medium deterioration.

4.1.2.2 Preparation of serum and packed red blood cells (PRBCs) for malaria parasite culture

The human AB or B serum and whole blood group O of human in an anticoagulant CPD-adenine containing bag was tested for HIV and hepatitis B antibodies. Packed red blood cells (PRBCs) were prepared by centrifugation whole blood with incomplete medium at 2,000 $\times$ g for 10 min for three times. The packed red blood cells were stored at 4ºC for up to one week and the serum was stored at -20ºC until use.

4.1.2.3 *In vitro* cultivation of malaria parasite

Blood stages of the laboratory clones chloroquine resistant (K1) and chloroquine-sensitive (3D7) *P. falciparum* were cultured *in vitro* according to the method of Trager and Jensens.[122] All culture steps were performed using aseptic technique in the NuAire laminar flow class II safety cabinet. All glassware was autoclaved at 121ºC (15 atmosphere) for at least 15 min. Malaria parasite was maintained in continuous culture with human packed red blood cells (blood group O$^+$) in RPMI 1640 medium supplemented with 10% human AB$^+$ serum, 25 mM N-2-hydroxyethylpiperazine-N-2-ethanesulfonic acid (HEPES), 25 mM sodium bicarbonate, and gentamycin sulfate (60 µg/ml, pH 7.2). The culture was incubated at 37ºC in an atmosphere consisting of 90% N_2, 5% O_2, and 5% CO_2. Parasite culture was synchronized to the ring stage by treatment with 5% (w/v) D-sorbitol.[123] Parasites at the ring stage are impermeable to osmotic sorbitol solution. Other stage parasites are more permeable to sorbitol, causing them to swell and lyse. Starting from malaria culture with a high percentage of ring stage was transferred to centrifuge tube and centrifuge at 2,000 $\times$ g for 5 min. The supernatant was removed and the packed red blood cells were resuspended in 5 volumes of 5% (w/v) sorbitol. The suspension was incubated at room temperature for 20 min with the occasional shaking and centrifuged at 2,000 $\times$ g for 5 min, respectively. After that, the supernatant was discarded and the packed red blood cells were washed two time with RPMI medium before continuous culture for 48 h in order to assessment of *in vitro* antimalarial activity.

4.1.2.4 Assessment *in vitro* antimalarial activity of plumbagin

Antimalarial activity of plumbagin was investigated using SYBR Green I assay.[123,124] Highly synchronous ring stage parasite was used in each assay. An aliquot of parasite inoculum (50 µl) with 2% parasitaemia and 1% haematocrit was added into each well of microtiter plate. Plumbagin was dissolved in DMSO and diluted with RPMI 1640 to final concentration of DMSO<1%. Plumbagin (50 µl) was added to the malaria culture at eight final concentrations of 210, 420, 840, 1,680, 3,360, 6,720, 13,440, and 26,880 nM. Chloroquine (3.89-498.15 nM) and artesunate (0.39-50.00 nM) were used as standard antimalarial drugs. The microtitre plate was covered incubated a 37ºC with 5% CO_2 for 48 h. Following 48 h incubation, packed red blood cells were hemolyzed by fluorescent hemolysis reagent (1 ml lysis buffer blend with 0.1 µl SYBR Green I) 100 µl per well and then incubated in dark at room temperature for 1 h. After that, the plate was measured of parasites' survival by plate reader (Varioskan Thermo, Massachusetts, USA) with excitation and emission wavelengths of 485 and 530 nm, respectively. The fluorescent was intercalated in the nucleic acid of malarial DNA. The experiment was repeated three times. IC_{50} value (drug concentration that inhibits the parasite growth by 50%) was used as an indicator of antimalarial activity and was determined from a logdose-response curve plotted using the Calcusyn™ version 1.1 (BioSoft, Cambridge, UK).

4.1.3 *In vivo* experiments

4.1.3.1 Animals

ICR (Imprinting Control Region) mice (5-7 weeks of age, weighting 20-40 g) of both sexes were used in the study. All were obtained from the National Laboratory Animal Centre, Thailand. Animal experiments were carried out in accordance with the OECD Guideline for chemicals.[125] The animals were housed under standard conditions and fed with a stock diet and water ad labitum. Approval of the study protocol was obtained from the Ethics Committee for Animal Research, Thammasat University, Thailand.

4.1.3.2 Toxicity tests

Plumbagin was weighted and resuspended with 20% Tween-80 to obtain the desired concentrations. ICR mice were fasting 2 h before feeding with a single oral dose of plumbagin. Animals were divided into eight groups of six (3 males and 3 females for each group) for the acute toxicity and subacute toxicity (**Table 4.1**). For the acute toxicity test, mice in each group were fed with plumbagin at a single oral dose of 500, 200 and 100 mg/kg body weight; control group received a single oral dose of 20% Tween-80 (1 ml). For the subacute toxicity test, mice in each group were fed with plumbagin at a daily oral dose of 100, 50 and 25 mg/kg body weight for 28 days; control group received a daily oral dose 1 ml of 20% Tween-80 for 28 days.[126,127] General behavior of each mouse was observed continuously for 1 h after each dose, intermittently every 4 h, and thereafter over a period of 24 h.[128] Animals were observed for up to 14 days for the acute toxicity test and 28 days for the subacute toxicity test for any sign of toxicity (behavioral change related to central nervous, cardiovascular and gastrointestinal systems), body weight change and water and food consumption. At the end of the observational period, all animals were sacrificed under ether anesthesia and vital organs (heart, lung, liver, spleen and kidney) were removed from all animals for gross and histopathological examination.

4.1.4 Histopathology

The vital organs (heart, lung, liver, spleen and kidney) from animal were washed with 0.85% normal saline and fixed by using 10% formalin (37% formaldehyde in DW) with 10 fold volume of the organs. The fixed organs were preserved in 10% formalin until performed tissue processing.

4.1.4.1 Tissue processing

The fixed organs were cut into cross sections by microtome. Tissue sections were processed by using STP120 Microm model STP 20-3 automate (MM France, Francheville, France). After that, the processing step was strating by soaking tissues sections in 95% ethanol and absolute ethanol, respectively

in order to remove water. To remove alcohol residue, tissue sections were soaked in xylene. Finally, xylene in tissues sections was replaced by paraffin wax.

4.1.4.2 Tissue embedding, sectioning and staining

The embedding step was performed by using Embedding Microm model EC 350 automate (Dotmed, Walldrof, Germany). The heating paraffin and tissues were put into the cooling molds. Then, hardened blocks containing the tissue samples were sectioned by Leica Microsystms model RM212S (Leica Microsystems Inc., Richmond, Germany). After that, the tissue slides were deparaffinized by heating at 80 °C and using xylene solvent. In order to remove water from tissue, alcohol which higher concentration than water was used. The tissue slides were stained with hematoxylin dye for nuclei of cell and eosin dye for cell cytoplasm

4.1.5 Assessment of antimalarial activity of plumbagin in *P. berghei-*infected mouse model (4-day suppressive test)

The *in vivo* antimalarial activity of plumbagin was evaluated using a 4-day suppressive test in *P. berghei*-infected mouse model.[106] *P. berghei* (ANKA) strain used in the experiment was obtained from the National Center for Genetic Engineering and Biotechnology (BIOTEC), Thailand. The parasite had been maintained by serial blood passage in mice, and blood stage stored at −196°C until use. ICR mice were divided into five groups (3 males and 3 females for each group) (**Table 4.2**). The donor mice were infected with 200 μl of *P. berghei* parasite inoculum. The parasitized blood of each donor mouse was collected from the tail vein and diluted with 0.9% sodium chloride. Mice were infected with saline suspension of 1×10^7 parasitized erythrocytes (0.2 ml) by intraperitoneal injection (Day 0). Four hours after infection, animals were treated with plumbagin at oral daily doses of 1, 10, or 25 mg/kg body weight of plumbagin for four consecutive days (test group 1, 2, and 3, respectively). Positive and negative control groups were fed with the antimalarial chloroquine at oral daily doses of 10 mg/kg body weight of plumbagin and 20% Tween-80, respectively. On day 4 (96 h post infection), parasitaemia of individual mouse was determined under light microscope by examination of giemsa-stained

thin blood smears prepared from mouse tail blood.[129] The mean parasitaemia in each group of mice was used to calculate the % suppression for each dose using the formula:

$$\% \text{ Suppression} = \frac{\text{Parasitaemia of negative control - Parasitaemia of test}}{\text{Parasitaemia of negative control}} \times 100$$

The antimalarial activity of plumbagin was determined from the ratio of percentage of parasite reduction in treated and negative control groups.[130] Results are expressed as median (range) values. Comparison of difference in quantitative variables between more than two and two groups was performed using Kruskal Wallis and Mann–Whitney U tests (SPSS version 16.0, SPSS Inc., CO, USA). Statistical significance level was set at $\alpha < 0.05$ for all tests.

Table 4.1 Allocation of mice into eight groups of six mice each (3 males and 3 females for each group) for assessment of toxicity

	Test group
Acute toxicity	Control (20% Tween-80)
	Plumbagin: 500 mg/kg body weight
	Plumbagin: 200 mg/kg body weight
	Plumbagin: 100 mg/kg body weight
Subacute toxicity	Control (20% Tween-80)
	Plumbagin: 100 mg/kg body weight
	Plumbagin: 50 mg/kg body weight
	Plumbagin: 25 mg/kg body weight

Table 4.2 Allocation of mice into five groups of six mice each (3 males and 3 females for each group) for assessment of antimalarial activity

Group	Treated
Group 1 (negative control)	Mice were received 20% Tween-80 (1 ml)
Group 2 (positive control)	Mice were received chloroquine at a single oral dose of 10 mg/kg body weight/day
Group 3 (test)	Mice were received the plumbagin at a single oral dose of 1 mg/kg body weight/day
Group 4 (test)	Mice were received the plumbagin at a single oral dose of 10 mg/kg body weight /day
Group 5 (test)	Mice were received the plumbagin at a single oral dose of 25 mg/kg body weight /day

4.2 Permeability of plumbagin in caco-2 cell monolayers and their effects on the P-glycoprotein

The aim of this part was to investigate the permeability of plumbagin through Caco-2 cell monolayers. In addition, the effect of plumbagin on MDR-1 mRNA expression and function of the transport protein P-glycoprotein in the Caco-2 cell monolayers was also investigated.

4.2.1 Chemicals

The authentic plumbagin (purity 98.2%) was obtained from Apin chemicals Co. Ltd. (Oxford, UK). Verapamil, rhodamine 123 (R123), dimethylsulfoxide (DMSO), and 3-(4,5-dimethylthiazolyl-2)-2,5-diphenyltetrazolium bromide (MTT) were purchased from Sigma Chemical Co. Ltd. (Saint Louis, MO, USA). Triton X100 was purchased from Bio-Rad Laboratories Inc. (Hercules, CA, USA). Minimum Essential Medium (MEM) powder containing Earle's salts, L-glutamine, non-essential amino acids, antibiotic-antimycotic 100x, fetal bovine serum, 0.25% trypsin-EDTA solution and N-2-Hydroxyethylpiperazine-N'-2-ethanesulfolic acid (HEPES) were obtained from Gibco BRL Life Technologies (Grand Island, NY, USA). TRIzolTM reagent, SuperScript™ III Reverse Transcriptase kit, Hanks' balanced salt solution (HBSS) and SYBR® Green Real-Time PCR Master Mixes were purchased from Invitrogen Life Technologies Inc. (Carlsbad, CA, USA). RQ1 RNase-Free DNase was purchased from Promega (Mannheim, Germany). Cell culture flasks and 24-transwell plates were obtained from Coring Incorporated Co. Ltd. (NY, USA). Caco-2 cell was obtained from the American Type Culture Collection (Rockville, MD). Millicell-ERS volt-ohm meter was purchased from Millipore (Temecular, CA, USA). All solvents were of LC/MS grade and all chemicals were of analytical grade.

4.2.2 Caco-2 cell culture

Caco-2 cells were cultured in MEM medium with 1 mM sodium pyruvate, 20% fetal bovine serum, and 100 U/ml antibiotic–antimycotic. Cells were grown in a humidified atmosphere of 5% CO_2 at 37°C. Caco-2 cells were harvested at approximately 80% confluence using 0.25% trypsin–EDTA solution and mixed with

complete MEM medium. The cells were separated through centrifugation at $100 \times g$ for 5 min.

4.2.3 *In vitro* cytotoxicity of plumbagin

Cytotoxic activity of plumbagin on Caco-2 cells was performed using MTT assay according to the method described by Wang *et al.* with modification[131] to select the concentrations that were not toxic to the cells. After harvesting, Caco-2 cells were cultured in 96-well plates at a seeding cell suspension density of 1.5×10^4 cells/well in a final volume 100 µl for 48 h. Plumbagin was dissolved in 50% DMSO, diluted with complete MEM medium to different concentrations and the final concentrations of DMSO were less than 0.1% (v/v). Varying concentrations of plumbagin (at final concentrations 0-125 and 0-62.5 µM for a 4- and 48-h exposure experiment, respectively) were added with a total volume of 200 µl. DMSO in complete MEM medium (0.1%, v/v), Triton X100 in MEM and complete MEM medium were used as vehicle control, positive control and negative control, respectively. The plates were incubated in an atmosphere of 5% CO_2 (Thermo Electron Corporation, Vantaa, Finland). Following 4 or 48 h incubation, MTT reagent (20 µl, 5 mg/ml) in 0.1 mM PBS pH 7.4 was added to each well. The plates were incubated at 37°C for another 4 h and the medium was removed. The intracellular reduced product formed in the cells-formazan (dark purple), was solubilized with 100 µl DMSO and quantified at the absorbance at 590 nm on a Micro-plate Multi-detection Instrument (Varioskan Flash, Thermo Electron Corporation, Vantaa, Finland).[131] Percentage of cell viability was calculated based on the absorbance measured following exposure to plumbagin relative to the absorbance of cells exposed to the negative control.

4.2.4 Transportation of plumbagin across Caco-2 cell monolayers

Caco-2 cells (passage 30-40) were seeded at $3.2\text{-}3.6 \times 10^4$ cells/insert in 24-transwell permeable supports with 0.4 µM polyester membrane, 6.5 mm insert (Corning cat. No. 3470) and grown in a humidified chamber (37°C, 5% CO_2). The culture medium was changed every 2-3 days (0.2 ml for apical side, and 0.6 ml for basolateral side). The cells were used for transport experiments after 21 days post

seeding. The integrity of the monolayer cells was determined by measuring Trans Epithelial Electrical Resistance (TEER) across the monolayers using Millicell-ERS Volt-Ohm Meter (Millipore, Temecular, CA, USA). TEER was measured at six time points with two points at the last day and the day before (*i.e.* on days 4, 7, 10, 14, 20, and 21). The TEER value was calculated according to the following equation:

$$\text{TEER } (\Omega.\text{cm}^2) = (R_{total} - \text{filter}_{w/o\ cells}) * A$$

where R_{total} is the resistance measured (Ω), R_{filter} w/o cells (Ω) is the resistance of inserts alone and A is the surface area (cm^2). Cell integrity was also investigated through monitoring of leakage of the marker compound Lucifer yellow across the monolayers. The transport mechanism of this marker compound is mainly through paracellular diffusion with only limited permeability across monolayer cells. Lucifer yellow (0.2 ml, 100 µg/ml in transport buffer) was added into apical side, whereas transport buffer (0.6 ml) was added into basolateral side. The plates were incubated at 37°C for 90 min under gentle shaking (100 rpm).[131-133] Aliquots of the samples (150 µl) were collected and Lucifer yellow was measured using by Micro-plate Multi-detection Instrument. The excitation and emission wavelengths were set at 428 and 540 nm, respectively.[134,135] Calibration curve of Lucifer yellow was constructed using linear regression analysis of the Relative Fluorescence Units (RFU) versus concentrations of Lucifer yellow. HBSS (w/o phenol red) with 10 mM HEPES (pH 7.4) served as a blank. The transport rate (V) and P_{app} and efflux ratio were calculated as:

$$V \text{ (nmole.cm}^{-2}.\text{sec}^{-1}) \quad = \quad \frac{dQ/dt}{A}$$

$$P_{app} \text{ (cm/s)} \quad = \quad \frac{dQ/dt}{A*C_0}$$

$$\text{Efflux ratio} \quad = \quad \frac{P_{app(B-A)}}{P_{app(A-B)}}$$

where dQ/dt is the flux of drug across the cell monolayer (nmole/s), C_0 is the initial concentration in the donor compartment (nM), and A is the surface area of the cell monolayer (cm^2).

Acceptable TEER value was>400 $\Omega.cm^2$ and acceptable apparent permeability coefficient (P_{app}) for Lucifer yellow was<0.5×10^{-6} cm/s.[131,136]

Before starting the experiment, the inserts were washed twice and equilibrated for 30 min with transport buffer (HBSS containing 10 mM HEPES, pH 7.4). Stock solution of plumbagin was prepared in DMSO and diluted to the desired final concentrations with transport buffer. Transportation of plumbagin (2, 4 and 8 µM) across Caco-2 cells was measured by adding the solution on either the apical (0.2 ml) or the basolateral (0.6 ml) side of the inserts. The corresponding volumes of transport buffer were added in the receiving compartment. The investigation was performed either in the apical to basolateral (A to B) or the basolateral to apical (B to A) direction. The plates were incubated at 37°C with gentle shaking (100 rpm) for 60 min. Aliquots of 150 µl were collected from both the apical and basolateral sides and immediately refilled with an equal volume of transport buffer. Samples were stored at -80°C until analysis. The plates were washed and equilibrated and the permeability of Lucifer yellow was measured as described above. Concentrations of the plumbagin in the transport buffer were measured using high-performance liquid chromatography with tendem mass spectrometric (LC-MS/MS).

4.2.5 Effect of plumbagin on rhodamine 123 transport

Rhodamine 123 (R123) is a chemical compound and dyes fluoresce which is the substrate of P-glycoprotein.[137] In this experiment, R123 was used to detect the activity of P-glycoprotein efflux in the Caco-2 cell monolayers. Caco-2 cell monolayer in 24-transwell plates with insert was used for R123 transport studies after 21 days. The integrity of the monolayer was evaluated based on TEER value and apparent permeability coefficient (P_{app}) of Lucifer yellow. Prior to the experiment, Caco-2 cell monolayers on insert and 24-transwell plates were washed and equilibrated as described above. R123 (5 µM), a mixture of R123 (5 µM) and verapamil (100 µM), and a mixture of R123 (5 µM) and plumbagin (1, 2, 4 and 8 µM)

in transport buffer were added to the apical (A) or basolateral (B) side of the chamber. Verapamil was used as a positive P-glycoprotein inhibitor. The plate was incubated at 37℃ for 120 min with gentle shaking (100 rpm) and aliquots of samples (150 µl) were collected from the receiver chamber and an equal volume of HBSS was immediately replenished to the chamber. The 24-transwell plate with insert was washed and equilibrated as described above. Concentrations of R123 were immediately analyzed using Micro-plate Multi-detection Instrument at 485/535 nm (excitation/emission).[131] The calibration curve of R123 (5-5,000 nM) versus Relative Fluorescence Units (RFU) was constructed.

4.2.6 Effect of plumbagin on the function of P-glycoprotein in Caco-2 cells

To investigate the effect of plumbagin on P-glycoprotein function in Caco-2 cells, the cell monolayer in 24-Transwell® insert was exposed to DMSO (0.1% v/v, vehicle), plumbagin (1, 2 and 4 µM), verapamil (100 µM) or complete MEM medium for 24 or 48 h on day 19 or 20 after seeding. Cell monolayer was washed and equilibrated as described above. R123 (5 µM) in transport buffer was added to the apical (A) or basolateral (B) side of the chamber. R123 transport experiment was performed as described above.

4.2.7 Determination of plumbagin concentrations

Concentrations of plumbagin in the transport buffer collected from both apical and basolateral sides of the chamber were measured by liquid chromatographic-mass spectrometry (LC-MS/MS). The system included Agilent 1100 Separation Module (Agilent Technologies, CA, USA) solvent and sample delivery, Av QTRAP 5500 Triple Quadrupole Mass Spectrometer (AB sciex, Foster City, CA, USA) equipped with CID, and Multiple Reactions Monitoring (MRM). Separation was performed using Hypersil gold C18 column (50 mm × 4.6 mm *i.d.,* 5 µM: Thermo Scientific, Fremont, CA, USA) with the mobile phase consisting of a mixture of (A) water containing 0.1% formic acid and (B) 100% methanol, running with isocratic mode. The ratio of mobile phase components (A:B) was 20:80 at the flow rate of 0.6 ml/min at room temperature. The total running time was 5 min for each sample.

Mass spectrometric analysis was performed in the negative-ion mode (ESI). The internal standard honokiol (3 µl, 10 ng/ml) was added into sample. The calibration curve of plumbagin was prepared at the concentration range of 10-5,000 nM. On the basic of the full-scan mass spectra of each analyze, the most abundant ions were selected and the mass spectrometer was set to monitor the transitions of the precursors to the product ions as follow: m/z 187→159 for plumbagin, 265→224 for honokiol (internal standard). The system was controlled by AnalystTM solfware (AB Sciex, Foster City, CA, USA). Proteins in samples were precipitated using cold acetonitrile (100 µl). Samples were centrifuged at 12,000 ×g for 15 min and 3 µl was injected onto the LC-MS/MS. Quality control (QC) samples were run in duplicate in each analytical batch at low, medium, and high concentrations. Criteria for acceptability were four out of six of the QC analyses to lie inside 100±15% of the nominal values. Intra and inter-assay accuracy and precision of the analytical method were<10%. The limit of quantitation of plumbagin (LOQ, signal to- noise ratio≥10) was 10 nM (RSD<7.0%, n = 3).

4.2.8 Effect of plumbagin on MDR-1 mRNA expression

Caco-2 cells ($5×10^5$ cells) were seeded on a 6-well plate in culture medium (2 ml). The culture medium was changed every 2 days. Cells were incubated at 37°C for 10 days in a humidified atmosphere of 5% CO_2. The culture medium was replaced with plumbagin at the concentrations of 0, 1, 2, and 4 µM and further incubated for an additional 24 and 48 h.[138,139]

4.2.8.1 Preparation of RNA from Caco-2 cells

Total RNA was prepared using TrizolTM reagent according to the manufacturer's protocol (Invitrogen, Karlsruhe, Germany). Briefly, following an exposure of to plumbagin for 24 or 48 h, the cell monolayer was rinsed with ice cold PBS and the lysed cells were added into a culture dish with TRIZOL Reagent (1 ml per 3.5 cm diameter dish). Cells were scrapped and cell lysate was mixed thoroughly. The homogenized sample was incubated at room temperature for 5 min, followed by centrifugation (12,000 × g for 10 min, 2-8°C) to remove cell debris and the supernatant was transferred to a new tube. Chloroform was added (0.2 ml

per 1 ml of TRIZOL reagent). Cells were scaped and thoroughly mixed for 15 sec. Following centrifugation (12,000 × *g* for 15 min, 2-8°C), cell suspension was separated into a lower red phenol-chloroform phase, an interphase and a colorless upper aqueous phase. The upper aqueous phase was transferred carefully into a fresh tube and RNA was separated by mixing the suspension with 0.5 ml isopropyl alcohol and incubated at 15-30°C for 10 min. Following centrifugation (12,000 × *g* for 10 min, at 2-4°C), the RNA was precipitated and washed with 1 ml of 75% ethanol and centrifuged at 7,500 × *g* for 5 min (2-8°C). The RNA pellets were dried and dissolved in 20 µl DEPC-treated water. The concentration of RNA was quantitated using NanoDrop Spectrophotometry (NanoDrop Technologies, Wilmington, DE, USA). The RNA samples were treated with RQ1 RNase-Free DNase according to the manufacturer's protocol (Promega, Mannheim, Germany) to degrade both double-stranded and single-stranded DNA.

4.2.8.2 Preparation of first-strand cDNA synthesis

The cDNA was prepared using the SuperScript™ III Reverse Transcriptase according to the manufacturer's protocol (Invitrogen, Karlsruhe, Germany). Briefly, total RNA (10 pg–5 µg) from Caco-2 cells and 1 µl of 50 µM oligo(dT)$_{20}$ were incubated at 55ºC for 50 min. The reaction was inactivated by heating at 70ºC for 15 min and chilled on ice for 2 min. cDNA was synthesized in a total volume of 20 µl containing 5x First-Strand Buffer (250 mM Tris–HCl (pH 8.3), 375 mM KCl, and 15 mM MgCl2), 0.1 M DTT, 40 U RNaseOUT™ Recombinant RNase Inhibitor, 10 mM dNTPs, and 200 U Superscript III Reverse Transcriptase Rnase H (Invitrogen).

4.2.8.3 Quantification of MDR1 mRNA expression

The forward and reverse primers for the selected genes used in the study are shown in **Table 4.3**. The platinum SYBRTM Green qPCR Supermix-UDG (invitrgen, Carsbad, CA, USA) was used for real-time PCR (RT-PCR) analysis using iCycler IQ machine (BioRad Laboratories Inc., Hercules, CA, USA). The reaction mixture (25 µl) consisted of 50 ng/µl cDNA, platinum SYBRTM Green qPCR Supermix-UDG mixture, 10 µM forward primer, 10 µM reverse primer, and sterile

double distilled water. The following PCR cycles for MDR-1 and GAPDH were initiated: denaturation at 95°C for 10 min followed by 40 cycles of amplification at 95°C for 15 sec and annealing at 60°C for 1 min. Each RT-PCR was performed in duplicate. Ct values (threshold cycle) which is the intersection between an amplification and threshold line was generated to reflect relative measure of the concentration of target in the RT-PCR reaction.

The delta-delta Ct method was used to calculate MDR-1 gene expression level relative to control and the housekeeping gene GAPDH was used for normalization of MDR-1 expression. The delta-delta Ct calculation for the relative quantification of target gene was as follows:

$$\Delta Ct\ (1) = [Ct\ (MDR\text{-}1)\text{-}Ct(GAPDH)]$$

$$\Delta Ct\ (2) = [Ct(control\ for\ MDR\text{-}1) - Ct(control\ for\ GAPDH)$$

$$\Delta\Delta Ct\ \ = \Delta Ct(1) - \Delta Ct(2)$$

$$Relative\ expression = 2^{-\Delta\Delta Ct}$$

where $\Delta Ct\ (1)$ = delta Ct of unknown sample, $\Delta Ct\ (2)$ = delta Ct of control, MDR-1 = target gene, and GAPDH = housekeeping gene.

Table 4.3 Primer sequences for determination of MDR-1 mRNA expression

Gene	Primer sequence
MDR-1	Forward: 5'- GTC TTT GGT GCC ATG GCC GT-3'
	Reverse: 5'- ATG TCC GGT CGG GTG GGA TA-3'
GAPDH	Forward: 5'- TGA AGG TCG GAG TCA ACG GAT TTG-3'
	Reverse: 5'- GCG CCA GTA GAGGCA GGG ATG ATG-3'

4.2.9 Data analysis

Statistical analysis was performed using SPSS version 16.0 (SPSS Inc., CO, USA). Quantitative data are presented as mean±SD of four experiments (duplicate each). Comparison of quantitative variables between the two sets of data

was performed using independent t-test. Statistical significance level was set at α=0.05 for all tests.

4.3 Inhibitory activities of Thai medicinal plants with promising activities against malaria on human cytochrome P450

The aim of this part was to investigate the propensity to inhibit CYP-mediated hepatic metabolism (CYP1A2, CYP2C19, CYP2D6 and CYP3A4) of five the Thai medicinal plants with promising activities against malaria (**Table 1.1**) using human liver microsomes *in vitro*.

4.3.1 Chemicals

Phenacetin, paracetamol, caffeine, nifedipine, oxidized nifedipine, diazepam, omeprazole, 5-hydroxyomeprazole, dextromethorphan hydrobromide, dextromethorphan, ketoconazole, nootkatone, α-napthoflavone, propranolol, dioscorealide B, myristicin, plumbagin and α-mangostin were purchased from Sigma-Aldrich (St. Louis, MO, USA). 1,4-naphthoquinone were obtained from Wako Pure Chemical Industries (Osaka, Japan). β-Nicotinamide adenine dinucleotide phosphate tetrasodium salt (NADPH) was purchased from Merck KGaA (Darmstadt, Germany). Loureirin B was obtained from ApexBio Technology (Boston MA, USA). Pooled human liver microsomes (from 50 donors, catalog number: HMMC-PL, lot number: PL050B, 20 mg/ml) were obtained from Gibco BRL Life Technologies (Grand Island, NY, USA). Solvents and other reagents were purchased from common commercial sources.

4.3.2 Plant materials

Plant materials were collected from different regions of Thailand and some were purchased from the city markets. Authentication of the plant materials was performed at the herbarium of the Department of Forestry, Bangkok, Thailand, where the herbarium vouchers had been archived. Information on the plant species under investigation including their botanical voucher numbers and traditional uses in medicine are shown in **Table 1.1**.

4.3.3 Preparation of crude extracts

Extraction was performed using the maceration method.[140] In brief, plant materials were washed with water to remove contaminants and cut into small pieces, oven-dried at 50ºC until stability of dry weight was observed, and then ground into powder. Extraction was carried out by macerating the powdered plant materials (100 g) in flasks containing 500 ml of 95% ethanol at room temperature (25-30ºC) for 7 days. The extracted solvent was separated and filtered through Whatman no. 1 filter paper (GE Healthcare Bio-Sciences, NJ, USA). After filtration, the extract was evaporated under reduced pressure by rotary evaporation. The dried powder was weighed and stored at -20ºC until used. Stock solutions of the ethanolic extracts were prepared at the concentration of 100 mg/ml. Plant materials were standardized using reversed phase HPLC with UV detection to quantify specific biomarker compounds.[23,25,27,28,141] The extraction yields (%) including relative amounts of biomarker compounds used are summarized in **Table 1.1**.

4.3.4 Assay validation

4.3.4.1 Precision

The precision of analytical method is a measure of random error and is defined as the agreement between replicate measurements of the same sample. It is expressed as the percentage coefficient of variation (% CV) or percentage relative standard deviation (%RSD) of replicate measurements. The percentage RSD or CV was calculated from the equation:

$$\% \text{ RSD} = \frac{\text{Standard deviation} \times 100}{\text{Mean}}$$

Precision can be considered as having an intra assay batch (repeatability) and the ability to repeat the same methodology in three replicates within one day and on three consecutive days. The precision of the method based on intraday repeatability was determined by analyzing five series concentration of selective metabolized spiked phosphate buffer. The repeatability between days of the method was established using the same range of selective metabolized in phosphate buffer on three consecutive days.

4.3.4.2 Accuracy

The accuracy of analytical method is a measure of the systemic error or bias and is defined as the agreement between the measured value and the true value and expressed as percent deviation of mean value (% DMV). Accuracy was reported as percentage bias calculated from the equation:

% Bias =   [(Measure value - True value)/True value] ✗ 100

The accuracy of the method was determined by comparing the measured concentration of selective metabolized in phosphate buffer at each concentration level (n=5) to the true concentration spiked into the phosphate buffer in three replicates within one day and on three consecutive days.

4.3.4.3 Sensitivity

Sensitivity of analytical method was obtained by the determination the limit of quantification (LOQ). The LOQ of the method is based on signal-to-noise approach by comparing measured signals from samples with known lowest concentrations of analyze and by establishing the minimum concentration at which the analyses can be reliably quantified.   The typical signal-to-noise ratio is 10:1.

4.3.5 Inhibitory effects on human cytochrome P450

Phenacetin O-deethylation, omeprazole 5-hydroxylation, dextromethorphan O-demethylation and nifedipine oxidation were used as selective markers for CYP1A2,[142] CYP2C19,[16] CYP2D6[14] and CYP3A4[143] activities, respectively. The selective inhibitors used for the inhibition of CYP1A2, CYP2C19, CYP2D6 and CYP3A4 were α-napthoflavone, nootkatone, quinidine and ketoconazole, respectively.   The substrate concentration similar to the apparent K_m (substrate concentration at which the reaction rate is half value of the maximal velocity) of each individual CYP was used in the experiment.   Various concentrations of the test extract (0-400 µg/ml in methanol) were added into the incubation mixture (final concentration of methanol in the incubation mixture<1%).   The incubation condition for the determination of the inhibitory activities of the crude extract of each plant to each CYP is summarized in **Table 4.4**.   The incubation mixture of 500 µl containing

the test extract, selective substrate and human liver microsomes (in 100mM phosphate buffer pH 7.4) was preincubated at 37ºC for 5 min in a shaking water bath. Methanol in water (<1%) was used as a vehicle control. The reaction was initiated and terminated by the addition of NADPH and cold acetonitrile (500 µl), respectively. The incubation time and protein concentration used were within the linear range for respective CYP activity. Each experiment was repeated four times (duplicated each). **Table 4.5** summarizes HPLC conditions including analytical assay performances for the four CYP-mediated metabolites. The analysis was performed using Spectra System HPLC with P4000 solvent delivery system, equipped with an AS3000 auto sampler, UV1000 detector, FL 300 fluorescence detector, SN4000 controller (Thermo Finnigan, San Jose, CA, USA) and Chrome Quest software (version 4.0). The linearity of the calibration curve for each analytical assay was demonstrated with the determination coefficient (r^2) of greater than 0.995. Quality control (QC) samples were run in duplicate in each analytical batch at low, medium and high concentrations. Criteria for acceptability were four out of six of the QC analyses to lie inside 100±15% of the nominal values.

4.3.6 Data analysis

Metabolite formation for each CYP-mediated reaction was expressed as a percentage of control in the absence of inhibitor. Data are presented as mean±SD of four experiments. The inhibitory potency of each extract was determined by the IC_{50} value (concentration which inhibits enzyme activity by 50%) estimated from dose response analysis using Calcusyn™ version 1.1 (BioSoft, Cambridge, UK). Statistical analysis was performed using SPSS version 16.0 (SPSS Inc., CO, USA). The IC_{50} of the selective inhibitor of each CYP isoform was used as the cut-off value and IC_{50} of the plant extract similar to or significantly lower than the cut-off value was considered significant enzyme inhibition. Comparison of the IC_{50} values between each selective CYP inhibitor and medicinal plant was performed using independent t-test at a statistical significance level of α=0.05.

Table 4.4 Specific enzyme reactions for CYP1A2, CYP2C19, CYP2D6 and CYP3A4

CYP	Reaction	Substrate (Concentration)	Metabolite	Internal Standard (Concentration)	Incubation Time (min)	Microsomal protein (concentration)	Selective inhibitor
1A2	Phenacetin O-deethylation	Phenacetin (20 μM)	Paracetamol	Caffeine (500 μM)	60	0.3 mg/ml	α-naphthoflavone
2C19	Omeprazole 5-hydroxylation	Omeprazole (10 μM)	5-hydroxy omeprazole	1,4-Naphthoquinone (10 μM)	30	0.5 mg/ml	Nootkatone
2D6	Dextromethorphan O-demethylation	Dextromethorphan (20 μM)	Dextrophan	Propanolol 50 μM	45	0.4 mg/ml	Qunidine
3A4	Nifedipine oxidation	Nifedipine (40 μM)	Oxidized nifedipine	Diazepam (80 μg/ml)	40	0.3 mg/ml	Ketoconazole

Table 4.5 Summarizes HPLC conditions including analytical assay performances for the four CYP-mediated metabolites

CYP	Metabolites	HPLC Methods	Sensitivity (LOQ: µM)	Precision (%)		Accuracy (%)		Recovery (%)
				Intra-assay	Inter-assay	Intra-assay	Inter-assay	
1A2	Paracetamol	HPLC-UV (Lavhekar *et al.*, 2006)	1	6.3	7.1	10	12	75
2C19	5-hydroxy omeprazole	HPLC-UV (Tassaneeyakul *et al.*, 2000)	0.04 (mM)	4.3	5.2	8.7	12.1	85
2D6	Dextrophan	HPLC- fluorescence (Taesotikul *et al.*, 2011)	0.02 (nmole)	9.8	11.2	9	10.3	79
3A4	Oxidized nifedipine	HPLC-UV (Patki *et al.*, 2003)	1	7.1	8.2	6	8.3	81

4.4 Investigation of the *in vitro* inhibition and *in vivo* induction of CYP-mediated hepatic metabolism of plumbagin

The aim of the present study was to further investigate the propensity of plumbagin to inhibit the three isoforms of human cytochrome P450 (CYP), *i.e.*, CYP1A2, CYP2C19 and CYP3A4 using human liver microsomes *in vitro*. In addition, evaluate the induction effect of plumbagin on hepatic cytochrome P450 1A2 and 3A11 in mice using the RT-PCR methodology in combination with enzyme activity measurements.

4.4.1 Chemicals

The authentic plumbagin (purity 98.2%) was obtained from Apin chemicals Co. Ltd (OX, UK). Tween-80, phenacetin, paracetamol, caffeine, omeprazole, 5-hydroxyomeprazole, nifedipine, oxidized nifedipine, ketoconazole, nootkatone, α-napthoflavone, and diazepam were purchased from Sigma-Aldrich (St. Louis, MO, USA). 1, 4-naphthoquinone was purchased from Wako Pure Chemical Industries, Co. Ltd. (Osaka, Japan). β-nicotinamide adenine dinucleotide phosphate (reduced form) tetrasodium salt (NADPH) was purchased from Merck KGaA (Darmstadt, Germany). Pooled human liver microsomes (from 50 donors) were obtained from Gibco BRL Life Technologies (Grand Island, NY, USA). TRIzolTM reagent, SuperScript™ III Reverse Transcriptase kit, and SYBR® Green Real-Time PCR Master Mixes were purchased from Invitrogen Life Technologies Inc. (Carlsbad, CA, USA). RQ1 RNase-Free DNase was purchased from Promega (Mannheim, Germany).

4.4.2 CYP inhibition

Inhibitory effects of plumbagin on CYP1A2, CYP2C19 and CYP3A4 activities were investigated *in vitro* using pooled human liver microsomes in a total volume of 500 µl of 0.1 M sodium phosphate buffer (pH 7.4). The concentration range of each substrate used was approximately equal to its K_m (Michaelis constant) value. Each experiment was repeated four times.

4.4.2.1 HPLC system

Analysis of concentrations of each CYP-mediated metabolite was performed using the validated high-performance liquid chromatography (HPLC) method. The HPLC system consisted of TSP HPLC with P4000 solvent delivery system, equipped with an AS3000 auto sampler, UV1000 detector, SN4000 controller (Thermo Finnigan, San Jose, CA, USA), and Chrome Quest software (version 4.0). The HPLC column used was a Thermo Hypersil Gold C-18 reversed phase column (210 mm × 4.6 mm, 5 µm particle size). Quality control (QC) samples were run in duplicate in each analytical batch at low, medium, and high concentrations. Criteria for acceptability were four out of six of the QC analyses to lie inside (100±15)% of the nominal values.

4.4.2.2 Analytical assay validation

The precision of the assay methods based on intraday repeatability was determined by analyzing five series concentrations of paracetamol, 5-hydroxyomeprazole, or oxidized nifedipine in phosphate buffer. The repeatability between days was established using the same concentration range of the three compounds, but the analysis was performed on three consecutive days. Results are expressed as relative standard deviation (%RSD) of replicate measurements as follow:

$$\% \text{ RSD} = \frac{\text{Standard deviation}}{\text{Mean}} \times 100$$

The accuracy of the analytical methods was determined by comparing the measured concentration of paracetamol, 5-hydroxyomeprazole and oxidized nifedipine in phosphate buffer at each concentration level (n=5) to the true concentration in three replicates within one day and on three consecutive days. Accuracy was reported as percentage bias calculated from the equation:

$$\% \text{ Bias} = [(\text{Measure value - True value})/\text{True value}] \times 100$$

Sensitivity of the analytical methods was obtained by the determination the limit of quantification (LOQ). The LOQ was determined based on signal-to-noise approach by comparing measured signals from samples with known lowest concentrations of the test compounds (paracetamol, 5-

hydroxyomeprazole, and oxidized nifedipine) and by establishing the minimum concentrations at a typical signal-to-noise ratio is 10:1.

4.4.2.3 CYP inhibition

The inhibitory effect of plumbagin on CYP1A2-mediated phenacetin O-deethylation was performed using α-naphthoflavone as a selective inhibitor.[142] In brief, the reaction mixture was pre-incubated (at 37°C, 5 min) with human liver microsomes (0.3 mg/ml, 100 µl), 20 µM phenacetin, and plumbagin (0-10 µM). The reaction was initiated with the addition of 1 mM NADPH. Following an incubation (at 37°C) for 60 min, the reaction was stopped by the addition of 500 µl of cold acetonitrile. The internal standard caffeine (500 µM, 50 µl) was added and the incubation mixture was cooled on ice for 5 min and centrifuged at 12,000 × g for 15 min. The supernatant was transferred to an autosampling vial and an aliquot of 20 µl was injected onto the HPLC column. The concentrations of paracetamol (metabolite) were measured by HPLC with UV detection (240 nm).[142] The gradient mobile phase consisted of a mixture of (A) acetonitrile and (B) distilled water; the initial ratio of mobile phase components (A:B) was 10:90 at a flow rate of 1 ml/min. The calibration curve was plotted using high ratio of paracetamol to caffeine on the ordinate, and concentrations of paracetamol (1-50 µM) on the abscissa.

The inhibitory effect of plumbagin on CYP2C19-mediated omeprazole hydroxylation was performed using nootkatone as a selective inhibitor.[16] In brief, the reaction mixture was pre-incubated (at 37°C for 5 min), with human liver microsomes (0.5 mg/ml, 100 µl), 10 µM omeprazole, and plumbagin (0-200 µM). The reaction was initiated with the addition of 1 mM NADPH. Following an incubation (at 37°C for 60 min), the reaction was stopped by the addition of 500 µl of cold acetonitrile. The internal standard 1,4-naphthoquinone (10 µM, 50 µl) was added and the incubation mixture was cooled on ice for 5 min and centrifuged at 12,000 × g for 15 min. The supernatant (800 µl) was transferred to an eppendorf tube and evaporated using speed vacuum concentrator (FTS System, Stone Ridge, NY, USA). The dried residue was reconstituted with 100 µl of a mixture of acetonitrile and water (50%:50%, v:v) and 10 µl injected onto the HPLC column. The concentrations

of the metabolite 5-hydroxyomeprazole were measured by HPLC with UV detection (302 nm).[16] The gradient mobile phase consisted of a mixture of (A) acetonitrile and (B) distilled water; the initial ratio of mobile phase components (A:B) was 10:90 at a flow rate of 1 ml/min. The calibration curve was plotted using high ratio of 5-hydroxyomeprazole to 1,4-napthoquinone on the ordinate, and concentrations of 5-hydroxyomeprazole (40-2,500 nM) on the abscissa.

The inhibitory effect of plumbagin on CYP3A4-mediated nifedipine oxidation was performed using ketoconazole as a selective inhibitor.[143] In brief, the reaction mixture was pre-incubated (at 37°C, 5 min, with human microsomes (0.3 mg/ml, 100 µl), 40 µM nifedipine, and plumbagin (0-20 µM). The reaction was initiated with the addition of 1 mM NADPH. Following an incubation (at 37°C for 40 min), the reaction was stopped by the addition of 500 µl of cold acetonitrile. The internal standard diazepam (80 ng/ml, 50 µl) was added and the incubation mixture was cooled on ice for 5 min and centrifuged at 12,000 $\times$ g for 15 min. The supernatant was transferred to an autosampling vial and an aliquot of 20 µl was injected onto the HPLC column. The concentrations of oxidized nifedipine (metabolite) were measured by HPLC with UV detection (270 nm).[7,143,144] The gradient mobile phase consisted of a mixture of (A) methanol and (B) distilled water; the initial ratio of mobile phase components (A:B) was 55:45 at a flow rate of 1 ml/min. The calibration curve was plotted using high ratio of oxidized nifedipine to diazepam on the ordinate, and concentrations of oxidized nifedipine (1-25 µM) on the abscissa

4.4.3 CYP induction
4.4.3.1 Animals and treatments

Male ICR (Imprinting Control Region) mice (5-7 weeks of age, weighting 20-40 g) were used in the study. All were obtained from the National Laboratory Animal Centre, Thailand. Animal experiments were carried out in accordance with the *Guidelines for the Care and Use of Laboratory Animals.* These animals were housed under controlled light (12 h light and 12 h dark) and temperature (22-24ºC) in animal house facility at Thammasat University. All animals

were fed with a stock diet and water *ad labitum*. Approval of the study protocol was obtained from the Ethics Committee for Animal Research, Thammasat University, Thailand. The number of the certification was 005/2558.

Mice were divided into four groups (3 mice for each group). Mice in the treated group were fed with plumbagin at a daily oral dose of 25.00, 12.25 and 6.25 mg/kg body weight for 28 days. The control group received a daily oral dose (1 ml) of 20% Tween-80 for 28 days.[145] At the end of the experiment period, all animals were sacrificed under ether anesthesia and liver organs were removed for investigation of *in vivo* induction on hepatic CYP 1A2 and 3A11 by the RT-PCR methodology and measurement of enzyme activity.[146,147]

4.4.3.2 Preparation of mice liver microsomes

The liver samples were rinsed with ice-cold, 0.9 % NaC1, homogenized in 50 mM sodium phosphate buffer (pH 7.4) containing 0.1 mM EDTA and centrifuged at 9,000 $\times$ g for 20 min. The supernatant was ultracentrifuged at 105,000 $\times$ g for 60 min, and the resulting microsomal pellets were suspended with ice cold 1.15% KCl solution and ultracentrifuged at 105,000 $\times$ g for 60 min. The resulting pellets were homogenized with 50 mM potassium phosphate (pH 7.4) containing 0.1 mM EDTA and 10% glycerol. Following of protein concentration determination by Bradford protein assay,[148] the suspended microsomes were aliquoted and stored at -80ºC until used.

4.4.3.3 Effect of plumbagin on CYP1A2 and CYP3A11 activities

Phenacetin *O*-deethylation and nifedipine oxidation were used as selective markers for CYP1A2 and CYP3A11 activities, respectively.[149] The substrate concentration equivalent to the apparent K_m value of each individual CYP was used in the experiment. Final concentration of organic solvent in the incubation mixture was<1%. The incubation conditions for determination enzyme activity to each CYP are according to that previously discussed in scheme.[14,16,142,143]

The incubation mixture of 500 µl containing the selective substrate, mice liver microsomes (in 100 mM phosphate buffer pH 7.4) was pre-incubated at 37ºC for 5 min in a shaking water bath. The reaction was initiated by the addition of NADPH

and further incubated for the specified periods. The incubation time and protein concentration used were within the linear range for respective CYP activity. Each experiment was performed in triplicate. CYP1A2-mediated phenacetin *O*-deethylation and CYP3A11-mediated nifedipine oxidation reactions were terminated by the addition of 500 µl of cold acetonitrile. The internal standard (50 µl) caffeine (for CYP1A2) or diazepam (for CYP3A11) was added. After centrifugation at 12,000 *x g* for 15 min, concentrations of the metabolites of CYPA2 and CYP3A11 produced in the supernatant (20 µl) was measured by HPLC. Concentrations of the paracetamol (metabolite for CYP1A2) and oxidized nifedipine (metabolite for CYP3A11) in the incubation mixtures were determined using HPLC with UV detection.[149] HPLC analysis was performed with HPLC system consisted of Spectra System HPLC with P4000 solvent delivery system, equipped with an AS3000 auto sampler, UV1000 detector, SN4000 controller (Thermo Finnigan, San Jose, CA, USA), and Chrome Quest software (version 4.0). Twenty microliters sample was injected onto the HPLC column for analysis. HPLC condition for determination of paracetamol (metabolite for CYP1A2) consisted of: C-18 reversed phase column (Thermo Hypersil Gold, 210 × 4.6 mm, 5 µm particle size), gradient mobile phase a mixture of acetonitrile and distilled water, with an initial ratio of 10:90 at the flow rate of 1 ml/min, and UV detection at 240 nm. The calibration curve was prepared at the concentration range of 1-50 µM. HPLC condition for determination of oxidized nifedipine consisted of: C-18 reversed phase column (Thermo Hypersil Gold, 210 × 4.6 mm, 5 µm particle size), mobile phase (a mixture of methanol and water at the ratio of 65:35% v/v) with a flow rate of 1.0 ml/min and UV detection at 270 nm. The calibration curve was prepared at the concentration range of 1-25 µM. The linearity of the calibration curve for each analytical assay for the CYP-mediated production of metabolite was demonstrated with the determination coefficient (r^2) of greater than 0.995. Quality control (QC) samples were run in duplicate in each analytical batch at low, medium, and high concentrations. Criteria for acceptability were four out of six of the QC analyses to lie inside 100±15% of the nominal values.

4.4.3.4 Inducing activity of plumbagin on CYP1A2 and CYP3A11 mRNA expression

Preparation of RNA from liver sample: The liver sample isolated from each mouse was rinsed with ice-cold, 0.9 % NaCl and total RNA was prepared using Trizol^{TM} reagent according to the manufacturer's protocol (Invitrogen, Karlsruhe, Germany). Briefly, homogenize liver sample in 1 ml of TRIZOL reagent *per* 50-100 mg of tissue using power homogenizer. Homogenized sample was incubated at 25°C for 5 min and chloroform (0.2 ml) *per* 1 ml of TRIZOL reagent was added. The sample was thoroughly mixed and incubated at 25°C for 3 min. Following centrifugation (12,000 $\times$ g for 15 min, 2-8°C), homogenized sample was separated into a lower red phenol-chloroform phase, an interphase, and a colorless upper aqueous phase. The upper aqueous phase was transferred carefully into a fresh tube and RNA was separated by mixing the suspension with 0.5 ml isopropyl alcohol and incubated at 15-30°C for 10 min. Following centrifugation (12,000 $\times$ g for 10 min, at 2-4°C), the RNA was precipitated and washed with 1 ml of 75% ethanol and centrifuged at 7,500 $\times$ g for 5 min (2-8°C). The RNA pellets were dried and dissolved in 20 µl DEPC-treated water. The concentration of RNA was quantitated using NanoDrop Spectrophotometry (NanoDrop Technologies, Wilmington, DE, USA). The RNA samples were treated with RQ1 RNase-Free DNase according to the manufacturer's protocol (Promega, Mannheim, Germany) to degrade both double-stranded and single-stranded DNA.

Preparation of first-strand cDNA synthesis: The cDNA was prepared using the SuperScript™ III Reverse Transcriptase according to the manufacturer's protocol (Invitrogen, Karlsruhe, Germany). Briefly, total RNA (10 pg-5 µg) from Caco-2 cells and 1 µl of 50 µM oligo(dT)$_{20}$ were incubated at 55ºC for 50 min. The reaction was inactivated by heating at 70ºC for 15 min and chilled on ice for 2 min. cDNA was synthesized in a total volume of 20 µl containing 5x First-Strand Buffer (250 mM Tris–HCl (pH 8.3), 375 mM KCl, and 15 mM MgCl$_2$), 0.1 M DTT, 40 U RNaseOUT™ Recombinant RNase Inhibitor, 10 mM dNTPs, and 200 U Superscript III Reverse Transcriptase Rnase H (Invitrogen).

Quantification of CYP1A2 and CYP3A11 mRNA expression:
The forward and reverse primers for the selected genes used in the study are shown in **Table 4.6.** The platinum SYBRTM Green qPCR Supermix-UDG (Invitrgen, Carsbad, CA, USA) was used for real-time PCR (RT-PCR) analysis using iCycler IQ machine (BioRad Laboratories Inc., Hercules, CA, USA). The reaction mixture (25 µl) consisted of 50 ng/µl cDNA, platinum SYBRTM Green qPCR Supermix-UDG mixture, 10 µM forward primer, 10 µM reverse primer, and sterile double distilled water. The PCR cycles for CYP1A2, CYP3A11 and GAPDH consisted of denaturation at 95°C for 10 min followed by 40 cycles of amplification at 95°C for 15 sec, and annealing at 60°C for 1 min. Each RT-PCR was performed in duplicate. Ct values (threshold cycle) which is the intersection between an amplification and threshold line was generated to reflect relative measure of the concentration of target in the RT-PCR reaction.

The delta-delta Ct method was used to calculate MDR-1 gene expression level relative to control and the housekeeping gene GAPDH was used for normalization of MDR-1 expression. The delta-delta Ct calculation for the relative quantification of target gene was as follows:

ΔCt (1) = [Ct (CYP1A2 or CYP3A11)-Ct(*GAPDH*)]

ΔCt (2) = [Ct(control for CYP1A2 or CYP3A11)- Ct(control for *GAPDH*)

$\Delta\Delta$Ct = ΔCt(1) - ΔCt(2)

Relative expression = $2^{-\Delta\Delta Ct}$

where ΔCt (1) = delta Ct of unknown sample, ΔCt (2) = delta Ct of control, CYP1A2 and CYP3A11 = target gene, and GAPDH = housekeeping gene.

Table 4.6 Primer sequences for determination of CYP1A2 and CYP3A11 mRNA expression

Gene	Primer sequence
CYP1A2	Forward: 5'-TGGTGGAATCGGTGGCTAAC-3'
	Reverse: 5'- GACCGGGAAGAAGTCCACTG-3'
CYP3A11	Forward: 5'- ACCTGGGTGCTCCTAGCAAT-3'
	Reverse: 5'- GCACAGTGCCTAAAAATGGCA-3'
GAPDH	Forward: 5'- GGAGAGTGTTTCCTCGTCCC-3'
	Reverse: 5'- ATGAAGGGGTCGTTGATGGC-3'

4.4.4 Data analysis

IC_{50} (concentration causing 50% inhibition of enzyme activity) values were calculated from a log dose–response curve plotted using the Calcusyn™ version 1.1 (BioSoft, Cambridge, UK). Data are presented as mean±SD of the four experiments. Statistical analysis was performed using SPSS version 16.0 (SPSS Inc., CO, USA). The statistical significance of difference between treatments and control group was performed using independent-sample t Test. Statistical significance level was set at α=0.05.

4.5 Toxicity and pharmacokinetics of plumbagin in wistar rats model

The aim of this part was to evaluate the toxicity and pharmacokinetics of plumbagin in wistar rats model.

4.5.1 Chemicals

The authentic plumbagin (purity 98.2%) was purchased from Apin chemicals Co. Ltd (Oxford, UK). Tween-80 and honokiol (internal standard) were purchased from Sigma-Aldrich (St. Louis, MO, USA). Stock solutions of plumbagin and the internal standard were prepared in methanol. MS grade water, methanol and acetonitrile were purchased from Yes-sci Co., Ltd. Isoflurane was purchased from Wako Pure Chemical Industries, Ltd. (Osaka, Japan).

4.5.2 Animals

Wistar rats (5-8 weeks of ages, weighting 200-300 g) of both sexes were obtained from the National Laboratory Animal Centre, Thailand. Animal experiments were carried out in accordance with the Guidelines for the Care and Use of Laboratory Animals. These animals were housed under controlled light (12 h light and 12 h dark) and temperature (22-24°C) in animal house facility at Thammasat University. All animals were fed with a stock diet and water ad labitum. Approval of the study protocol was obtained from the Ethics Committee for Animal Research, Thammasat University, Thailand. The number of the certification was 005/2558.

4.5.3 Toxicity testing in wistar rat model

4.5.3.1 Acute toxicity tests

Plumbagin was dissolved with 20% Tween-80 to make the desired concentrations. Wistar rats were fasting 2 h before administration a single oral dose of the plumbagin. Animals were divided into four groups, six for each (3 males and 3 females) as follows,[126] wistar rats were fed with plumbagin at a single oral dose of 500, 250 and 150 mg/kg body weight. Control group were received a single oral dose of 20% Tween-80 (1 ml). Behavioral changes and other physiological activities[150] of rats were observed continuously for 1 h after dosing and intermittently 4 h, and thereafter over a period of 24 h.[128] Animals were observed for up to 14

days following dosing for any signs of toxicity, the latency of death and the body weight were recorded. At the end of the experiment, all animals were sacrificed under ether anesthesia and vital organs (liver, lung, kidney, heart and spleen) were removed from all animals for gross and histopathological examination.

4.5.3.2 Subacute toxicity test

Wistar rats were devided into four groups, six for each (3 males and 3 females) as follows,[127] fed with plumbagin by oral dose of 100, 50 and 25 mg/kg body weight for 28 days. Control group were received oral dose of 20% Tween-80 (1 ml) for 28 days. All animals were fasting 2 h before administration by oral dose of the plumbagin. Behavioral changes and other physiological activities[150] of rats were observed continuously for 1 h after dosing and intermittently 4 h, and thereafter over a period of 24 h.[128] They were observed for up to 28 days following dosing for any signs of toxicity, the latency of death, blood chemistry, hematology test and the body weight as well as complete blood count, liver and kidney function tests) were monitored. At the end of the experiment, all animals were sacrificed under ether anesthesia and vital organs (liver, lung, kidney, heart and spleen) were removed from all animals for gross and histopathological examination.

4.5.3.3 Histopathology

At the end of the experiment, animals were sacrificed using isoflurane. The organs from all animal were washed with 0.85% NaCl, then fixed with 10% formalin (37% formaldehyde in water) with 10x volume of the organs. The fixed organs from all rats were preserved until performed tissue processing. Histopathological examination of heart, lung, kidney, liver, and spleen were performed.

Tissue processing: The organs of rats were cut into cross sections by microtome. These tissue sections were then processed by using STP120 Microm model STP 20-3 automate (MM France, Francheville, France). The processing method was starting by soaking tissues sections in 95% ethanol and absolute ethanol to remove water. The tissue sections were soaked in xylene to remove alcohol residue. Finally, xylene was replaced by paraffin wax.

Tissue embedding, sectioning and staining: The embedding step was performed by using Embedding Microm model EC 350 automate (Dotmed, Walldrof, Germany). The heating paraffin and tissues were put into the cooling molds. Then, hardened blocks containing the tissue samples were sectioned by Leica Microsystms model RM212S (Leica Microsystems Inc., Richmond, Germany). After that, the tissue slides were deparaffinized by heating at 80ºC and using xylene solvent. In order to remove water from tissue, alcohol which higher concentration than water was used. The tissue slides were stained with hematoxylin dye for nuclei of cell and eosin dye for cell cytoplasm

4.5.4 Pharmacokinetics of plumbagin in rat

Four male wistar rats (weighing 200-350 g) were received an oral dose of 100 mg/kg body weight plumbagin. The control group was received 20% Tween-80 (1 ml). Blood sample (500 µl) was collected from the tail vein of each rat at 0, 1, 2, 3, 5, 8, 24, 48 and 72 h after dosing. Then plasma was separated from whole blood samples through centrifugation at 3,000 x g for 10 min. The resulting plasma (100 µl) were mixed with 10 ng/ml honokiol (5 µl) and ethyl acetate (1 ml) and centrifuged at 12,000 x g for 15 min.[120] The upper layer was transferred to a new tube and evaporated to dryness under nitrogen flow. The dried residue was reconstituted with 100 µl of the mobile phase and a 5 µl aliquot were injected onto the LC-MS/MS. Urine samples were collected from the metabolic cages at 24, 48, 72, 96 and 120 h. Urine samples were centrifuged at 1,500 x g for 10 min. The urine supernatant sample (100 µl) was extracted with ethyl acetate (1 ml).[120] The extract was dried and the residue was reconstituted with 100 µl of the mobile phase and a 5 µl aliquot were injected onto the LC-MS/MS.

4.5.4.1 Plasma and urine calibration curve

The stock solution of plumbagin was prepared at a concentration of 1 mg/ml by dissolving in methanol and stored at -20ºC. The solution was then diluted with water to make the desired concentrations. Working solution for the internal standard (honokiol) was prepared at a concentration of 10 ng/ml with methanol. The plasma standard samples of plumbagin were prepared at

concentrations of 10, 50, 100, 250, 500, 1,000 and 2,000 ng/ml by using drug-free rat plasma. Quality control samples were prepared at concentrations of 25, 125 and 1,250 ng/ml in blank rat plasma. The urine standard samples of plumbagin were prepared at concentrations of 50, 100, 500, 1,000, 5,000, 10,000, and 50,000 ng/ml by using drug-free rat urine. Quality control samples were prepared at concentrations of 250, 2,500 and 25,000 ng/ml in blank rat urine. Quality control (QC) samples were run in duplicate in each analytical batch at low, medium, and high concentrations. Criteria for acceptability were four out of six of the QC analyses to lie inside 100±15% of the nominal values. The intra and inter-assay accuracy and precision of the assay methods were determined. Accuracy was reported as percentage bias which calculated from the equation:

$$\% \text{ Bias} = [(\text{Measure value - True value})/\text{True value}] \times 100$$

Precision was reported as the relative standard deviation (RSD) which calculated from the equation:

$$\% \text{ RSD} = \frac{\text{Standard deviation}}{\text{Mean}} \times 100$$

4.5.4.2 Recovery of rat plasma and urine

The recovery of rat plasma, solution of plumbagin was added into rat plasma to yield final concentrations of 50, 500 and 2,000 ng/ml. The recovery of rat urine, plumbagin solution was added into urine to yield final concentrations of 500, 5,000 and 20,000 ng/ml. The individual experiment was repeated three times. Meanwhile plumbagin solution was diluted to 50, 500, 2,000 and 5,000 ng/ml in methanol. The plasma sample, urine sample and the diluted solution were extracted using the sample preparation method described above. The ratio of peak area (plasma or urine sample/diluted solution) for plumbagin was used to calculate the recovery in plasma and urine.

4.5.4.3 Determination of plasma and urine concentrations of plumbagin

Concentrations of plumbagin in plasma and urine of wistar rats were measured using liquid chromatographic-mass spectrometry (LC-MS/MS). The system included Agilent 1100 Separation Module (Agilent Technologies, CA, USA) solvent and sample delivery, Av QTRAP 5500 Triple Quadrupole Mass Spectrometer (AB Sciex, Foster City, CA, USA) equipped with CID, and Multiple Reactions Monitoring (MRM). Mass spectrometric analysis was performed in the negative-ion mode (ESI). The following parameters of the turbo ionspray were used: ionspray voltage,-4500V; the ion source gas 1 (GS1), gas 2 (GS2), curtain gas (CUR) and collision gas (CAD) were 50, 60, 25 and 5, respectively and desolvation gas (nitrogen) heated to 500°C. Separation was performed using Hypersil gold reversed-phase C18 column (50 mm × 4.6 mm i.d., 5 µM: Thermo Scientific, Fremont, CA, USA) with the mobile phase consisting of a mixture of (A) water containing 0.1% formic acid and (B) 100% methanol, running with gradient mode at the flow rate of 0.6 ml/min at room temperature (**Table 4.7**). On the basic of the full-scan mass spectra of each analyze, the most abundant ions were selected and the mass spectrometer was set to monitor the transitions of the precursors to the product ions as follow: m/z 187→159 for plumbagin, 265→224 for honokiol (internal standard). The system was controlled by AnalystTM solfware (AB Sciex, Foster City, CA, USA).

Table 4.7 HPLC condition for quantitative analysis plumbagin using gradient mobile phase of (A) water containing 0.1% formic acid and (B) 100% methanol

Time (min)	0.1% formic acid in water	100% Methanol
0-2	60	40
2-2.5	20	80
2.5-7.5	20	80
7.5-8	60	40
8-10	60	40

4.5.5 Pharmacokinetic analysis

Pharmacokinetic parameters of plumbagin were determined using the PKSolver software version 2.0 (Nanjing, China).[151] Non-compartmental analysis models 101 (Noncompartmental analysis, extravascular) was used with log-linear trapezoidal estimation. The pharmacokinetic estimates included time to reach maximum blood concentration (T_{max}), maximum blood concentration (C_{max}), area under the tissue concentration-time curve (AUC_{0-inf}), clearance (CL), volume of distribution (Vd), elimination half-life ($T_{1/2}$), and mean residence time (MRT).

4.5.6 Statistical analysis

Statistical analysis was performed using SPSS version 16.0 (SPSS Inc., CO, USA). All quantitative variables are presented as mean±SD. Comparison of difference in quantitative variables between two groups and more than two groups was performed using independent sample t-test and one-way analysis of variance (ANOVA). Statistical significance level was set at α=0.05 for all tests.

4.6 Application of SPECT/CT imaging system and radiochemical analysis for investigation of blood kinetics and tissue distribution of radiolabeled plumbagin in healthy and *P. berghei*-infected mice

The aim of this part was to investigate blood kinetics and tissue distribution of radiolabeled plumbagin in healthy and *P. berghei*-infected mice by using application of SPECT/CT imaging system and radiochemical analysis

4.6.1 Chemicals

Plumbagin (purity 98.2%) was obtained from Apin chemicals Co. Ltd. (Oxford, UK). Methanol, chloroform, chromato sheet, stannous chloride dihydrate ($SnCl_2.2H_2O$) acetone, ethyl acetate, and ammonium hydroxide were purchased from Wako Pure Chemical Industries, Ltd. (Osaka, Japan). Pooled human liver microsomes (50 donors) were purchased from Gibco BRL Life Technologies (Grand Island, NY, USA). Other reagents used were purchased from local market and

were of analytical grade. Technetium-99m (^{99m}Tc) freshly eluted from ^{99}Mo by solvent extraction method was purchased from Nihon Mediphysics (Tokyo, Japan).

4.6.2 Animals

ICR (Imprinting Control Region) mice (5-7 weeks of age, weighting 20-40 g) of both genders were used in the study. All were purchased from Japan SLC Inc., Japan. Animal experiments were housed under controlled light (12 h light and 12 h dark) and temperature (22-24°C) in animal house facility at Nagasaki University Radioisotope Center.[152] All were fed with a stock diet and water *ad libitum*. Approval of the study protocol was obtained from the Ethics Committee for Animal Research, Nagasaki University, Japan (approval date 27/11/2013, certification number 131104-1).

4.6.3 *Plasmodium berghei*-infected mice model

P. berghei (ANKA), the rodent *Plasmodium* species was kindly provided by Animal Research Center for Tropical Infections, Institute of Tropical Medicine (NEKKEN), Nagasaki University, Nagasaki, Japan. The donor mice were infected with 200 μl of *P. berghei* suspension to increase parasite inoculum and were sacrificed by cervical dislocation after 7 days of infection (5-10% parasitemia). The parasitized blood of each donor mouse was collected *via* heart puncture and blood was smeared and stained with 10% Giemsa stain solution. Blood film was examined on light microscope under immersion oil at ×100 magnification.[129] The parasitemia was determined by counting the number of infected erythrocytes and expressed as percentage of total number of cells in approximately 5-10 fields of blood film. Suspension (200 μl in normal saline) of 1×10^{7} parasitized erythrocytes was infected to each mouse by intraperitoneal injection.

4.6.4 Radiolabeling of plumbagin with technetium-99m (^{99m}Tc)

^{99m}Tc-Plumbagin was prepared by dissolving 0.5 mg of plumbagin in normal saline (0.9% NaCl), followed by a reducing agent for radiolabeling stannous chloride dihydrate (50 μg/ml). The pH of the solution was adjusted to 6.5 using 0.1 M NaOH and ^{99m}Tc (30-40 MBq) was added. The solution was incubated at 37°C for 30 min.[152-154] The radiolabeled complex was filtered through low protein GV 0.22

micron filter (Millex, Merck Millipore, Darmstadt, Germany). The radiochemical purity of the labelled complex was determined using Instant Thin Layer Chromatography (ITLC).[155]

4.6.5 Effects of pH and concentration of stannous chloride dihydrate on the labelling efficiency

To determine the effect of pH on the labelling complex, the pH of plumbagin-radiolabeled solution was varied from 4.5 to 7.5 using 0.1 M NaOH solution, with a fixed concentration of stannous chloride dehydrate at 50 µg/ml. To determine the effect of stannous chloride dihydrate concentration on the labelling efficiency, concentrations of the compound were varied from 25 to 200 µg/ml, with constant solution pH at 6.5.[152] Each experiment was repeated six times. The percentage of labelling yield and was determined using a mixture of acetone, ethyl acetate, water, and ammonium hydroxide (at a ratio of 7:3:3:0.3, v:v:v:v) as the mobile phase. The reported retardation factor (Rf) values of ^{99m}Tc-plumbagin complex and reduced/hydrolyzed (R/H) technetium are 0.9-1 and 0, respectively.[153]

4.6.6 Radiochemical purity analysis

The labelling purity of ^{99m}Tc-plumbagin was assessed by ascending ITLC using chromate sheets (Wako Pure Chemical Industries, Ltd., Osaka, Japan). The radiolabel complex (5 µl) was applied onto the sheet at distance 1 cm from the end of the sheet with the mobile phase consisting of a mixture of acetone, ethyl acetate, water, and ammonium hydroxide (at the ratio of 7:3:3:0.3, v:v:v:v). The reported Rf values of ^{99m}Tc-plumbagin complex and reduced/hydrolyzed (R/H) technetium are 0.9-1 and 0, respectively.[153] The ITLC sheet was divided into two equal halves and radioactivity in each segment of the ITLC sheet was counted using 2470 Automatic Gamma Counter (PerkinElmer Life and Analytical Sciences Ltd., Turku, Finland). Labelling efficiency was calculated using the following equation.[156]

$$\% \text{ Labelling efficiency} = \frac{\text{Total counts} - \{\text{Counts of reduced/hydrolyzed (R/H) technetium} + \text{Counts of free technetium}\}}{\text{Total counts}}$$

4.6.7 *In vitro* and *in vivo* stability of radiolabeling ^{99m}Tc-plumbagin complex

In vitro stability of ^{99m}Tc-plumbagin complex was determined using ITLC. Normal saline and/or mice plasma (630 µl) were mixed separately with 70 µl of the ^{99m}Tc-plumbagin complex and incubated at 37°C for 24 h. An aliquot of sample was collected at 0, 1, 2, 4, 6 and 24 h and radiolabeled compound was determined by ITLC, using a mixture of acetone, ethyl acetate, water and ammonium hydroxide (7:3:3:0.3, v:v:v:v) as the mobile phase. Radioactivity in each segment of ITLC sheet was counted using 2470 Automatic Gamma Counter. The experiment was repeated four times.

In vivo stability of ^{99m}Tc-plumbagin complex was assessed by injection (intravenously) of ^{99m}Tc-plumbagin (740 KBq, 200 µl) through the tail vein of mice (2 female and 2 male mice each). Blood samples were collected into red micro-hematocrit capillary tubes (75 µl) at different time intervals, *i.e.,* 0, 1, 2, 4, 6, and 24 h after injection by tail clip. Plasma samples were separated through centrifugation (2,500 *x g*, 15 min). Stability of the ^{99m}Tc-plumbagin complex in plasma was determined by ITLC. The radioactivity in each segment of ITLC sheet was counted using 2470 Automatic Gamma Counter.

4.6.8 Blood kinetics of ^{99m}Tc-plumbagin complex

Blood kinetics of the radiolabeled plumbagin was investigated in healthy and *P. berghei*-infected mice (4 mice per group, 2 males and 2 females each). Animals were injected with 740 KBq ^{99m}Tc-plumbagin complexes intravenously through the tail vein. Blood sample (1 ml) was withdrawn from each animal *via* heart puncture at 5 min, 1, 2, 4, 6 and 24 h after injection. The radioactivity was measured using 2470 Automatic Gamma Counter, and the concentration was normalized to percentage of injected dose *per* gram (% ID/g).[157]

Pharmacokinetic parameters of ^{99m}Tc-plumbagin were determined using the PKSolver software version 2.0 (Nanjing, China)[151]. Non-compartmental analysis models 102 (IV-bolus input) was used with log-linear trapezoidal estimation. The pharmacokinetic estimates included time to reach maximum blood

concentration (T_{max}), maximum blood concentration (C_{max}), area under the tissue concentration-time curve (AUC_{0-inf}), clearance (CL), volume of distribution (Vd), elimination half-life ($T_{1/2}$), and mean residence time (MRT).

4.6.9 Biodistribution of ^{99m}Tc-plumbagin complex in healthy and *P. berghei*-infected mice

Healthy and *P. berghei*-infected mice were divided into six groups (2 male and 2 female mice each) for six sampling time points. Animals were fasted overnight before the experiment but allowed free access to water. ^{99m}Tc-plumbagin complex (200 µl, 0.5 mg/ml) was intravenously injected (740 KBq) through the tail vein of each mouse. Animals were humanely sacrificed by cervical dislocation and blood samples (1 ml each) were collected *via* heart puncture at 5 min, and 1, 2, 4, 6, and 24 h after injection. All vital organs including liver, kidney, spleen, stomach, small intestine, large intestine, heart, lung, and brain were removed, washed with normal saline, dried with filter paper, and weighed. The radioactivity of the radiolabeled complex accumulated in each organ was counted using 2470 Automatic Gamma Counter. Data are expressed as percent of the injected dose *per* whole organ (%ID/whole organ).[154,157,158]

4.6.10 SPECT/CT imaging studies in healthy and *P. berghei*-infected mice

SPECT images and X-ray CT scans were acquired using a SPECT/CT imaging system (FLEXTM TriumphTM, Gamma Medica Ideas Innovation for life, Northridge, CA, USA). SPECT imaging was performed using high-resolution single pinhole collimators at 30 min, and 2, and 4 h after an intravenous injection of ^{99m}Tc-plumbagin complex (2 male mice each). The detector was mounted on a circular gantry, allowing it to rotate 360° around the animal positioned on a stationary bed. The radius of rotation (ROR) was set at 70 mm with a field of view (FOV) of 91.08 mm. The imaging acquisition was accomplished using 64 projections at 20 sec per projection. CT image acquisition (X-ray source: 70 kV, 170µA; 256 projections) was then performed with the animal in exactly the same position. The Triumph[TM] X-OTM CT system software 4.2.0.0 was used for CT image reconstruction, and the vivid

software was used for SPECT/CT imaging fusion. At 30 min, 2, and 4 h after the intravenous injection of ^{99m}Tc-plumbagin complex (0.5 mg/ml, 200 µl) through the tail vein of each mouse (injected dose: 740 KBq), the animal was anesthetized with 1.5% isofluran and SPECT/CT image was monitored.[159,160]

4.6.11 *In vitro* hepatic metabolism of plumbagin

Pooled human liver microsomes from 50 donors (Gibco BRL Life Technologies (Grand Island, NY, USA) were used to investigate the role of liver in the biotransformation of plumbagin. In brief, plumbagin (2.5 µM) was pre-incubated (at 37°C for 5 min) with 0.6 mg/ml of pooled human liver microsomes in 0.1 M potassium phosphate buffer (pH 7.4) in a total volume of 0.5 ml. The reaction was initiated and terminated by the addition of 1 mM NADPH and 500 µl ice-cold acetonitrile, respectively. The internal standard honokiol (10 µM, 50 µl) was added to the incubation mixture at 0, 5, 10, 15, 20, 30, 40, 50 and 60 min. Samples were thoroughly mixed and centrifuged (12,000 x g, 15 min) before HPLC analysis.

Concentrations of plumbagin (substrate) and honokiol (internal standard) in the incubation mixture collected at each time point were determined by HPLC. The HPLC system consisted of Spectra P400 HPLC solvent system (P400, Thermo Finnigan, CA, USA), equipped with a Rheodyne 7125 injector (Rheodyne, Berkeley, CA, USA) with a 20 µl loop, degasser, SCM1000, AS3000 auto sampler, and ultraviolet detector (Spectra System UV1000, ThermoFinnigan, CA, USA). Separation of plumbagin and honokiol was performed on a Thermo Hypersil Gold C-18 reversed phase column (210 × 4.6 mm, 5 µm *i.d.*) and the mobile phase consisting of a mixture of methanol (A) and (B) distilled water running with gradient elution mode at the flow rate of 1 ml/min. The initial ratio of the mobile phase was set at 60:40 (A:B, v:v). UV detection was set at the wavelength of 210 nm. Twenty microliters of sample was injected onto the HPLC column for analysis. The standard curve was plotted using peak height ratio of plumbagin to internal standard on the ordinate and concentration of plumbagin in the concentration range 0.1-5 µM on the abscissa.

4.6.12 Statistical analysis

Statistical analysis was performed using SPSS version 16.0 (SPSS Inc., CO, USA). All quantitative variables are presented as median with 95% CI (confidence interval) for median. Comparison of the quantitative variables between healthy and *P. berghei*-infected mice in each organ at each time point was performed using Mann-Whitney U test. For the quantitative two-related groups, Wilcoxon Signed Rank test was applied. Statistical significance level was set at α=0.05 for all tests.

CHAPTER 5

RESULTS

5.1 Antimalarial activity of plumbagin *in vitro* and in animal models

5.1.1 Assessment of *in vitro* antimalarial activities of plumbagin

The median IC_{50} values for antimalarial activity of plumbagin against 3D7 chloroquine-sensitive *P. falciparum* and K1 chloroquine-resistant *P. falciparum* clones were 580 and 370 nM, respectively. The corresponding IC_{50} values for chloroquine and artesunate were 10.5 *vs* 128.7 and 2.1 *vs* 1.91 nM, respectively (**Table 5.1**).

Table 5.1 *In vitro* antimalarial activity of plumbagin, chloroquine and artesunate

Compound	IC_{50} against 3D7 chloroquine-sensitive *P. falciparum* clones (nM)	IC_{50} against K1 chloroquine resistant *P. falciparum* clones (nM)
Plumbagin	580 (270–640)	370 (270–490)
Chloroquine	10.5 (9.4–12.1)	128.7 (109.3–139.2)
Artesunate	2.1 (1.98–2.54)	1.91 (16.1–2.1)

Data are presented as median (range) of IC_{50} values (nM).

5.1.2 Toxicity tests

The toxicity of plumbagin when given as a single oral dose (acute toxicity) and 28-day daily doses (subacute toxicity) in mice was investigated in order to define optimal dose of plumbagin to be used for evaluation of its *in vivo* antimalarial activity in malarial mouse model. Results indicated virtually no toxicity of plumbagin at a maximum single oral dose of 100 mg/kg body weight (acute toxicity). All mice survived following a single oral dose of 100 mg/kg body weight of plumbagin and 20% Tween-80 (control) (**Table 5.2**). There was neither sign of toxicity nor significant change in water and food consumption and body weights of

mice in both groups during the 14 days observation period (**Figure 5.1**). Toxic signs and symptoms including anxiety and agitation were however observed in 6/6 and 2/6 of mice following the doses of 500 and 200 mg/kg body weight, respectively; all subsequently died within 24 h. The gross examination of vital organs, *i.e.,* heart, lung, liver, spleen and kidney in both treated (all dose levels) and control groups were similar either in size and cell morphology.

For the subacute toxicity test, all mice survived following daily oral doses of 25 mg/kg body weight plumbagin and 20% Tween-80 (control) for 28 days (**Table 5.2**). There was neither abnormality in behavior, sign of toxicity, nor significant change in water and food consumption and body weights during the 28 days observation period (**Figure 5.2**). Toxic signs and symptoms including anxiety and agitation were however observed in all mice following the doses of 100 and 50mg/kg body weight of plumbagin (for 28 days). Mice receiving 100 mg/kg body weight of plumbagin died within 4-8 days, whereas those receiving 50 mg/kg body weight dosing died within 8-11 days. The gross examination of vital organs, i.e., heart, lung, liver, spleen and kidney in both treated and control groups were similar in size and cell morphology.

Table 5.2 Number of survived ICR mice following a single (acute toxicity) and multiple (subacute toxicity) oral dosing of plumbagin

	Test group	Number of mice (survived/total)
Acute toxicity	Control (20% Tween-80)	6/6
	Plumbagin: 500 mg/kg body weight	0/6
	Plumbagin: 200 mg/kg body weight	4/6
	Plumbagin: 100 mg/kg body weight	6/6
Subacute toxicity	Control (20% Tween-80)	6/6
	Plumbagin: 100 mg/kg body weight/day	0/6
	Plumbagin: 50 mg/kg body weight/day	0/6
	Plumbagin: 25 mg/kg body weight/day	6/6
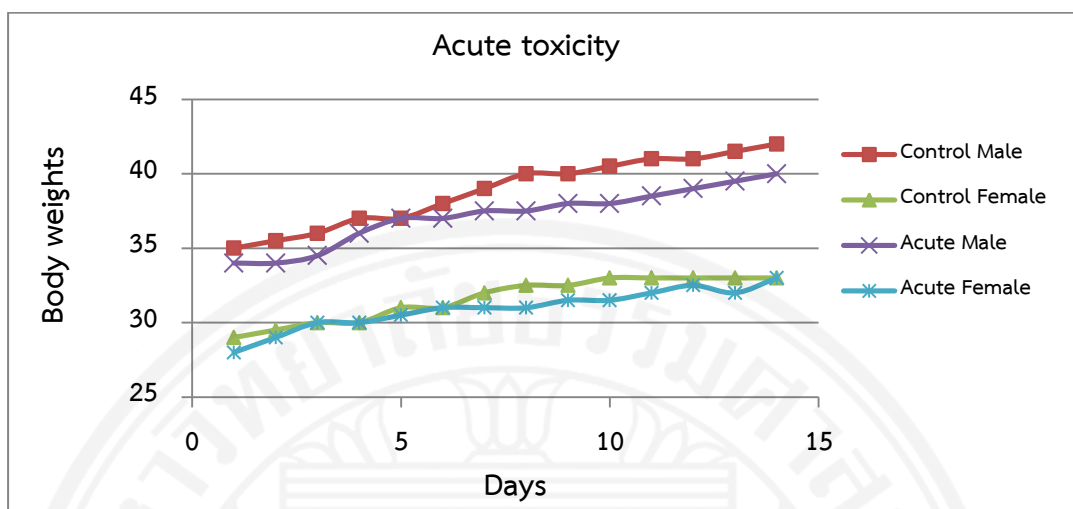
Figure 5.1 Median body weight (g) of male and female mice (n=6 for each group) during the first 14 days in the administration of a single oral dose of 100 mg/kg body weight of plumbagin and following 20% Tween-80 (control) in the acute toxicity test.
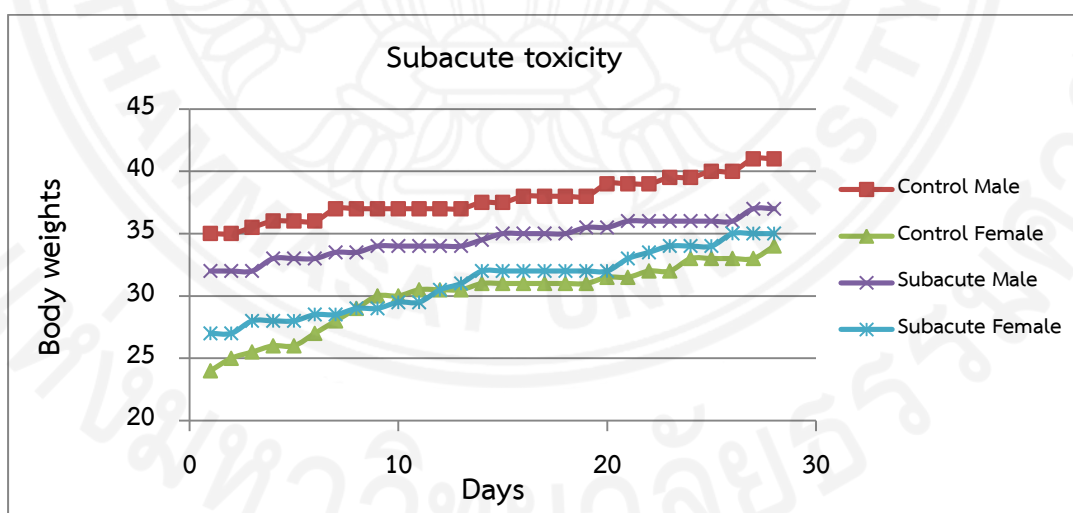
Figure 5.2 Median body weight (g) of male and female mice (n=6 for each group) during the 28 days following the administration of daily oral doses of 25 mg/kg body weight of plumbagin and 20% Tween-80 (control) in the subacute toxicity test.

5.1.3 Assessment of antimalarial activity of plumbagin in *P. berghei-*infected mouse model (4-day suppressive test)

Results of the 4-day suppressive antimalarial test of plumbagin and chloroquine in mice infected with *P. berghei* ANKA strain are summarized in **Table 5.3**. Median (range) parasite density on day 4 of the negative control group (20% Tween-80), mice treated with 1, 10 and 25 mg/kg body weight of plumbagin, and 10 mg/kg body weight of chloroquine were 37.8 (46.9-41.8), 35.6 (31.7-39.6), 35.05 (31.2-38.8), 22.3 (19.2-25.7) and 0 (0-0)%, respectively. Parasite density on day 4 in the control group treated with 20% Tween-80 was higher than the groups treated with chloroquine and 25 mg/kg body weight plumbagin. Chloroquine exhibited the most potent antimalarial activity with respect to its activity on reduction of parasitaemia on day 4 and prolongation of survival time. Parasite density (%) on day 4 following chloroquine treatment (0%) was significantly lower than 20% Tween 80 (negative control) and plumbagin at all dose levels ($p<0.05$). In addition, parasite suppression (%) of mice treated with chloroquine (100%) was significantly higher than the negative control group (0%) and the groups treated with 1 (5.5%), 10 (7.3%), and 25 (41%) mg/kg/day plumbagin ($p<0.01$). The survival time in the group treated with chloroquine was also significantly longer than the negative control and the groups treated with plumbagin at all dose levels ($p<0.01$).

Table 5.3 Antimalarial activity of plumbagin compared with chloroquine and negative control (treated with 20% Tween-80) against *P. berghei* ANKA strain in mice (4-day suppressive test)

Treatment	Dose (mg/kg body weight/day)	Parasite density (range: %) on Day 4	% Suppression at Day 4	Survival time (days)
Negative Control (20% tween 80)	-	37.8 (36.9-41.8)[a]	0	7 (6-7)
Plumbagin	1	35.6 (31.7-39.6)	5.8	7.5 (6-9)
	10	35.05 (31.2-38.8)	7.3	8 (8-9)
	25	22.3 (19.2-25.7)	41	10 (9-11)
Chloroquine	10	0 (0-0)[b]	100[c]	> 15[d]

Data are presented as median (range) values (6 mice for each group) of parasite density, % suppression and survival time.

[a] Significantly higher than the groups treated with 10 and 25 mg/kg body weight/day of plumbagin and 10 mg/kg body weight/day of chloroquine ($p < 0.05$).

[b] Significantly lower than negative control and the groups treated with 1, 10 and 25 mg/kg body weight/day of plumbagin ($p < 0.05$).

[c] Significantly higher than negative control and the groups treated with 1, 10 and 25 mg/kg body weight/day of plumbagin ($p < 0.05$).

[d] Significantly longer than negative control and the groups treated with 1, 10 and 25 mg/kg body weight/day of plumbagin ($p < 0.05$).

5.2 Permeability of plumbagin in caco-2 cell monolayers and their effects on the P-glycoprotein

5.2.1 *In vitro* cytotoxicity of plumbagin on Caco-2 cells

The viability of Caco-2 cells after exposure to plumbagin at the concentration ranges of 0-125 µM for 4 h and 0-62.50 for 48 h µM are shown in **Figure 5.3a** and **5.3b**, respectively. Following exposure for 4 h, plumbagin at 7.81, 15.63, 31.25, 62.50 and 125 µM inhibited cell growth to 83, 61, 37, 26 and 10% cell viability comparing with control, respectively. No toxic effect on Caco-2 cells was observed following exposure to 0.1% DMSO, 1.95, and 3.91 µM plumbagin (**Figure 5.3a**). For the 48 h exposure, plumbagin at 1.95, 3.91, 7.81, 15.63, 31.25 and 62.50 µM inhibited cell growth to 96.57, 88.92, 71.34, 35.09, 3.50 and 0.84% cell viability, respectively. No toxic effect on Caco-2 cells was observed following exposure to 0.1% DMSO, and 0.98 µM plumbagin (**Figure 5.3b**).
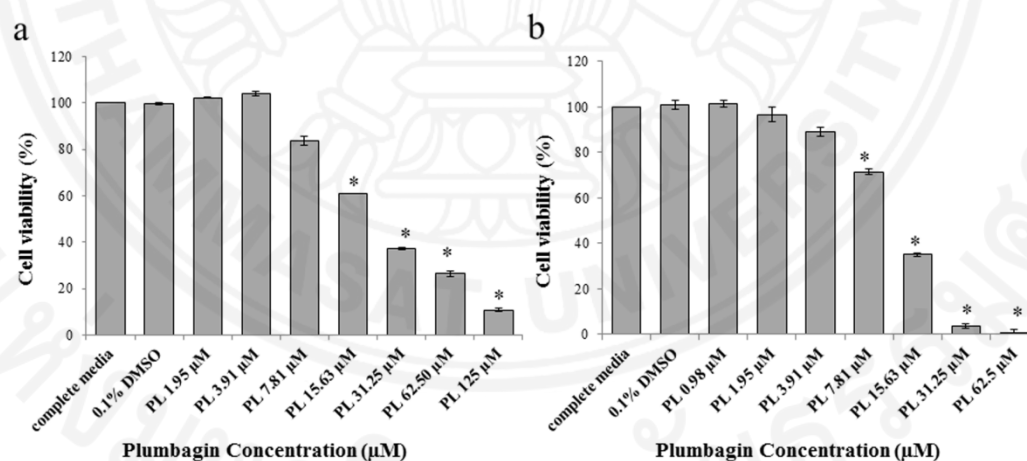
Figure 5.3 Effects of plumbagin on Caco-2 cell viability (MTT assay) following 4 (a) and 48 h (b) exposure. Data are presented as mean±SD values from triplicate determinations (duplicate of each). Complete medium, 0.1%DMSO and TritonX-100 were used as negative control, vehicle control and positive control, respectively.

* Statistically significant difference from control with $p<0.05$.

5.2.2 Caco-2 cell monolayers integrity

The baseline TEER values (mean±SD) of all Caco-2 cell monolayers of 1,479±111 Ω.cm^2 indicated the tightness of the junctions between cells.[131,161] The integrity of the cell monolayers during the experimental period was confirmed by the impermeability of Lucifer yellow across Caco-2 cell monolayers. After exposure to plumbagin, the average Lucifer yellow P_{app} values observed after 21 days were less than 0.5×10^{-6} cm/sec.[131]

5.2.3 Permeability of plumbagin across Caco-2 cell monolayers

The rate of transport of plumbagin at the concentration range of 2-8 µM across Caco-2 cell monolayers in the apical to basolateral (A-B) direction was much higher than that in the basolateral to apical (B–A) direction (**Figure 5.4**). Mean (±SD) values of apparent permeability coefficient (P_{app}) of plumbagin at 2, 4 and 8 µM for the A-B and B-A transport directions including the efflux ratio after 60 min incubation are presented in **Table 5.4**.
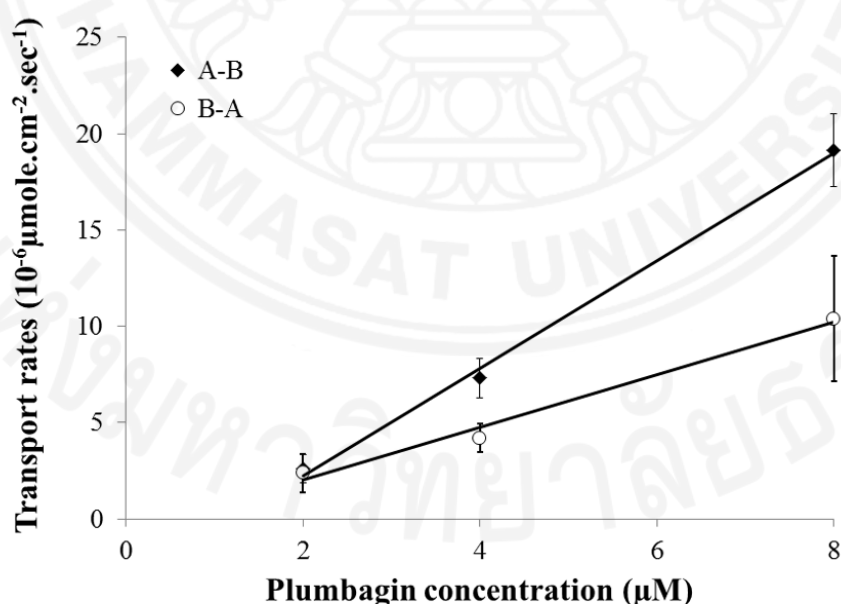
Figure 5.4 Transport rates of plumbagin across Caco-2 cell monolayers in the apical to basolateral (A-B) and the basolateral to apical (B-A) directions. Each data point represents the mean±SD for six independent experiments.

Table 5.4 Permeability of plumbagin (2, 4 and 8 µM) across Caco-2 cell monolayers. Results are expressed as mean±SD for six independent experiments.

Plumbagin	P_{app} ($\times 10^{-6}$ cm/s)		Efflux ratio
(µM)	B-A	A-B	
2	7.40±2.80	10.29±1.86	0.73±0.30
4	7.70±0.85	12.18±1.71	0.64±0.13
8	9.02±2.16	15.96±1.57	0.57±0.16

5.2.4 Effect of plumbagin on rhodamine 123 transport

Apparent permeability coefficient (P_{app}) and the efflux ratios of R123, R123 in the presence of plumbagin, and R123 in the presence of verapamil are summarized in **Table 5.5**. Plumbagin at all concentrations (1, 2, 4 and 8 µM) produced no effect on P-glycoprotein-mediated R123 transport across Caco-2 cell monolayers. On the other hand, verapamil (100 µM) significantly interfered with R123 transport, as indicated by a significant reduction in the mean efflux ratio (p<0.0001).

5.2.5 Effect of plumbagin on the function of P-glycoprotein in Caco-2 cells

Plumbagin at the concentrations of 1, 2 and 4 µM had no effect on the function of P-glycoprotein in Caco-2 cells. Following exposure to plumbagin at all concentrations for 24 or 48 h, the mean P_{app} of R123 transport across Caco-2 cells in the B–A and A–B directions were similar to that following exposure to 0.1 % DMSO and untreated cells. On the other hand, P_{app} of R123 transport across Caco-2 cells in the B–A and A–B directions were significantly difference from control (p = 0.004 and 0.006 for 24 and 48 h exposure, respectively) when exposing to verapamil (**Figure 5.5a and 5.5b**).

Table 5.5 Effect of plumbagin and the p-glycoprotein inhibitor verapamil on the bidirectional transport of R123. All the test compounds were added to donor side of the cell monolayers. Samples from the received compartment were collected at 120 min, and R123 concentration was measured using Micro-plate Multi-detection Instrument. Results are expressed as mean±SD of four independent experiments.

	Papp ($\times 10^{-6}$ cm/s)		Efflux ratio
	B-A	A-B	
R123 (control group)	12.18±1.96	1.99±0.19	6.11±0.47
R123 + 1 µM Plumbagin	10.98±2.59	1.77±0.33	6.15±0.38
R123 + 2 µM Plumbagin	11.06±2.04	1.81±0.24	6.10±0.66
R123 + 4 µM Plumbagin	11.68±1.37	1.92±0.17	6.11±0.66
R123 + 8 µM Plumbagin	10.87±1.00	1.76±0.20	6.20±0.33
R123 + 100 µM Verapamil	6.27±1.56[*]	3.15±0.48[**]	2.03±0.56[***]

[*] Statistically significant difference from control with p=0.011 (t-test)

[**] Statistically significant difference from control with p=0.004 (t-test)

[***] Statistically significant difference from control with p<0.0001 (t-test)
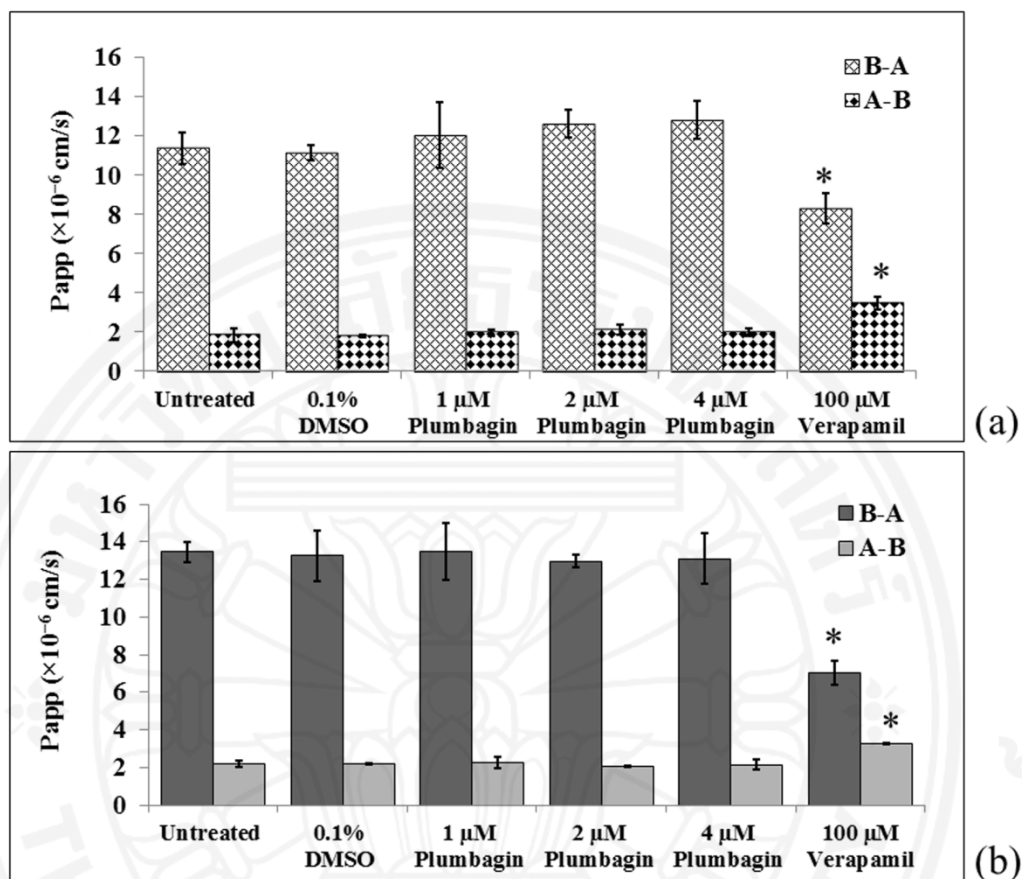
Figure 5.5 R123 transport across Caco-2 cell monolayers following 24 h (a) and 48 h (b) exposure to plumbagin (1, 2 and 4 µM), 01% DMSO, untreated control and verapamil (100 µM). Results are expressed as mean±SD of three independent experiments.

* For 24 h, statistically significant difference from control with p=0.004 (t-test)

* For 48 h, statistically significant difference from control with p=0.006 (t-test)

5.2.6 Effect of plumbagin on MDR-1 mRNA expression

Plumbagin at the concentrations of 1, 2 and 4 µM did not significantly interfere (up- or down-regulated) with MDR-1 expression in Caco-2 cell monolayers following 24 and 48 h exposure (**Figure 5.6**).
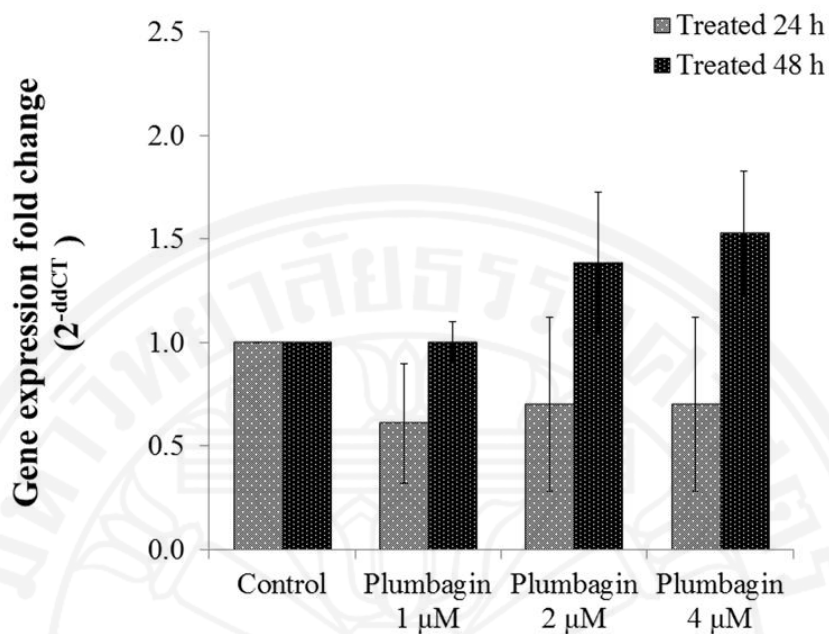
Figure 5.6 MDR-1 mRNA expression levels in Caco-2 cell monolayers following exposure for 24 and 48 h to plumbagin (1, 2 and 4 μM) and untreatd control. GAPDH was used as an internal control. MDR-1 mRNA expression was quantified by RT-PCR analysis in relation to GAPDH. Data are expressed as mean±SD of duplicated experiments.

5.3 Inhibitory activities of Thai medicinal plants with promising activities against malaria on human CYP

The inhibitory effects of all the plant extracts on CYP1A2, CYP2C19, CYP2D6 and CYP3A4 are presented in **Table 5.6.** The selective inhibitor of CYP1A2 α-naphthoflavone, exhibited the most potent inhibitory activity on enzyme activity with mean IC_{50} of 0.01 µg/ml. DM exhibited most potent activity with IC_{50} values higher than α–naphthoflavone about 100 fold ($p<0.05$). DM, DL and GM were classified in the moderate potencies (IC_{50} 1.04-9.87 µg/ml), whereas PI and MF exhibited relatively low potencies (IC_{50} 12.95 and 22.05 µg/ml, respectively).

With regard to the inhibitory activity on CYP2C19, mean IC_{50} of the selective inhibitor nootkatone was 5.64 µg/ml. The inhibitory activities of PI and DM were classified in the most potent group with potency comparable to that of nootkatone (mean IC_{50} 4.71 and 6.92 µg/ml, respectively, $p>0.05$). DL and MF exhibited moderate potencies (mean IC_{50} 10.83-12.31 µg/ml), while GM exhibited the lowest potency (mean IC_{50} 61.75 µg/ml).

The selective inhibitor quinidine showed the most potent inhibitory activity on CYP2D6 activity with mean IC_{50} of 0.97 µg/ml. DM, DL and PI showed the highest inhibitory activities (mean IC_{50} 2.93-9.57 µg/ml). The potency of inhibitory activitiy of DM was comparable to that of quinidine ($p>0.05$). GM exhibited moderate potencies (mean IC_{50} 23.40 µg/ml) while MF exhibited relatively low potencies (mean IC_{50} 195.83 µg/ml).

The selective inhibitor ketoconazole showed the most potent inhibitory activity on CYP3A4 with mean IC_{50} of 0.23 µg/ml. DM, DL and PI were most potent with mean IC_{50} 3.06-6.43 µg/ml. GM exhibited moderate potencies (mean IC_{50} 11.33 µg/ml) while MF exhibited relatively low potencies (mean IC_{50} 41.91 µg/ml,) (**Table 5.6**).

Table 5.6 Mean±SD IC_{50} values for CYP1A2, CYP2C19, CYP2D6 and CYP3A4 activities by crude ethanolic extracts of five Thai medicinal plants with promising activities against malaria (DM, DL, MF, PI and GM) compared with selective inhibitors in each CYP in pooled (50 donor) human liver microsomes (n=4).

Plant Name	CYP1A2		CYP2C19		CYP2D6		CYP3A4	
	IC_{50} (µg/ml)	*p*-value	IC_{50} (µg/ml)	*p*-value	IC_{50} (µg/ml)	*p*-value	IC_{50} (µg/ml)	*p*-value
Selective inhibitor	0.01± 0.00	-	5.64±0.32	-	0.97±0.06*	-	0.23±0.004	-
Dioscorea membranacea Pierre (DM)	1.04±0.14	0.045[**]	6.92±1.07	0.246	2.93±0.24	0.052	4.35±0.35	0.038[**]
Dracaena loureiri Gagnepv (DL)	1.97±0.02	0.005[**]	10.83±0.35	0.004[**]	9.57±0.48	0.025[**]	3.06±0.13	0.02[**]
Myristica fragrans Houtt (MF)	22.05±0.88	0.018[**]	12.31±0.93	0.011[**]	195.83±3.66	0.008[**]	41.91±2.19	0.001[**]
Plumbago indica Linn (PI)	12.95±1.25	0.044[**]	4.71±0.21	0.076	7.20±0.44	0.031[**]	6.43±0.42	0.031[**]
Garcinia mangostana Linn (GM)	9.87±0.22	0.01[**]	61.75±1.59	0.0001[**]	23.40±1.05	0.021[**]	11.33±0.42	0.001[**]

*Taesotikul et al., 2011

[**] *Significantly higher than the selective inhibitor*

5.4 Investigation the *in vitro* inhibition and *in vivo* induction CYP-mediated hepatic metabolism of plumbagin

5.4.1 Analytical *in vitro* inhibition assay validation

The analytical methods for determination of paracetamol, 5-hydroxyomeprazole, and oxidized nifedipine used in the study was found to be sensitive and accurate. The linearity of all calibration curves were demonstrated with coefficient (r^2) of greater than 0.995.

CYP1A2-mediated metabolism: The LOQ of paracetamol at a signal-to-noise ratio≥10 was 1 µM. The precision (intra- and inter-) of analytical method (% RSD) was<6.3% and the accuracy (intra- and inter-) of the method was <±10% (**Table 5.7**). CYP2C19-mediated metabolism: The LOQ of 5-hydroxyomeprazole at a signal-to-noise ratio≥10 was 40 nM. The precision (intra- and inter-) of analytical method (% RSD) was<6.22% and the accuracy (intra- and inter-) of the method was<±7% (**Table 5.8**). CYP3A4-mediated metabolism: The LOQ of oxidized nifedipine at a signal-to-noise ratio≥10 was 1 µM. The precision (intra- and inter-) of analytical method (% RSD) was<7.05% and the accuracy (intra- and inter-) of the method was<±6% (**Table 5.9**).

5.4.2 CYP inhibition

The inhibitory effects of plumbagin and positive controls on the activities of three major human CYP isoforms, *i.e.*, CYP1A2, CYP2C19 and CYP3A4 are shown in **Figure 5.7A–C** and the IC_{50} values are presented in **Table 5.10.** Plumbagin clearly inhibited CYP1A2-mediated phenacetin *O*-deethylation, CYP2C19-mediated omeprazole hydroxylation and CYP3A4-mediated nifedipine oxidation in concentration-dependent manners. Among the three CYP isoforms, the inhibitory activity was most potent for CYP2C19, of which its potency was about 35-fold of the selective inhibitor nootkatone (mean IC_{50} values of 0.78 µM *vs* 27.31 µM). The inhibitory activities on CYP1A2 and CYP3A4 were moderate (about 13- to 69-fold lower than the selective inhibitors).

Table 5.7 Intra- and inter-assay accuracy and precision values of the HPLC method for determination inhibitory effect of plumbagin on CYP1A2-mediated phenacetin *O*-deethylation (n=3).

Quantity of paracetamol	Accuracy (%Bias)		Precision (%RSD)	
spiked (µM)	Intra-assay	Inter-assay	Intra-assay	Inter-assay
1	-4.63	-9.18	1.32	6.21
5	-8.10	-4.44	6.30	6.28
10	3.17	-1.92	2.85	5.73
25	4.46	3.54	3.01	5.70
50	-1.13	-0.78	0.86	1.23

Table 5.8 Intra- and inter-assay accuracy and precision values of the HPLC method for determination inhibitory effect of plumbagin on CYP2C19-mediated omeprazole hydroxylation (n=3).

Quantity of 5-hydroxy	Accuracy (%Bias)		Precision (%RSD)	
omeprazole spiked (nM)	Intra-assay	Inter-assay	Intra-assay	Inter-assay
40	3.21	3.23	1.46	2.69
200	-5.86	-6.43	2.03	1.80
800	0.89	2.26	3.93	4.64
1,600	3.25	3.52	4.63	2.16
2,500	4.45	4.06	4.08	6.22

Table 5.9 Intra- and inter-assay accuracy and precision values of the HPLC method for determination inhibitory effect of plumbagin on CYP3A4-mediated nifedipine oxidation (n=3).

Quantity of oxidized nifedipine spiked (µM)	Accuracy (%Bias)		Precision (%RSD)	
	Intra-assay	Inter-assay	Intra-assay	Inter-assay
1	-0.94	2.38	1.17	7.05
2.5	2.64	5.20	3.60	0.92
5	-1.41	-2.73	5.39	3.54
12.5	0.07	-1.19	4.51	3.23
25	0.01	0.35	0.93	0.72

Table 5.10 IC$_{50}$ values (µM) of plumbagin and selective inhibitors on CYP1A2-mediated phenacetin *O*-deethylation, CYP2C19-mediated omeprazole hydroxylation and CYP3A4-mediated nifedipine oxidation. Results are expressed as mean±SD (n=4).

Compound	CYP1A2	CYP2C19	CYP3A4
α-naphthoflavone (selective inhibitor for CYP1A2)	0.02±0.36	-	-
Nootkatone (selective inhibitor for CYP2C19)	-	27.31±0.66	-
Ketoconazole (selective inhibitor for CYP3A4)	-	-	0.18±0.06
Plumbagin	1.39±0.01	0.78±0.01	2.37±0.10
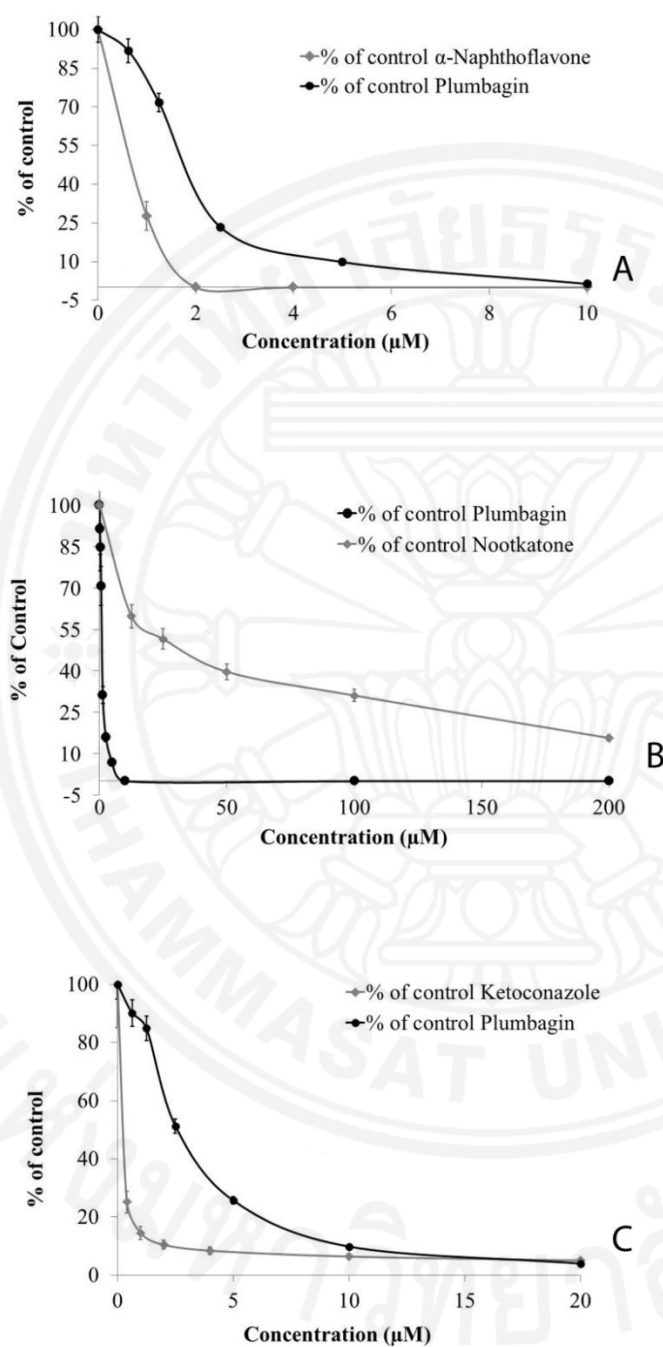
Figure 5.7 Inhibitory activities of plumbagin and selective inhibitors on (A) CYP1A2-mediated phenacetin *O*-deethylation, (B) CYP2C19-mediated omeprazole hydroxylation, and (C) CYP3A4-mediated nifedipine oxidation (n=4 for each experiment).

5.4.3 CYP induction

5.4.3.1 Inducing activity of plumbagin on CYP1A2 and CYP3A11 activity

Inducing activity of plumbagin on CYP1A2 and CYP3A11 activities was determined by comparison of CYP1A2 and CYP3A11 activities from mouse liver microsomes between the treated (induced with plumbagin for 28 days) and control groups. CYP1A2 and CYP3A11 activities were determined through investigation of the concentration of each CYP-mediated metabolite (**Figure 5.8**). Plumbagin slightly inhibited CYP1A2 activity but did not to significant level. Plumbagin did not induce CYP1A2-mediated phenacetin *O*-deethylation and CYP3A11-mediated nifedipine oxidation.
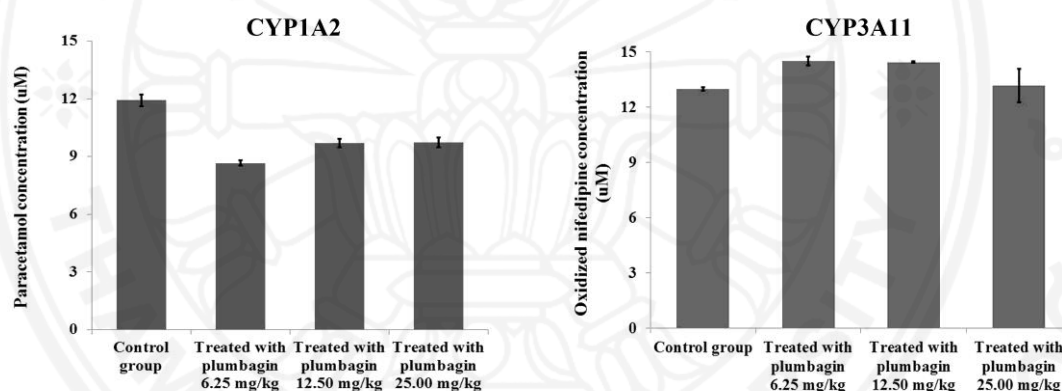
Figure 5.8 CYP1A2 and CYP3A11-mediated metabolite in mouse liver microsomes from the treated (induced by plumbagin for 28 days) and the control groups. Data were expressed as mean±SD from triplicated experiments (n=3).

5.4.3.2 Inducing activity of plumbagin on CYP1A2 and CYP3A11 mRNA expression

The inducing activity of plumbagin on CYP1A2 and 3A11 at mRNA level was evaluated by using RT-PCR. Plumbagin (6.25, 12.50 and 25.00 mg/kg body weight) did not up-regulate the CYP1A2 and 3A11 mRNA expression (**Figure 5.9**). On the other hand, plumbagin of all dose levels down-regulate of the CYP1A2 mRNA expression, but did not reach the level of significance (**Figure 5.9**).
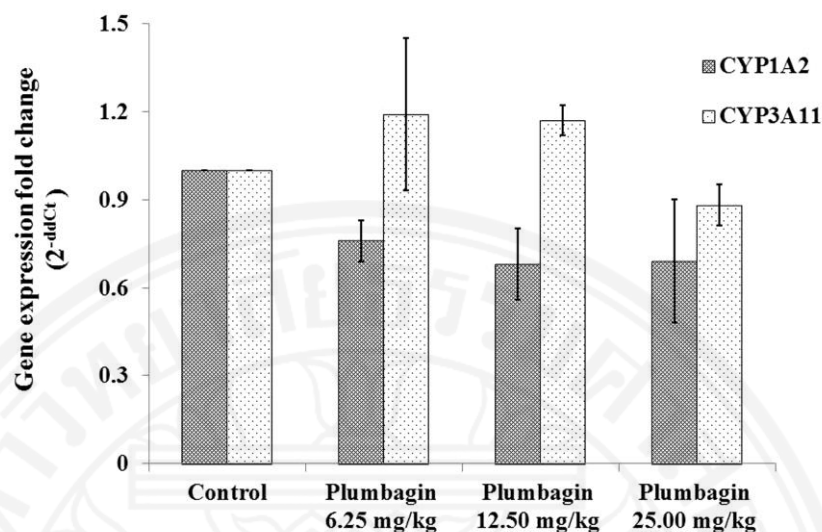
Figure 5.9 CYP1A2 and 3A11mRNA expression levels in mouse liver cells treated (6.25, 12.50 and 25.00 mg/kg body weight for 28 days of plumbagin) and control groups. GAPDH was used as an internal control. CYP1A2 and 3A11mRNA expression levels were quantified by RT-PCR analysis in relation to GAPDH. Data are expressed as mean±SD from triplicated experiments (n=3).

5.5 Toxicity and pharmacokinetics of plumbagin in wistar rats model

5.5.1 *In vivo* toxicity test

The toxicity of plumbagin in rats was investigated in order to define optimal dose of plumbagin to be used for investigation of its pharmacokinetics study in wistar rats model. Results indicated virtually no toxicity of plumbagin at a maximum single oral dose of 150 mg/kg body weight. All rats survived following a single oral dose of 150 mg/kg body weight plumbagin and 20% Tween-80 (control) **(Table 5.11)**. There was no visible sign of toxicity, or any change in water and food consumption and the body weights of rats in both groups during the 14 days of observation **(Figure 5.10).** At higher doses (250 and 500 mg/kg body weight), it produced toxic signs and symptoms including anxiety, salivation, exhibited chewing, and agitation. Then were observed in in 3/6 and 6/6 of rats following the doses of 250 and 500 mg/kg body weight, respectively; all subsequently died within 24 h.

Plumbagin at a single dose 150 mg/kg body weight was considered well tolerated. Three rats survived following a single oral dosing of 250 mg/kg body weight plumbagin. The LD_{50} of the plumbagin was 250 mg/kg body weight. Histopathological examination of various organs (liver, kidney, heart, spleen, and lung) revealed no significant change in size and morphology in both treated single dose 150 mg/kg body weight and control.

For subacute toxicity test, all rats survived following a daily oral dose of 25 mg/kg body weight plumbagin and 20% Tween-80 (control) for 28 days **(Table 5.14)**. There was no abnormality in behavior, sign of toxicity, nor changes in water and food consumption in both groups during the 28 days observation period. There was no significant difference (p>0.05) in body weights between both groups **(Figure 5.11)**. Histopathological examination of various organs (liver, kidney, heart, spleen, and lung) revealed no significant change in size and morphology in animals of both group. Plumbagin at a repeated dose of 25 mg/kg body weight daily for 28 days considered well tolerated. Blood chemistry and hematology of rats treated with 25 mg/kg body weight plumbagin daily for 28 days and control group are summarized in **Table 5.12** and **Table 5.13**, respectively. Blood morphology of both groups was normal. There were no significant differences (p>0.05) in red blood cells (RBC), hemoglobin, hematocrit, white blood cells (WBC), neutrophils, eosinophils, lymphocytes, monocytes and platelets count between both groups. In addition, there were no significant differences (p>0.05) in serum AST and ALT levels in both groups. Furthermore, serum glucose, BUN, creatinine, cholesterol and triglyceride levels of rats following a daily oral dose of 25 mg/kg body weight plumbagin for 28 days were not significantly different from the control group (p>0.05). Toxic signs and symptoms including anxiety, salivation, exhibited chewing and agitation were observed in 2/6 and 6/6 of rats following the doses of 50 and 100 mg/kg body weight, respectively. All rats receiving 100 mg/kg body weight of plumbagin daily for 28 days died within 6-10 days, whereas two rats receiving 50 mg/kg body weight dosing died within 12-16 days.

Table 5.11 Number of survived wistar rats following a single (acute toxicity) and multiple (subacute toxicity) oral dosing of plumbagin

	Test group	Number of rats (survived/total)
Acute toxicity	Control (20% Tween-80)	6/6
	Plumbagin: 500 mg/kg body weight	0/6
	Plumbagin: 250 mg/kg body weight	3/6
	Plumbagin: 150 mg/kg body weight	6/6
Subacute toxicity	Control (20% Tween-80)	6/6
	Plumbagin: 100 mg/kg body weight	0/6
	Plumbagin: 50 mg/kg body weight	4/6
	Plumbagin: 25 mg/kg body weight	6/6
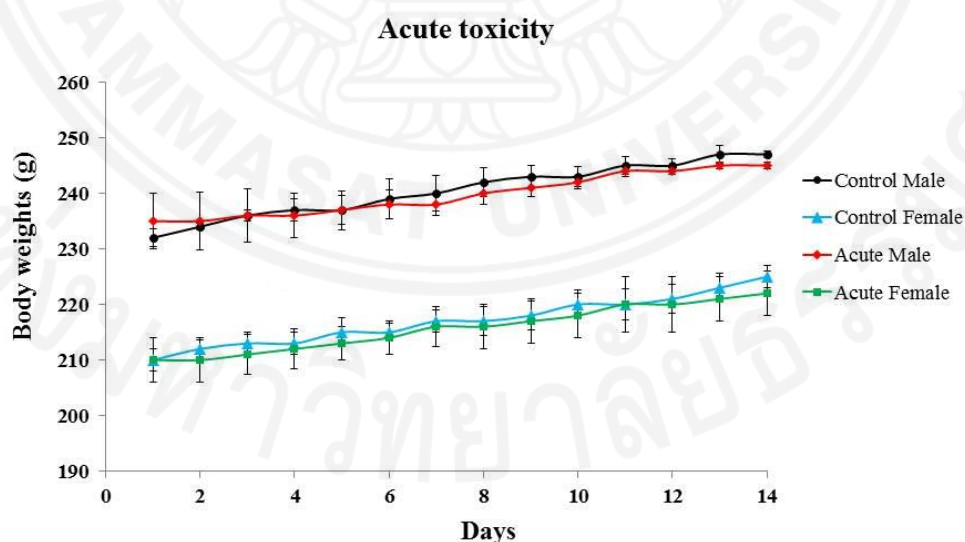
Figure 5.10 Body weights of male and female rats during the first 14 days following the administration of a single oral dose of 150 mg/kg body weight of plumbagin compared with control (n=6 for each group). Data are presented mean±SD.
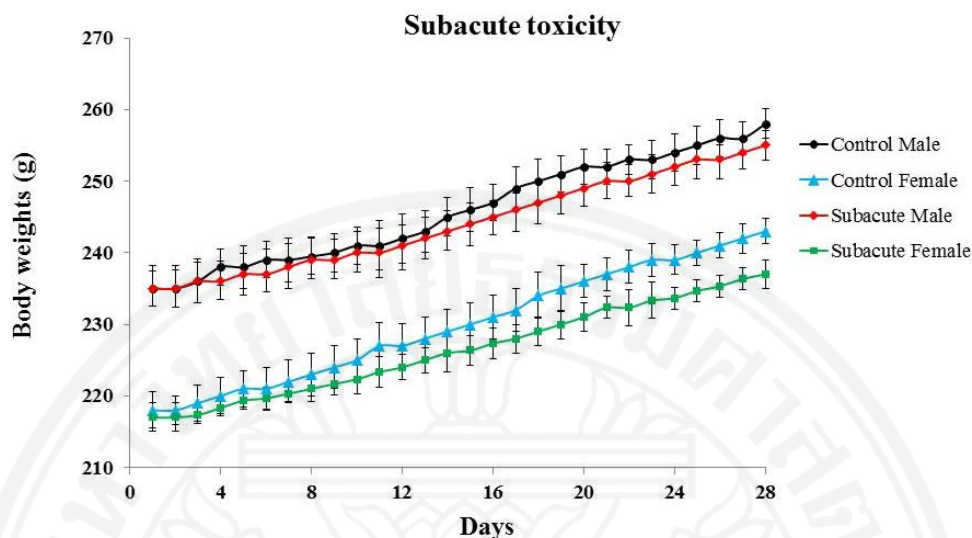
Figure 5.11 Body weights of male and female rats following the administration of oral dose of 25 mg/kg body weight of plumbagin for 28 days compared with control (n=6 for each group). Data are presented as mean±SD.

Table 5.12 Effects of plumbagin on blood chemistry parameters in serum of rats after daily oral administration at 25 mg/kg body weight for 28 days (n = 6 for each group). Data are presented as mean±SD.

Parameter	Control	Plumbagin 25 mg/kg body weight
Glucose (mg/dl)	254±47.92	240.00±33.76
BUN (mg/dl)	20.17±3.19	20.67±3.83
Creatinine (mg/dl)	0.50±0.00	0.50±0.00
Cholesterol (mg/dl)	68.17±2.32	73.33±5.65
Triglyceride (mg/dl)	106.00±7.75	110.50±7.61
AST (U/L)	144.50±22.45	155.50±16.74
ALT (U/L)	36.00±5.44	36.83±3.49

Table 5.13 Hematological parameters of rats after treatment with 25 mg/kg body weight plumbagin given daily for 28 days (n=6 for each group). Data are presented as mean±SD.

Parameter	Control	Plumbagin 25 mg/kg body weight
RBC $(\times 10^6/\mu l)$	8.24±0.29	8.03±0.36
Hemoglobin (g/dl)	14.93±0.37	14.63±0.62
Hematocrit (%)	47.80±1.66	47.13±2.05
WBC $(\times 10^3/\mu l)$	8.97±0.43	9.27±0.51
Neutrophils $(\times 10^3/\mu l)$	1.92±0.06	2.18±0.36
Eosinophils $(\times 10^3/\mu l)$	0.50±0.55	0.33±0.52
Lymphocytes $(\times 10^3/\mu l)$	7.46±0.16	7.54±0.17
Monocytes $(\times 10^3/\mu l)$	0.33±0.52	0.34±0.52
Platelets count $(\times 10^3/\mu l)$	876.17±92.41	861.33±75.99
Blood morphology	Normal	Normal

5.5.2 LC-MS/MS analysis of plumbagin concentrations in plasma and urine samples

C18 reversed-phase column with the mobile phase consisting of a mixture of (A) water containing 0.1% formic acid and (B) 100% methanol, running with gradient mode provided a good separation of plumbagin eluted within 10 min. This specificity method was showed by MRM chromatograms of plumbagin and honokiol (IS) for drug-free plasma, a spiked plumbagin 500 ng/ml in plasma sample and a plasma sample from a rat 3 h after oral administration. As shown in **Figure 5.12**, no significant interfering peaks were present near the analyte peak in the drug-free rat plasma. The linearity of plumbagin 10-2,000 ng/ml in plasma and 50-50,000 ng/ml in urine for calibration curves were demonstrated with correlation coefficients greater than 0.999. The limit of quantitation of plumbagin (LOQ, signal-to-noise ratio≥10) was 10 ng/ml with accuracy (intra- and inter-) within ±15% and precision

(intra- and inter-) of analytical method (% RSD) was≤15%. Precision and accuracy of the analytical method were determined by replicate analyses (n=3).

Ethyl acetate was choosed as the organic solvent for liquid/liquid extraction method due to ethyl acetate is a high polarity and volatility solvent. This extraction method was modified from Hsieh *et al*.[120] The extraction recovery of plumbagin were determined by comparing the peak area of plumbagin in plasma and urine samples that had been spiked with the analyte extraction with that for samples to which plumbagin had been added post-extraction. Ethyl acetate produced in about 43-63% recovery of plumbagin from plasma and urine. A plasma concentration–time profile of plumbagin is shown in **Figure 5.13**. Plumbagin was detected in the plasma samples collected within 1-48 h after the oral administration, but was not detected in the samples collected after oral administration 72 h. Concentrations determined from four rats were averaged and used for estimation of the pharmacokinetic parameters of plumbagin (**Table 5.14).**

Plumbagin was found in the urine samples collected from Day 1 to Day 4 after dosing in all rats, but was not detected on Day 5 (**Table 5.15**). The half-life of plumbagin was 9.98±1.63 h (mean±SD). Time to reach maximum blood concentration (T_{max}) and maximum blood concentration (C_{max}) were 5.00±0.00 h and 0.46±0.08 µg/ml, respectively. The mean residence time (MRT) was 13.67±1.62 h. The area under the time curve for (AUC_{0-inf}) and (AUC_{0-48h}) were 6.72±0.74 and 6.47±0.62 µg•h/ml, respectively. Systemic clearance (CL) and volume of distribution (Vd) were 7.51±0.84 (l/h) and 0.11±0.01 L, respectively.
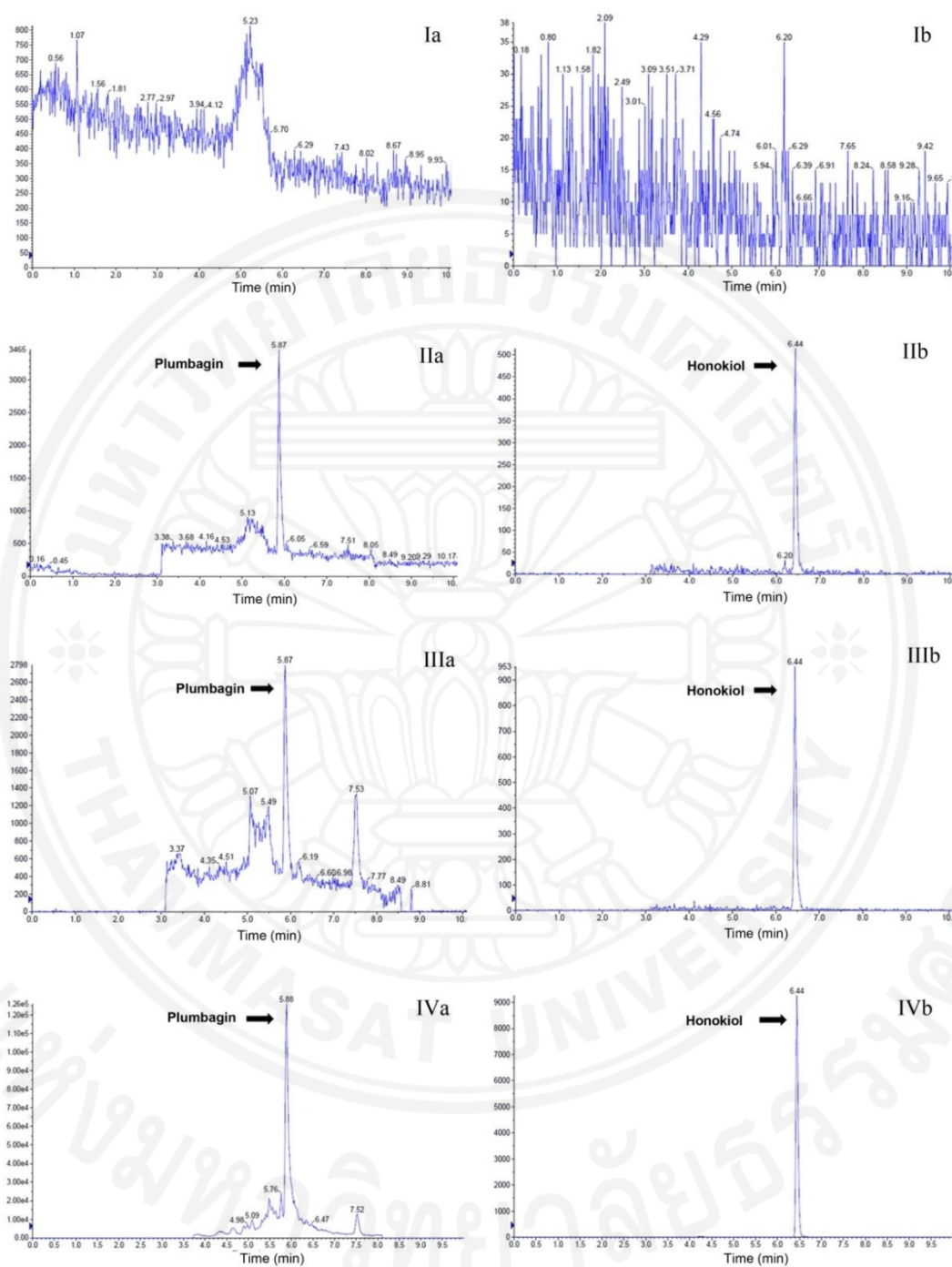
Figure 5.12 MRM chromatograms of plumbagin and honokiol as internal standard (a) plumbagin (m/z 187⟶159); (b) IS (m/z 265⟶224). (I) drug-free plasma; (II) plasma spiked with 500 ng/ml of plumbagin and 10 ng/ml of IS; (III) a plasma sample (435.12 ng/ml) 3 h and (IV) a urine sample (349.45 µg/ml) at 24 h after oral administration.
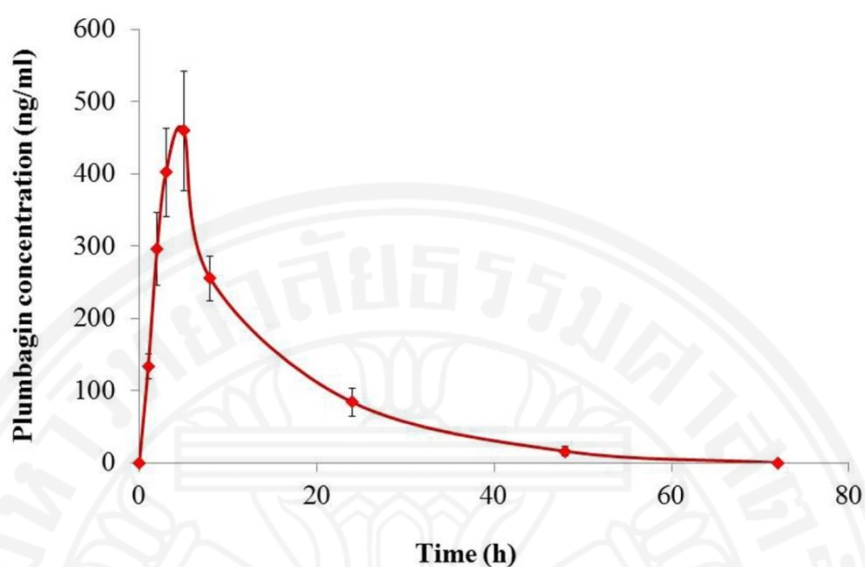
Figure 5.13 Mean plasma concentration–time profile of plumagin in wistar rats (n=4) after a single oral administration of 100 mg/kg body weight of plumbagin.

Table 5.14 The pharmocokinetic parameters of plumbagin after oral administration of 100 mg/kg body weight of plumbagin to healthy wistar rats (mean±SD, n=4)

Parameter	Plumbagin
$T_{1/2}$ (h)	9.98 ± 1.63
T_{max} (h)	5.00 ± 0.00
C_{max} (µg/ml)	0.46 ± 0.08
AUC_{0-48h} (µg•h/ml)	6.47 ± 0.62
AUC_{0-inf} (µg•h/ml)	6.72 ± 0.74
MRT (h)	13.67 ± 1.62
Vd (l)	0.11 ± 0.01
CL (l/h)	7.51 ± 0.84

Table 5.15 Amount of plumbagin in urine sample collected from wistar rats after a single oral administration of 100 mg/kg body weight of plumbagin (mean±SD, n=4)

Urine samples	Amount of plumbagin (µg)
DAY 1 (24 h)	371.55±68.19
DAY 2 (48 h)	242.69±156.88
DAY 3 (72 h)	14.62±13.19
DAY 4 (96 h)	1.75±0.70
DAY 5 (120 h)	0.00±0.00

5.6 Application of SPECT/CT imaging system and radiochemical analysis for investigation of blood kinetics and tissue distribution of radiolabeled plumbagin in healthy and *P. berghei*-infected mice

5.6.1 Determination of radiolabeling efficiency

Plumbagin was labelled with ^{99m}technetium and stannous chloride dihydrate under various conditions and the labelling yield was optimized. The radiolabeling yield was found to be pH-dependent. The optimal condition for ^{99m}Tc-plumbagin labelling was obtained using 50 µg/ml of stannous chloride dihydrate at pH 6.5 with radiolabeling efficiency of greater than 98% (**Table 5.16 and Figure 5.14**).

5.6.2 *In vitro* and *in vivo* stability of ^{99m}Tc-plumbagin complex

Results of *in vitro* and *in vivo* stability studies suggested satisfactory stability profile of ^{99m}Tc-plumbagin complex. The *in vitro* stability of ^{99m}Tc-plumbagin complex in normal saline and plasma were 95 and 92% at 24 h of incubation (37ºC), respectively (**Table 5.17**). The *in vivo* stability was also correlated with the *in vitro* data with approximately 92 and 80% stability of the radiolabel complex up to 6 and 24 h of incubation (37ºC) (**Table 5.17**).

Table 5.16 Effect of stannous chloride dihydrate on the labelling efficiency of ^{99m}technetium with plumbagin. Data are expressed as median with 95% CI for median (n=6).

Stannous chloride dihydrate concentration (µg/ml)	% Label	% R/H
25	97.76 (97.67-97.81)	2.23 (2.11-2.33)
50	98.48 (98.07-98.72)	1.52 (1.32-1.64)
100	58.57 (50.48-63.74)	40.38 (33.91-48.07)
200	40.34 (28.57-48.11)	58.07 (50.57-66.84)

R/H = reduced/hydrolysed
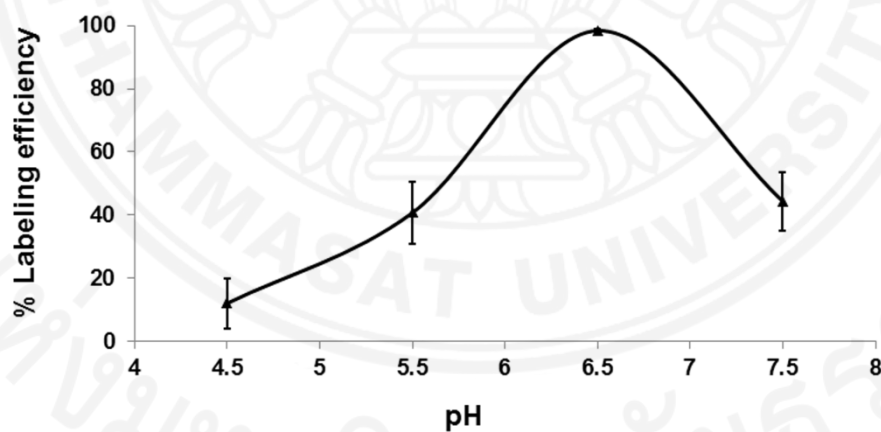
Figure 5.14 Effect of pH on labelling efficiency of ^{99m}Tc with plumbagin. Data are expressed as median with 95% CI for median (n=6).

Table 5.17 *In vitro* and *in vivo* stability of ^{99m}Tc-plumbagin complex at different time points up to 24 h after incubation in normal saline or mice plasma at 37°C. Data are expressed as median with 95% CI for median (n=4).

Incubation	% *In vitro* stability		% *In vivo* stability
Time (h)	Normal saline	Plasma	
0	99.09 (99.03-99.16)	98.99 (98.86-99.19)	98.23 (97.01-99.13)
1	98.97 (98.79-99.11)	98.74 (98.30-99.27)	98.23 (97.87-98.68)
2	98.73 (98.36-99.00)	98.33 (98.11-98.51)	92.57 (88.86-97.50)
4	98.45 (98.17-98.66)	98.03 (97.57-98.77)	93.02 (86.34-98.24)
6	97.77 (97.09-98.40)	97.65 (97.00-98.31)	91.63 (89.52-94.24)
24	95.47 (94.51-96.22)	92.21 (90.46-94.90)	80.42 (78.38-82.35)

5.6.3 Blood kinetics of ^{99m}Tc-plumbagin complex

Blood concentration-time profile of ^{99m}Tc-plumbagin complex in healthy mice and *P. berghei*-infected mice following intravenous injection of ^{99m}Tc-plumbagin complex (740 KBq) are presented in **Figure 5.15** and the pharmacokinetic parameters are summarized in **Table 5.18**. The mean residence time (MRT) of the labelled complex in healthy mice (3.16 h) was significantly longer than *P. berghei*-infected mice (2.21 h) ($p<0.001$). In addition, the area under the time curve (AUC$_{0-inf}$) was significantly higher in healthy (13.54 %ID/g*h) compared with *P. berghei*-infected (7.85 %ID/g*h) mice ($p<0.001$). On the other hand, systemic clearance (CL) and volume of distribution (Vd) of ^{99m}Tc-plumbagin were significantly higher in *P. berghei*-infected (12.76 l/h *vs* 41.95 ml) compared with healthy (7.39 l/h *vs* 29.56 ml) mice ($p<0.001$).
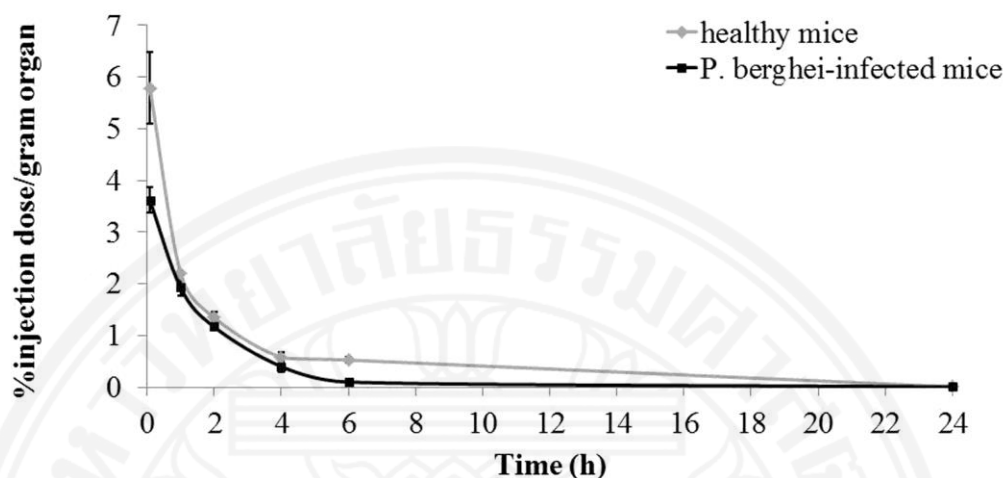
Figure 5.15 Blood concentration-time profiles of ^{99m}Tc-plumbagin following intravenous injection in healthy and *P. berghei*-infected mice. Data are expressed as median with 95% CI for median (n=4).

5.6.4 Biodistribution of ^{99m}Tc-plumbagin in healthy and *P. berghei*-infected mice

The biodistribution of the ^{99m}Tc-plumbagin complex in different organs of the healthy and *P. berghei*-infected mice at 5 min, 1, 2, 4, 6, and 24 h post intravenous injection are presented in **Figure 5.16** (a and b). In healthy mice, the labelled complex distributed to all organs but with high intensity in liver, followed by lung, stomach, large intestine, and kidney. Relatively lower levels of labelled complex uptake were observed in heart, brain, and spleen. The accumulation was markedly observed in liver and lung as early as 5 min after dosing [61.84 (56.38-67.3) and 12.14 (8.12-16.15) %ID/whole organs for liver and lung, respectively]. Clearance of the complex from blood circulation, as well as lung and liver was rapid and completed within 24 h of dosing (**Figure 5.16a**). In *P. berghei*-infected mice, ^{99m}Tc-plumbagin complex extensively distributed to liver, lung, spleen, kidney and stomach. It was noted that the accumulation of the complex in spleen was significantly higher than that in healthy mice [3.93 (2.07-5.79) *vs* 0.74 (0.52-0.95) % ID/whole organs] at 5 min of dosing (*p*=0.012). Clearance of the complex from blood

circulation and lung was rapid (**Figure 5.16b**). Relatively lower levels of ^{99m}Tc-plumbagin complex uptake were observed in heart and brain. Elimination of the complex from all organs was almost complete within 24 h of dosing.

Table 5.18 Pharmacokinetic parameters of ^{99m}Tc-plumbagin complex following intravenous injection in healthy and *P. berghei*-infected mice (4 mice each). Data are expressed as median with 95% CI for median (n=4).

Parameter	Healthy mice	*P. berghei*-infected mice
T_{max} (h)	0.08 (0.08-0.08)	0.08 (0.08-0.08)
C_{max} (%ID/g)	5.79 (4.68-6.89)[a]	3.50 (3.10-3.89)
AUC_{0-t} (%ID/g *h)	13.52 (12.80-14.24)[a]	7.84 (7.36-8.31)
AUC_{0-inf} (%ID/g *h)	13.54 (12.83-14.25)[a]	7.85 (7.36-8.33)
$T_{1/2}$ (h)	2.77 (2.49-3.05)[b]	2.28 (2.13-2.42)
MRT (h)	3.16 (2.85-3.47)[b]	2.21 (1.98-2.43)
V_d (ml)	29.56 (25.21-33.90)[c]	41.95 (38.38-45.52)
CL (l/h)	7.39 (7.01-7.77)[c]	12.76 (11.95-13.57)

T_{max} = time to maximum plasma maximum concentration (C_{max}), AUC_{0-t} = area under the blood concentration curve from administration to last observed concentration at t, AUC_{0-inf} = area under the plasma time curve extrapolated to infinity, $T_{1/2}$ = elimination half-life, MRT = mean residence time (MRT), Vd = volume of distribution, CL = clearance.

[a]*Significantly higher than P. berghei-infected group (p<0.001)*

[b]*Significantly longer than P. berghei-infected group (p<0.001)*

[c]*Significantly lower than P. berghei-infected group (p<0.001)*
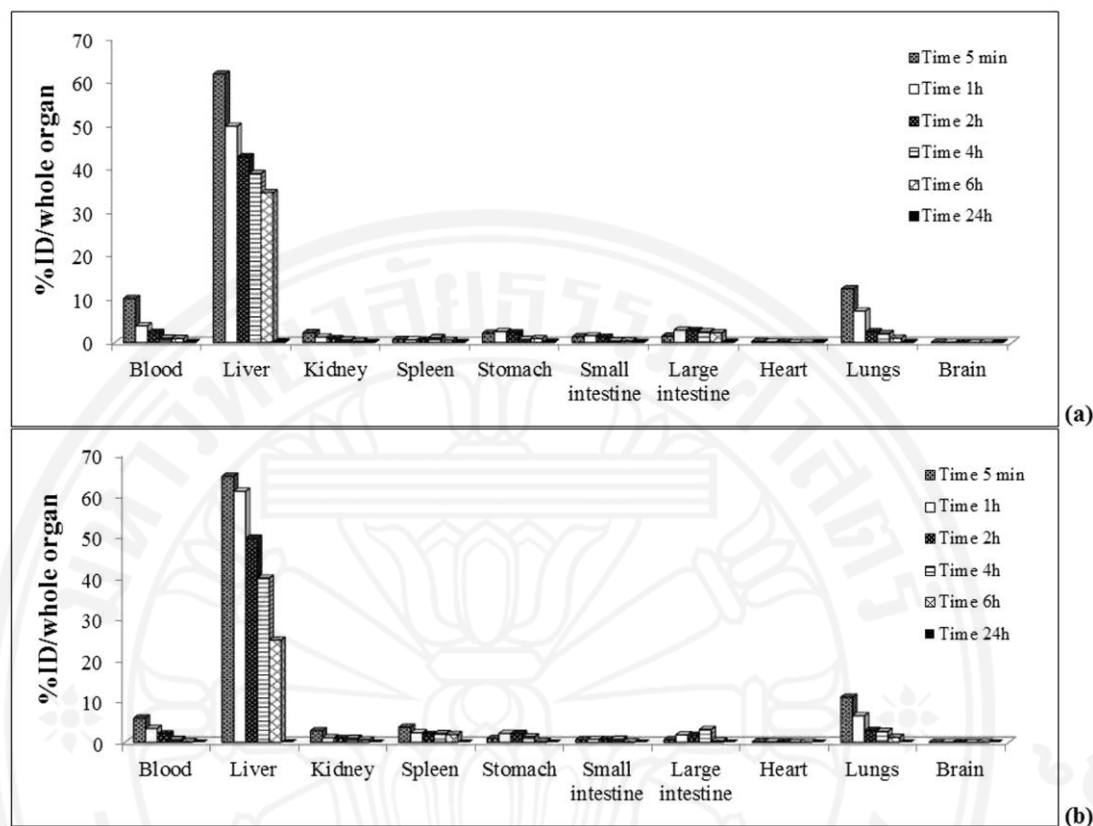
Figure 5.16 Biodistribution of ^{99m}Tc-plumbagin complex in (a) healthy and (b) *P. berghei*-infected mice (4 mice each). The accumulation of the complex in spleen was significantly higher than that in healthy mice at 5 min of dosing (p=0.012). Data are expressed as median of the percentage of injected dose *per* whole organ (%ID/ whole organ) (n=4).

5.6.5 SPECT/CT imaging of ^{99m}Tc-plumbagin complex in healthy and *P. berghei*-infected mice

The SPECT/CT images of ^{99m}Tc-plumbagin complex in healthy, *P. berghei*-infected mice and only ^{99m}Tc without plumbagin received mice are shown in **Figure 5.17**. Results indicated that the liver was an internal organ with highest accumulation of ^{99m}Tc-plumbagin complex and stomach was an internal organ with highest accumulation of only ^{99m}Tc without plumbagin. The distribution of the ^{99m}Tc-plumbagin complex to other organs such as lung, stomach, large intestine, and

kidney was relatively lower and was undetectable by SPECT/CT imaging system (lower sensitivity than radiochemical analysis by Gamma counter). Maximum accumulation of the ^{99m}Tc-plumbagin complex in the liver of healthy and *P. berghei-*infected mice was observed at 30 min after the intravenous dose [**Figure 5.17 (a)**]. At 2 h and 4 h, accumulation of radioactivity in the livers of both healthy and infected mice was relatively lower. The accumulation of ^{99m}Tc-plumbagin complex at 30 min and 2 h was more intensed in the infected mice compared with healthy mice. The accumulation profiles of the complex analysed by SPECT/CT imaging in both healthy and infected mice were in agreement with that observed in the biodistribution study (**Figure 5.16 a, b**). However, if we cannot label ^{99m}Tc with plumbagin, the SPECT/CT images of only ^{99m}Tc without plumbagin will accumulated in stomach, thyroid and urinary bladder (**Figure 5.17c**).

5.6.6 *In vitro* metabolism of plumbagin

Plumbagin was rapidly disappeared from the incubation mixture of pooled human liver microsomes during 0-10 min of reaction initiation (**Figure 5.18**). Thereafter, the concentration was gradually decreased from 2.5 µM to 0.3 µM within 60 min.

Figure 5.17 SPECT/CT images of ^{99m}Tc-plumbagin complex in healthy and *P. berghei-*infected mice (turning face position) at (a) 30 min, (b) 2 h, and (c) 4 h after intravenous injection. (a) Maximal accumulation of the labelled complex in liver was found at 30 min after injection, with relatively higher intensity in the infected compared with healthy mice. (b) At 2 h of injection, the intensity of the radiolabelled complex in liver was relatively higher in the infected compared with healthy mice. (c) At 4 h of injection, the intensity of the radiolabelled complex in liver was relatively low in both groups of mice.
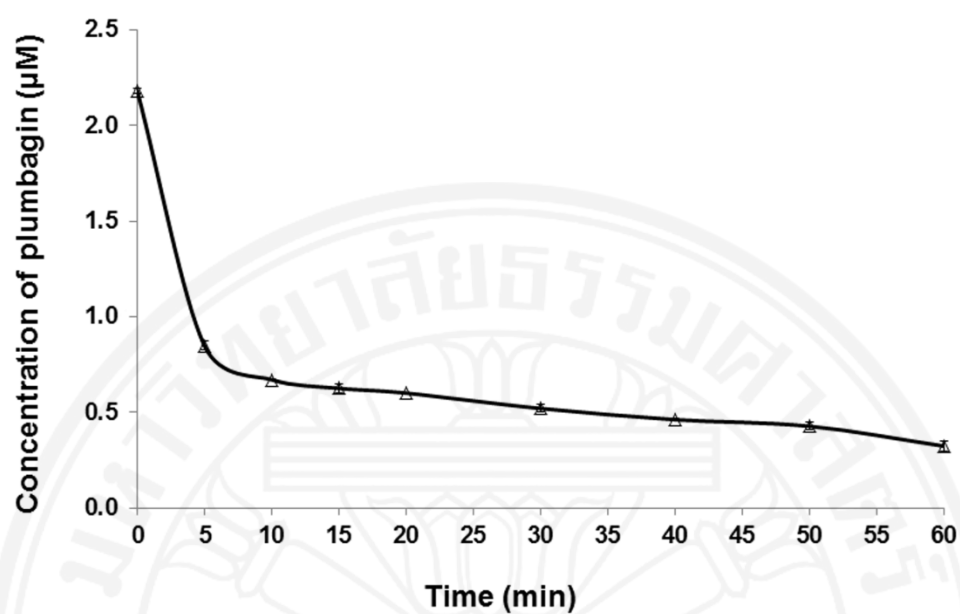
Figure 5.18 Disappearance of plumbagin from the incubation mixture of pooled human liver microsomes *in vitro*. Data are expressed as median with 95% CI for median (n=4).

CHAPTER 6

DISCUSSION

Plumbagin, a naturally occurring naphthoquinone widely distributed in the Plumbaginaceae family, has been reported to possess a wide spectrum of pharmacological properties. The crude ethanolic extract of *Plumbago indica* Linn. (root) has been shown to possess good to moderate antimalarial activity (class III antimalarial activity) in our previous *in vitro* screening.[12] Among the 32 plants investigated, *Plumbago indica* Linn. showed the most promising activity against both K1 chloroquine-resistant (IC_{50} 3 µg/ml) and 3D7 chloroquine-sensitive (IC_{50} 6.2 µg/ml) clones, with highest selectivity (SI=44.7 and 21.6, respectively). Its antimalarial potency against K1 chloroquine-resistant *P. falciparum* clone was about 2.2% of artesunate. In the present study, promising antimalarial activity of its active constituent plumbagin was initially demonstrated in the *in vitro* assay with median IC_{50} values against 3D7 chloroquine-sensitive and K1 chloroquine-resistant *P. falciparum* clones of 580 and 370 nM, respectively. It was noted for a relatively higher activity of plumbagin against chloroquine-resistant *P. falciparum* (class I: very good activity) compared with chloroquine-sensitive *P. falciparum* (class II: good) clone.[107] The difference in antimalarial activity between the two clones could be due to the difference in drug transportation mechanisms particularly that involving *P. falciparum* chloroquine resistance transporter (pfcrt). Parasite chromosomal loci associated with these differential chemical phenotypes should be investigated to clarify this issue.[162] This activity however, should be of advantage for the treatment of patients in areas where *P. falciparum* is still sensitive to chloroquine.

Based on the results of the *in vivo* antimalarial testing, plumbagin at the dose of 25 mg/kg body weight given for 4 days exhibited moderate to weak antimalarial activity with regards to its inhibitory activity on the reduction of parasitaemia and the prolongation of survival time. The compound at daily doses of 10 mg/kg body weight/ day for 4 days showed only weak activity, while at daily doses of 1 mg/kg body weight did not produce any significant activity.[107] The

antimalarial drug chloroquine exhibited the most potent antimalarial activity with 100% suppression of parasitaemia on day 4 (0% parasite density) and a significant prolongation of survival time (>15 days). This result of the *in vivo* antimalarial activity of plumbagin was however, inconsistent with the observed *in vitro* showing the compound to be of good to moderate antimalarial activity. Plumbagin is poorly water soluble which results in poor absorption across gastrointestinal mucosa and thus low systemic bioavailability.[163] In a previous study, mice treated with liposomal formulation of plumbagin was shown to achieve higher plasma and tissue level and area under the concentration-time curve (AUC) compared with those treated with the water-soluble plumbagin. Moreover, high concentration was found in liver and spleen of mice.[164] *In vivo* pharmacokinetics study also demonstrated that orally administered plumbagin produced only 39% systemic bioavailability due to its limited biopharmaceutical properties such as high lipophilicity (log P 3.04) and insolubility in water.[120]

Plumbagin was observed by oral administration in the absence of significant toxicity both in acute and subacute toxicity testing in ICR mice with dose up to 100 mg/kg body weight and 25 mg/kg body weight/day for 28 days, respectively. Results obtained from the acute and subacute toxicity testing in wistar rats demonstrated that maximum tolerated dose of plumbagin was 150 (single oral dose) and 25 (daily doses for 28 days) mg/kg body weight after oral administration, respectively. Oral LD_{50} value of plumbagin in wistar rats was 250 mg/kg body weight after oral administration.

For the permeability of plumbagin in caco-2 cell monolayers and their effects on the p-glycoprotein study are the first that investigate the permeability of plumbagin across Caco-2 cell monolayers, including its effects on MDR-1 mRNA expression and function of P-glycoprotein in the cells. The concentrations of plumbagin used in all experiments were non-toxic as confirmed by MTT assay. The Caco-2 cells formed a robust monolayer structure with regard to the tight junctions (TEER>1300 $\Omega.cm^2$) and P_{app} for Lucifer yellow was 0.42±0.11 (mean±SD). The apparent P_{app} (A-B) and (B-A) values of plumbagin (2, 4 and 8 μM) were 10.29-

15.96×10^{-6} and $7.40\text{-}9.02 \times 10^{-6}$ cm/s, respectively. This allowed the passage of the plumbagin only through transcellular route. Compounds showing P_{app} values of $\geq 14.0 \times 10^{-6}$ cm/s are classified as compounds with highly permeable, whereas those with $< 5.0 \times 10^{-6}$ cm/s are classified as compounds with low permeability.[133,165] The permeability of plumbagin across Caco-2 cell monolayers was moderate in either the A-B or B-A direction. The efflux ratios of approaching 1.00 indicate passive transport mechanism[166] and the ratios of < 3 indicate absence of efflux.[167] The efflux ratios of plumbagin observed in this study (0.57-0.73) were close to 1.00, which suggest passive transport mechanism with no involvement of efflux transporters.

P-glycoprotein is the most important efflux transporters on the intestinal epithelial cells.[101,102] Co-administration of drugs that are substrates or inhibitors of P-glycoprotein may lead to clinically relevant drug-drug interactions.[168] Results of the present study suggest that plumbagin did not interfere with the P-glycoprotein mediated efflux in this cell. It did not inhibit nor induce P-glycoprotein function or gene expression. Plumbagin (1, 2, 4 and 8 μM) had no effect on R123 (P-glycoprotein substrate) transport in both directions (A-B and B-A). There was no change in the P_{app} of the R123 transport in both directions as well as the efflux ratio following exposing Caco-2 cell monolayers to plumbagin for 24 or 48 h. Furthermore, plumbagin produced no significant inhibitory effect of plumbagin at all concentration levels on MDR1 mRNA expression of P-glycoprotein. In contrast, Verapamil, a P-glycoprotein inhibitor, increased transport of R123 from A-B direction, but decreased transport of R123 from B-A direction.

Moreover, interactions between phytochemicals in herbal medicines and CYP are now well recognized because of their potential clinical and toxicological implications. These phytochemicals could act as substrates, inhibitors or inducers of the CYP isoforms, which can lead to pharmacokinetic interactions with the co-administered drugs metabolized by the same CYP isoform.[169,170] Various CYP isoforms including CYP1A2 (13%), CYP2A6 (4%), CYP2C (20%), CYP2D6 (2%), CYP2E1 (7%), and CYP3A (30%) are expressed in human liver.[69] Inhibition of CYP enzymes by drugs and food or supplement sources is well documented. The present study investigated the

potential of five Thai plants with promising activities against malaria for their propensity to inhibit hepatic CYP in humans. Specific inhibitors recommended by the U.S. FDA (Food and Drug Administration) were used as reference compounds for inhibitory activities on different isoforms of CYP.[171] For CYP2C19 however, since there has been no recommended selective inhibitor, nootakone was used as a reference compound because its inhibitory activity was shown to be selective toward CYP2C19.[16] The inhibitory activity of nootakone on CYP2C19 was comparable to that reported by Tassaneeyakul *et al.*[16] However, variation in inhibitory activities of the selective inhibitors for CYP1A2, CYP3A4, 2C19, and CYP 2D6 was observed in this study compared with those reported in previous studies. This could be due mainly to the choices of substrates used. Plants contain numerous classes of chemical constituents including pyrolizidine alkaloids which are hepatotoxic, pneumotoxic, genotoxic, neurotoxic, and cytotoxic. The observed inhibitory effect on drug metabolism can be highly variable as the constituent content can differ with plant species, source, environment, and processing and storage conditions. Results showed that all plants exhibited varying inhibitory potencies on various CYP isoforms. Most showed relatively potent inhibitory activities on CYP3A4 (3 plants with the potency order: DL>DM>PI), followed by CYP2D6 (3 plants with the potency order: DM>PI>DL), CYP2C19 (2 plants with the potency order: PI>DM) and CYP1A2 (2 plants with the potency order: DM>DL). With regard to the inhibitory activity of each plant extract on the four CYP isoforms, PI and DM showed potent inhibitory activities on most CYP isoforms (CYP2C19, CYP2D6, and CYP3A4). DL showed potent inhibitory activities on the two CYP isoforms (CYP3A4 and CYP2D6, respectively). According to U.S. FDA recommendation, clinical relevance enzyme inhibition is likely for test compounds/extracts with IC_{50} of ≤ that of the CYP selective inhibitors.[171] In the present study, the propensity of each plant extract to inhibit activity of each CYP isoform was determined by comparison of the IC_{50} value with that of the selective inhibitor of each CYP (cut-off IC_{50}).

CYP3A4 is the dominant CYP3A family enzyme expressed in the human liver and gastrointestinal tract.[172] CYP3A4 is reported to be involved in the

metabolism of 50% of all pharmaceuticals[173,174], it is therefore an enzyme of general interest for herb-drug interactions. Several herbs and natural remedies have been reported to induce or inhibit CYP3A4. These include grape fruit juice,[175,176] garlic,[177,178] black cohosh,[179,180] St. John's wort,[18,181,182] Echinacea,[18,181,182] and common valerian.[181] In this study, three plants showed potent inhibitory activity on CYP3A4-mediated nifedipine oxidation, of which DL was the most active with potency of about 13-fold lower than the selective inhibitor ketoconazole (mean IC_{50} 0.23 *vs.* 3.06 μg/ml). The inhibitory potencies of the other two plants (DM and PI) were about 19 to 28-fold lower than ketoconazole.

In our previous *in vitro* screening study,[183] the ethanolic extracts of PI, GM, DL, DM, and MF showed promising antimalarial activities with median IC_{50}<10 μg/ml against chloroquine resistant K1 and chloroquine sensitive 3D7 *P. falciparum* clones. Further development of PI and GM however was limited by their relatively weak *in vivo* activities in the *P. berghei* model, possibly due to poor absorption and pharmacokinetic characteristics of their active constituents.[28,184] Most of the currently used antimalarial drugs especially those which are the components of artemisinin-based combination therapy (ACT) are substrates of CYP, notably CYP3A4.[185] Further development of DM and DL as antimalarial candidates (either when given alone or in combination with standard antimalarial drugs) should be performed with caution for their potential to potently inhibit activities of various CYP isoforms particularly CYP3A4. DM or "Hua-Khao-Yen" has long been used in Thai traditional medicines as common ingredients in several preparations, including those used in the treatment of lymphopathy, dermopathy, venereal diseases, leprosy, and cancers.[21] DL is known in Thai as Chan-Daeng, Chan-Pha, or Lakka chan. It has been used in folk medicine as antipyretic, anti-analgesic, and anti-inflammatory.[24]

Furthermore, the present studies provide evidence for the inhibitory effect of plumbagin on the three major hepatic CYP isoforms, *i.e.,* CYP1A2, CYP2C19 and CYP3A4. CYP1A2, CYP2C and CYP3A are expressed in human liver at approximately 13, 20 and 30% of total CYP, respectively.[69] Among the three CYP isoform under investigation, the inhibitory activity of plumbagin on CYP2C19 was most evident, with potency of about 35-fold of the selective inhibitor nootkatone. CYP2C19 is a major metabolizing enzyme of several clinically important drugs such as proton-pump inhibitors like omeprazole and lanzoprazole, anti-epileptic-like mephenytoin, diazepam, antidepressants, the antiplatelet drug, clopidogrel, antifungal voriconazole and selective serotonin reuptake inhibitors like citalopram.[186] Previous investigations in man have shown that CYP2C19 activity is susceptible to induction by herbs and natural products, *e.g.,* St John's wort, Ginko biloba and the Chnes herbal mixture Yin Zhi Huang.[187-189] Nevertheless, there has been no clear evidence on the inhibitory effect of herbal remedies on CYP2C19. Although inhibitory activity on CYP3A4 was moderate (mean IC_{50}=2.37 µM), the clinical relevance of such interaction should not be overlooked as this CYP isoform is involved in the metabolism of 50% of all pharmaceuticals.[190] CYP1A2 is known to play a major role in the metabolism of pre-carcinogens and inhibitory effect of plumbagin to this CYP isoform may contribute only minor interaction with the co-administered drugs.[191] Several other factors are necessary to be considered for definitive conclusion on the clinical relevant metabolic drug interactions. These include comparative disposition of the individual constituents responsible for inhibition, as well as the locations of the affected CYP (intestine, liver, etc.).[192] Until further clinical investigations in healthy subjects are confirmed, the potential of this compound for use in treatment of malaria infection may be limited.

In vivo induction of CYP-mediated hepatic metabolism of plumbagin is the first report to demonstrate about inducing effect of plumbagin on hepatic drug metabolizing enzymes of mice. Nature has created the ability to induce metabolism in order to eliminate a drug or compound faster from the body during long-term exposure. Usually, enzyme induction leads to lower drug efficacy due to the

enhanced elimination of an active compound.[71] In some case, nature works against itself, and induction can lead to increased efficacy or even toxicity of metabolite.[72] In this study, induction of hepatic drug metabolizing enzymes by plumbagin in mice was clearly detected by the enzyme activities and expression of mRNA. Both CYP 1A2 and 3A11 activities and mRNA expression were not induced by plumbagin.

In the part of pharmacokinetics of plumbagin in wistar rats model, the dose selected to determine pharmacokinetics study of plumbagin was 100 mg/kg body weight, which was based on results of acute toxicity test (maximum tolerated dose=150 mg/kg body weight). Investigation of pharmacokinetics study of plumbagin suggested that the elimination half-life ($T_{1/2}$), and mean residence time (MRT) of the plumbagin in wistar rats mean (±SD) were 9.98±1.63 and 13.67±1.62 h, respectively whereas previous reported were 17.13±5.38 and 21.97±5.4 h, respectively.[120] Shorter half-life and mean residence time obtained from the present study compared with previous study may be due to the difference between the species of rats used in the study (wistar rats *vs* sprague–Dawley rats). The time to reach maximum blood concentration (T_{max}) of the plumbagin was slightly longer than that obtain in a previous study (5.0 *vs* 2.5 h). Plumbagin was rapidly cleared from blood circulation and was only detected in plasma up to 48 h and it was not detected in the plasma samples collected after oral administration 72 h. However, it was detected in the urine samples collected after oral administration up to 96 h. This could be explained by the greater lipophilicity of the plumbagin; the compound is likely to extensively distribute into the body tissue and causing slow elimination. Detection of plumbagin in the urine samples suggested that the major routes of excretion of plumbagin is probably *via* renal excretion since detectable with high amount of plumbagin in the urine samples. In addition, ^{99m}Tc-plumbagin complex was shown to be rapidly and extensively accumulated in livers and lungs of both healthy and infected mice as early as 5 min after dosing. Elimination of the complex from both organs was also rapid. These results suggested that the major routes of elimination of plumbagin are probably *via* hepatobiliary and pulmonary routes. Results of the *in vitro* study using human liver microsomes containing drug metabolizing enzymes

supported the role of liver in the biotransformation of plumbagin, which well explained the high accumulation of ^{99m}Tc-plumbagin complex in this organ. Plumbagin is a volatile compound which is likely to be excreted by pulmonary route through exhaled air.[193] It is noted that accumulation of ^{99m}Tc-plumbagin complex was markedly pronounced in spleens of *P. berghei*-infected mice compared with healthy mice. In a previous study, accumulation of plumbagin was shown to be high in liver and spleen of mice.[194] Spleen is an organ which is one of the components of host immune system to defense against foreign substances including following malaria infection. In animals or humans infected with malaria, spleen becomes enlarged as a consequence of its function in filtering out of excessive destroyed infected erythrocytes after the hemolysis.[195]

Investigation of blood kinetics of ^{99m}Tc-plumbagin complex suggested that malaria infection markedly influence the disposition of plumbagin in *P. berghei* infected mice. As a consequence of accelerated systemic clearance, the elimination half-life and mean residence time of the plumbagin in *P. berghei* infected mice was significantly shorter than healthy mice. This kinetic change together with the expansion of apparent volume of distribution resulted in a significant decrease in systemic bioavailability expressed as area under blood concentration-time profile (AUC_{0-inf}). The pharmacokinetics of antimalarial drug quinine during malaria infection has been shown to be markedly changed in such a way that its systemic bioavailability is increased. The elimination half-life is prolonged, while systemic clearance and apparent volume of distribution are decreased.[196,197] This kinetic change of plumbagin may well explain the inconsistent observation observed for its antimalarial activity *in vitro* and in infected mice in our previous study.[184] Apart from the influence of malaria infection, the pharmacokinetic characteristics of the compound itself may also contribute to the relatively low systemic bioavailability in infected mice following the administration of oral dose of an antimalarial drug.[120,184] Plumbagin is poorly water soluble which results in poor absorption across gastrointestinal mucosa and low systemic bioavailability.[194] Altogether, results of the present study as well as our previous studies, suggest that pharmacokinetic factors

and malaria disease state may limit the clinical use of plumbagin particularly if the drug is to be given as an oral formulation.

CHAPTER 7

CONCLUSIONS AND RECOMMENDATIONS

Results obtained from the dissertation could be summarized as follows;

Plumbagin exhibited promising antimalarial activity with *in vitro* IC_{50} (concentration that inhibits enzyme activity by 50%) against 3D7 chloroquine-sensitive *P. falciparum* and K1 chloroquine-resistant *P. falciparum* clones of 580 (270-640) and 370 (270-490) nM, respectively. *In vivo* antimalarial activity was investigated in *P. berghei* infected mouse model. Plumbagin at the dose of 25 mg/kg body weight given for 4 days produced moderate antimalarial activity with regards to its inhibitory activity on the reduction of parasitaemia and the prolongation of survival time.

Toxicity testing of plumbagin in ICR mice indicated maximum tolerated dose at the dose levels up to 100 (single oral dose) and 25 (daily oral doses for 28 days) mg/kg body weight for acute and subacute toxicity, respectively whereas toxicity testing in wistar rats indicated maximum tolerated dose at the dose levels up to 150 (single oral dose) and 25 (daily oral doses for 28 days) mg/kg body weight for acute and subacute toxicity, respectively. Fifty percent lethal dose (LD_{50}) of plumbagin in wistar rats was 250 mg/kg body weight.

Based on results of the Permeation (P_{app}) of plumbagin, plumbagin was moderately permeable across the Caco-2 cell monolayer. The compound was not found to be a substrate or inhibitor of P-glycoprotein (p-gp). It is therefore expected that drug-drug interactions at this level is unlikely following the co-administration of plumbagin with other drugs which as substrate of p-gp. Nevertheless, further investigation on the clearance of plumbagin by hepatic drug metabolizing enzymes is warranted. Among the five Thai medicinal plants with promising activities against malaria, *Dioscorea membranacea* Pierre and *Plumbago indica* Linn. significantly interfered with CYP2C19, CYP2D6 and CYP3A4. Clinical relevance of the inhibitory potential of *Dioscorea membranacea* Pierre and *Plumbago indica* Linn. should be of concern for further development of these plants for treatment of malaria.

Relationship between the concentrations of their active constituents in relation to pharmacological activities should be further investigated. Furthermore, the propensity of plumbagin to interfere with the three human hepatic CYP isoforms, *i.e.,* CYP1A2, CYP2C19 and CYP3A4 were determined. The inhibitory potency was highest on CYP2C19. Concurrent administration of plumbagin (as pure compound or as the extract of *Plumbago indica* Linn.) may result in highly toxic plasma concentrations of the co-administered drugs that are metabolized by these CYP isoforms. Clinical relevance of the interference of human drug metabolizing enzymes should be aware of for further development scheme of plumbagin as antimalarial drug when used co-administration with other antimalarial drugs which are metabolized by CYP1A2, 2C19 and 3A4, *i.e.*, quinine, mefloquine, and chloroquine. However, the result of *in vivo* inducing activity of plumbagin on hepatic cytochrome P450 of mice demonstrated that plumbagin did not significantly induce CYP1A2 and CYP3A11 activity and mRNA expression of treated mice with plumbagin (6.25, 12.50 and 25.00 mg/kg body weight) for 28 days. Base on pharmacokinetics of plumbagin studies, the results demonstrated that the average half-life ($T_{1/2}$) and time to reach maximum blood concentration (T_{max}) of plumbagin (in wistar rats model) were 9.98 and 5.00 h, respectively, after oral administration. Plumbagin was rapidly cleared from blood circulation and major routes of excretion were renal excretion, hepatobiliary and pulmonary routes. Malaria disease state influenced the pharmacokinetics and disposition of plumbagin in animal model.

Results suggest that clinical relevance of the interference of human drug metabolizing enzymes should be aware of for further development scheme of plumbagin as antimalarial drug when used in combination with other antimalarial drugs which are metabolized by these CYP isoforms. Preparation of modified formulation is required to improve its systemic bioavailability. Increase in the dose of plumbagin, together with improvement of its oral bioavailability may be required if the compound will be selected as a candidate compound for treatment of malaria.

REFERENCES

1.   Wang DQ, Xia ZG, Zhou SS, Zhou XN, Wang RB, Zhang QF. A potential threat to malaria elimination: extensive deltamethrin and DDT resistance to Anopheles sinensis from the malaria-endemic areas in China. Malar J. 2013;12(164):1475-2875.

2.   Namsa N, Mandal M, Tangjang S. Anti-malarial herbal remedies of northeast India, Assam: an ethnobotanical survey. J Ethnopharmacol. 2011;133(2):565-72.

3.   Na-Bangchang K. Pharmacodynamics of antimalarial chemotherapy. Expert Rev Clin Pharmacol. 2009;2(5):491-515.

4.   Na-Bangchang K, Karbwang J. Traditional Herbal Medicine for the Control of Tropical Diseases. Tropical Medicine and Health. 2014;42(2 Suppl):3-13.

5.   Muthaura C, Keriko J, Derese S, Yenesew A, Rukunga G. Investigation of some medicinal plants traditionally used for treatment of malaria in Kenya as potential sources of antimalarial drugs. Exp Parasitol. 2011;127(3):609-26.

6.   Robert A, Benoit-Vical F, Dechy-Cabaret O, Meunier B. From classical antimalarial drugs to new compounds based on the mechanism of action of artemisinin. Pure Appl Chem. 2001;73(7):1173–88.

7.   Foti RS, Pearson JT, Rock DA, Wahlstrom JL, Wienkers LC. *In vitro* inhibition of multiple cytochrome P450 isoforms by xanthone derivatives from mangosteen extract. Drug Metab Dispos. 2009;37(9):1848-55.

8.   Sandur SK, Ichikawa H, Sethi G, Ahn KS, Aggarwal BB. Plumbagin (5-hydroxy-2-methyl-1,4-naphthoquinone) suppresses NF-kappaB activation and NF-kappaB-regulated gene products through modulation of p65 and IkappaBalpha kinase activation, leading to potentiation of apoptosis induced by cytokine and chemotherapeutic agents. J Biol Chem. 2006 Jun 23;281(25):17023-33.

9.   Paiva SR, Silva Marques S, Figueiredo MR, Auxiliadora M. Plumbaginales: a pharmacological approach Brazilian Journal of Forestry and environment. 2003;10(1):98 - 105.

10.   Simonsen HT, Nordskjold JB, Smitt UW, Nyman U, Palpu P, Joshi P, *et al*. *In vitro* screening of Indian medicinal plants for antiplasmodial activity. J Ethnopharmacol. 2001 Feb;74(2):195-204.

11.   Suraveratum N, Krungkrai SR, Leangaramgul P, Prapunwattana P, Krungkrai J. Purification and characterization of *Plasmodium falciparum* succinate dehydrogenase. Mol Biochem Parasitol. 2000 Feb 5;105(2):215-22.

12.   Thiengsusuk A, Chaijaroenkul W, Na-Bangchang K. Antimalarial activities of medicinal plants and herbal formulations used in Thai traditional medicine. Parasitology Research. 2013 2013/04/01;112(4):1475-81.

13.   Bertz R, Granneman G. Use of *in vitro* and *in vivo* data to estimate the likelihood of metabolic pharmacokinetic interactions. Clin Pharmacokinet. 1997;32(3):210-58.

14.   Taesotikul T, Dumrongsakulchai W, Wattanachai N, Navinpipat V, Somanabandhu A, Tassaneeyakul W, *et al*. Inhibitory effects of Phyllanthus amarus and its major lignans on human microsomal cytochrome P450 activities: evidence for CYP3A4 mechanism-based inhibition. Drug Metab Pharmacokinet. 2011;26(2):154-61.

15.   Hellum B, Hu Z, Nilsen O. The induction of CYP1A2, CYP2D6 and CYP3A4 by six trade herbal products in cultured primary human hepatocytes. Basic Clin Pharmacol Toxicol. 2007;100(1):23-30.

16.   Tassaneeyakul W, Guo L, Fukuda K, Ohta T, Yamazoe Y. Inhibition selectivity of grapefruit juice components on human cytochromes P450. Arch Biochem Biophys. 2000;378(2):356-63.

17.   Usia T, Iwata H, Hiratsuka A, Watabe T, Kadota S, Tezuka Y. CYP3A4 and CYP2D6 inhibitory activities of Indonesian medicinal plants. Phytomedicine. 2006;13(1-2):67-73.

18.   Obach RS. Inhibition of human cytochrome P450 enzymes by constituents of St. John's Wort, an herbal preparation used in the treatment of depression. J Pharmacol Exp Ther. 2000;294(1):88-95.

19.   Markowitz JS, Donovan JL, DeVane CL, Taylor RM, Ruan Y, Wang JS, et al. Effect of St John's wort on drug metabolism by induction of cytochrome P450 3A4 enzyme. Jama. 2003;290(11):1500-4.

20.   Ueng YF, Don MJ, Peng HC, Wang SY, Wang JJ, Chen CF. Effects of Wu-chu-yu-tang and its component herbs on drug-metabolizing enzymes. Jpn J Pharmacol. 2002;89(3):267-73.

21.   Itharat A. Biological activity of bioactive compounds of five Thai medicinal plants called Hua-Khao-yen [Dissertation]. London: University of London; 2003.

22.   Itharat A, Plubrukarn A, Kongsaeree P, Bui T, Keawpradub N, Houghton PJ. Dioscorealides and dioscoreanone, novel cytotoxic naphthofuranoxepins, and 1,4-phenanthraquinone from Dioscorea membranacea Pierre. Org Lett. 2003;5(16):2879-82.

23.   Itharat A, Jaiaree N, Ruangnoo S, Thongdeeying P. Cytotoxic Compounds from Dioscorea Membranacea Against Three Types of Colon Cancer Cells. J Health Res. 2013;27(1):7-11.

24.   Pongbunrod S. Mai-Tet-Murng-Thai: Medicinal characteristic of foreign and Thai traditional medicines. 1st ed. Bangkok: : Khrungthon Press; 1979.

25.   Sattaponpan C, Kondo S. Antibacterial activity of crude extracts of prasaprohyai formula and its components against pathogenic bacteria. J Med Assoc Thai. 2011;94(7):S153-61.

26.   Phuphathanaphong L. Thai Medicinal Plants. 3rd, editor. Bangkok: Department of Forestry; 1982.

27.   Thitiorul S, Ratanavalachai T, Tanuchit S, Itharat A, Sakpakdeejaroen I. Genotoxicity and interference with cell cycle activities by an ethanolic extract from Thai Plumbago indica roots in human lymphocytes *in vitro*. Asian Pac J Cancer Prev. 2013;14(4):2487-90.

28.   Bunyong R, Chaijaroenkul W, Plengsuriyakarn T, Na-Bangchang K. Antimalarial activity and toxicity of Garcinia mangostana Linn. Asian Pac J Trop Med. 2014;7(9):693-8.

29.   Galinski M, Barnwell J. Monkey malaria kills four humans. Trends Parasitol. 2009;25(5):200-4.

30.   Jongwutiwes S, Buppan P, Kosuvin R, Seethamchai S, Pattanawong U, Sirichaisinthop J, et al. *Plasmodium knowlesi* Malaria in humans and macaques, Thailand. Emerg Infect Dis. 2011;17(10):1799-806.

31.   Jongwutiwes S, Putaporntip C, Iwasaki T, Sata T, Kanbara H. Naturally acquired *Plasmodium knowlesi* malaria in human, Thailand. Emerg Infect Dis. 2004;10(12):2211-3.

32.   Lee K, Cox-Singh J, Singh B. Morphological features and differential counts of *Plasmodium knowlesi* parasites in naturally acquired human infections

Malar J. 2009;8:73.

33.   Despommier., Gwads., Hotez., Knirsch. 5th edition of Parasitic Diseases. Apple Trees Productions. 2005:50-68.

34.   Olliaro P, Cattani J, Wirth D. Malaria, the submerged disease. Jama. 1996;275(3):230-3.

35.   WHO. World malaria report : 2010. Geneva, Switzerland: WHO Library Cataloguing-in-Publication Data; 2011 [cited 2015 Jan 5]. Available from: http://www.who.int/malaria/world_malaria_report_2011/en/.

36.   WHO. Malaria Situation in in SEA Region: WHO Press 2010 [cited 2015 Mar 4]. Available from: http://www.who.int/malaria/world_malaria_report_2010/ worldmalariareport2010.pdf.

37.   WHO. Malaria Situation in Thailand: WHO Press 2010 [cited 2014 Nov 30]. Available from: http://www.who.int/malaria/world_malaria_report_2010/ worldmalariareport2010.pdf?ua=1.

38.   Breman J. Clinical manifestations of malaria. In: Daily J, editor.2015.

39.   Trampuz A, Jereb M, Muzlovic I, Prabhu R. Clinical review: Severe malaria. Crit Care. 2003;7(4):315-23.

40.   CDC. Malaria. 2010 [updated 2010 Feb 8; cited 2015 Jun 2]; Available from: http://www.cdc.gov/malaria/about/disease.html.

41.   Ponnampalam JT. Chemotherapy of malaria. Ann Acad Med Singapore. 1981;10(1):99-106.

42.   WHO. Guidelines for the treatment of malaria 2015 [cited 2015 Feb 17]. Available from: http://www.who.int/malaria/publications/atoz/9789241549127/en/.

43.   Winstanley P, Ward S. Malaria chemotherapy. Adv Parasitol. 2006;61:47-76.

44.   Black R, Canfield C, Clyde D, Peters W, Wernsdorfer W, Organization WH. Chemotherapy of malaria. Geneva: World Health Organization; 1986 [cited 2014 Nov 27]. Available from: http://www.who.int/iris/handle/10665/38605# sthash.a1281rrM.dpuf.

45.   Peters W. The prevention of antimalarial drug resistance. Pharmacol Ther. 1990;47(3):499-508.

46.   Ariey F, Witkowski B, Amaratunga C, Beghain J, Langlois AC, Khim N, et al. A molecular marker of artemisinin-resistant *Plasmodium falciparum* malaria. Nature. 2014;505(7481):50-5.

47.   Ashley E, Dhorda M, Fairhurst R, Amaratunga C, Lim P, Suon S, et al. Spread of Artemisinin Resistance in *Plasmodium falciparum* Malaria. New England Journal of Medicine. 2014;371(5):411-23.

48.   Dondorp A, Nosten F, Yi P, Das D, Phyo A, Tarning J, et al. Artemisinin Resistance in *Plasmodium falciparum* Malaria. New England Journal of Medicine. 2009;361(5):455-67.

49.   Baird JK. Resistance to therapies for infection by *Plasmodium vivax*. Clin Microbiol Rev. 2009;22(3):508-34.

50.   Peter B. Drug resistance in malaria. United States of America: World Health Organization; 2001 [cited 2015 Jan 15]. Available from: http://www.who.int/csr/resources/publications/drugresist/malaria.pdf.

51.   Rosenthal PJ. Antimalarial drug discovery: old and new approaches. J Exp Biol. 2003 Nov;206(Pt 21):3735-44.

52.   Posner GH, Paik IH, Sur S, McRiner AJ, Borstnik K, Xie S, et al. Orally active, antimalarial, anticancer, artemisinin-derived trioxane dimers with high stability and efficacy. J Med Chem. 2003 Mar 13;46(6):1060-5.

53. Vennerstrom JL, Dong Y, Andersen SL, Ager AL, Jr., Fu H, Miller RE, et al. Synthesis and antimalarial activity of sixteen dispiro-1,2,4, 5-tetraoxanes: alkyl-substituted 7,8,15,16-tetraoxadispiro[5.2.5. 2]hexadecanes. J Med Chem. 2000 Jul 13;43(14):2753-8.

54. Tagboto S, Townson S. Antiparasitic properties of medicinal plants and other naturally occurring products. Adv Parasitol. 2001;50:199-295.

55. WHO. Health Situation Analysis in the African Region, Atlas of Health Statistics: WHO Regional Office for Africa; 2011 [cited 2015 Jan 3]. Available from: http://apps.who.int/medicinedocs/documents/s18863en/s18863en.pdf.

56. Tilak JC, Banerjee M, Mohan H, Devasagayam TP. Antioxidant availability of turmeric in relation to its medicinal and culinary uses. Phytother Res. 2004 Oct;18(10):798-804.

57. Botanical Dermatology Database. Plumbaginaceae. 1999 [updated 2012 Dec 5; cited 2015 Jun 10]; Available from: http://bodd.cf.ac.uk/BotDermP/PLUM.html.

58. Itoigawa M, Takeya K, Furukawa H. Cardiotonic action of plumbagin on guinea-pig papillary muscle. Planta Med. 1991;57(4):317-9.

59. Fournet A, Angelo A, Munoz V, Roblot F, Hocquemiller R, Cave A. Biological and chemical studies of Pera benensis, a Bolivian plant used in folk medicine as a treatment of cutaneous leishmaniasis. J Ethnopharmacol. 1992 Sep;37(2):159-64.

60. Bhargava SK. Effects of plumbagin on reproductive function of male dog. Indian J Exp Biol. 1984 Mar;22(3):153-6.

61. Premakumari P, Rathinam K, Santhakumari G. Antifertility activity of plumbagin. Indian J Med Res. 1977 Jun;65(6):829-38.

62. Paiva SR, Figueiredo MR, Aragao TV, Kaplan MA. Antimicrobial activity *in vitro* of plumbagin isolated from Plumbago species. Mem Inst Oswaldo Cruz. 2003;98(7):959-61.

63. Singh UV, Udupa N. Reduced toxicity and enhanced antitumor efficacy of betacyclodextrin plumbagin inclusion complex in mice bearing Ehrlich ascites carcinoma. Indian J Physiol Pharmacol. 1997;41(2):171-5.

64.   Rang H, Dale M, Ritter J, Flower R, Henderson G. Pharmacology. 7th ed: Elsevier Health Sciences; 2554.

65.   Roberts SA. Drug metabolism and pharmacokinetics in drug discovery. Curr Opin Drug Discov Devel. 2003 Jan;6(1):66-80.

66.   Mizuno N, Niwa T, Yotsumoto Y, Sugiyama Y. Impact of drug transporter studies on drug discovery and development. Pharmacol Rev. 2003 Sep;55(3):425-61.

67.   Amsterdam Institute of Molecules Medicines and Systems [internet]. Genetic factors and risks for severe adverse drugs reactions. 2013 [updated 2013 Apr 12; cited 2015 Jan 5]; Available from: http://aimms.vu.nl/en/news-events/news-archive/2013/genetic-factors-and-risks-for-severe-adverse-drugs-reactions.asp.

68.   Spatzenegger M, Jaeger W. Clinical importance of hepatic cytochrome P450 in drug metabolism. Drug Metab Rev. 1995;27(3):397-417.

69.   Shimada T, Yamazaki H, Mimura M, Inui Y, Guengerich FP. Interindividual variations in human liver cytochrome P-450 enzymes involved in the oxidation of drugs, carcinogens and toxic chemicals: studies with liver microsomes of 30 Japanese and 30 Caucasians. J Pharmacol Exp Ther. 1994;270(1):414-23.

70.   US FDA. Guidance for Industry: Drug Interaction Studies-Study Design, Data Analysis, Implications for Dosing, and Labeling Recommendations.: U.S. Department of Health and Human Services Food and Drug Administration Center for Drug Evaluation and Research (CDER). ; 2012 [updated 2012 Feb 5; cited 2015 Jan 5]; Available   from: http://www.fda.gov/downloads/drugs/guidancecompliance regulatoryinformation/guidances/ucm292362.pdf.

71.   Lin JH, Lu AY. Inhibition and induction of cytochrome P450 and the clinical implications. Clin Pharmacokinet. 1998;35(5):361-90.

72.   Pelkonen O, Maenpaa J, Taavitsainen P, Rautio A, Raunio H. Inhibition and induction of human cytochrome P450 (CYP) enzymes. Xenobiotica. 1998;28(12):1203-53.

73.   Handschin C, Meyer UA. Induction of drug metabolism: the role of nuclear receptors. Pharmacol Rev. 2003;55(4):649-73.

74.   Shih H, Pickwell GV, Guenette DK, Bilir B, Quattrochi LC. Species differences in hepatocyte induction of CYP1A1 and CYP1A2 by omeprazole. Hum Exp Toxicol. 1999 Feb;18(2):95-105.

75.   Li AP. Primary hepatocyte cultures as an *in vitro* experimental model for the evaluation of pharmacokinetic drug-drug interactions. Adv Pharmacol. 1997;43:103-30.

76.   Hollenberg PF. Characteristics and common properties of inhibitors, inducers, and activators of CYP enzymes. Drug Metab Rev. 2002;34(1-2):17-35.

77.   Olesen OV, Linnet K. Hydroxylation and demethylation of the tricyclic antidepressant nortriptyline by cDNA-expressed human cytochrome P-450 isozymes. Drug Metab Dispos. 1997 Jun;25(6):740-4.

78.   Sweeney BP, Bromilow J. Liver enzyme induction and inhibition: implications for anaesthesia. Anaesthesia. 2006;61(2):159-77.

79.   Marangoni A. Enzyme Kinetics: A Modern Approach. United States of America: John Wiley & Sons, Inc.; 2003.

80.   Teesside University. Enzyme Inhibition. 1999 [updated 1999 OCt 29; cited 2015 Jan 3]; Available from: http://sst-web.tees.ac.uk/external/U0000504/Notes/enzkin/Inhibition/Inhibition.html.

81.   IB Chemistry Human Biochemistry Wiki. Determine Vmax and the value of the Km by graphical means. 2015 [updated 2015 Jan 14; cited 2015 Jun 3]; Available from: https://ibhumanbiochemistry.wikispaces.com/C.7.2.

82.   Murzin D, Salmi T. Catalytic Kinetics. 1st ed: Elsevier Science; 2005.

83.   Department of Biochemistry the University of the West Indies. lineweaver-burk plot. 2013 [updated 2013 Apr 5; cited 2015 Jun 3]; Available from: https://msbellebiochemblogspot.wordpress.com/tag/lineweaver-burk-plot/.

84.   Molecular Imaging Program Stanford schol of medicine. Pharmacokinetics. 2015.

85.   Wikipedia the free encyclopedia. Hanes–Woolf plot. 2014 [updated 2014 Oct 18; cited 2015 Jun 8]; Available from: http://en.wikipedia.org/wiki/Hanes%E2%80%93Woolf_plot.

86.   Estudante M, Morais JG, Soveral G, Benet LZ. Intestinal drug transporters: an overview. Adv Drug Deliv Rev. 2013;65(10):1340-56.

87.   Petzinger E, Geyer J. Drug transporters in pharmacokinetics. Naunyn Schmiedebergs Arch Pharmacol. 2006;372(6):465-75.

88.   Mizuno N, Sugiyama Y. Drug transporters: their role and importance in the selection and development of new drugs. Drug Metab Pharmacokinet. 2002;17(2):93-108.

89.   Bosch I, Croop JM. P-glycoprotein structure and evolutionary homologies. Cytotechnology. 1998;27(1-3):1-30.

90.   Schinkel AH. P-Glycoprotein, a gatekeeper in the blood-brain barrier. Adv Drug Deliv Rev. 1999;36(2-3):179-94.

91.   Lugo MR, Sharom FJ. Interaction of LDS-751 with P-glycoprotein and mapping of the location of the R drug binding site. Biochemistry. 2005;44(2):643-55.

92.   Saeki T, Ueda K, Tanigawara Y, Hori R, Komano T. P-glycoprotein-mediated transcellular transport of MDR-reversing agents. FEBS Lett. 1993;324(1):99-102.

93.   Sukhai M, Piquette-Miller M. Regulation of the multidrug resistance genes by stress signals. J Pharm Pharm Sci. 2000;3(2):268-80.

94.   Texas Tech University. Anti-Cancer Drug Research with Purified P-glycoprotein. 2015.

95.   Artursson P. Epithelial transport of drugs in cell culture. I: A model for studying the passive diffusion of drugs over intestinal absorptive (Caco-2) cells. J Pharm Sci. 1990;79(6):476-82.

96.   Artursson P, Palm K, Luthman K. Caco-2 monolayers in experimental and theoretical predictions of drug transport. Adv Drug Deliv Rev. 2001;46(1-3):27-43.

97.   Artursson P, Ungell AL, Lofroth JE. Selective paracellular permeability in two models of intestinal absorption: cultured monolayers of human intestinal epithelial cells and rat intestinal segments. Pharm Res. 1993;10(8):1123-9.

98.   Thwaites DT, McEwan GT, Hirst BH, Simmons NL. H(+)-coupled alpha-methylaminoisobutyric acid transport in human intestinal Caco-2 cells. Biochim Biophys Acta. 1995;8(1):111-8.

99.	Borlak J, Zwadlo C. Expression of drug-metabolizing enzymes, nuclear transcription factors and ABC transporters in Caco-2 cells. Xenobiotica. 2003;33(9):927-43.

100.	Sambuy Y, De Angelis I, Ranaldi G, Scarino ML, Stammati A, Zucco F. The Caco-2 cell line as a model of the intestinal barrier: influence of cell and culture-related factors on Caco-2 cell functional characteristics. Cell Biol Toxicol. 2005;21(1):1-26.

101.	Beaulieu E, Demeule M, Ghitescu L, Beliveau R. P-glycoprotein is strongly expressed in the luminal membranes of the endothelium of blood vessels in the brain. Biochem J. 1997;326(Pt 2):539-44.

102.	Thiebaut F, Tsuruo T, Hamada H, Gottesman MM, Pastan I, Willingham MC. Cellular localization of the multidrug-resistance gene product P-glycoprotein in normal human tissues. Proc Natl Acad Sci U S A. 1987;84(21):7735-8.

103.	Taipalensuu J, Tornblom H, Lindberg G, Einarsson C, Sjoqvist F, Melhus H, et al. Correlation of gene expression of ten drug efflux proteins of the ATP-binding cassette transporter family in normal human jejunum and in human intestinal epithelial Caco-2 cell monolayers. J Pharmacol Exp Ther. 2001;299(1):164-70.

104.	US FDA DRAFT Guidance for Industry. Drug Interaction Studies-Study Design, Data Analysis and Implications for Dosing and Labeling. U.S. Department of Health and Human Services Food and Drug Administration Center for Drug Evaluation and Research (CDER). ; 2006 [updated 2006 Feb 19; cited 2015 Jan 5]; Available from: http://www.fda.gov/OHRMS/DOCKETS/98fr/06d-0066-gdl0001.pdf.

105.	Stevenson MM, Kraal G. Histological changes in the spleen and liver of C57BL/6 and A/J mice during *Plasmodium chabaudi* AS infection. Exp Mol Pathol. 1989;51(1):80-95.

106.	Peters W, Portus J, Robinson B. The chemotherapy of rodent malaria, XXII. The value of drug-resistant strains of *P. berghei* in screening for blood schizontocidal activity. Ann Trop Med Parasitol. 1975 Jun;69(2):155-71.

107.	Willcox M, Gamaniel S, Matsabisa M, Randriasamimanana J, Wambebe C, Rasoanaivo P. Guidelines for the Preclinical Evaluation of the Safety of Traditional Herbal Antimalarials. Traditional Medicinal Plants and Malaria: CRC Press; 2004.

108.	Carter R, Diggs CL. Plamodia of rodents. Academic Press. 1977;3:359-465.

109.	Perkins S, Sarkar I, Carter R. The phylogeny of rodent malaria parasites: simultaneous analysis across three genomes. Infect Genet Evol 2007 Jan;7(1):74-83 Epub 2006 Jun 9. 2007;7(1):74-83.

110.	Sanni LA, Fu S, Dean RT, Bloomfield G, Stocker R, Chaudhri G, et al. Are reactive oxygen species involved in the pathogenesis of murine cerebral malaria? J Infect Dis. 1999;179(1):217-22.

111.	Fidock DA, Rosenthal PJ, Croft SL, Brun R, Nwaka S. Antimalarial drug discovery: efficacy models for compound screening. Nat Rev Drug Discov. 2004;3(6):509-20.

112.	Lindenberg L, Thomas A, Adler S, Mena E, Kurdziel K, Maltzman J, et al. Safety and biodistribution of ^{111}In-amatuximab in patients with mesothelin expressing cancers using single photon emission computed tomography-computed tomography (SPECT-CT) imaging. Oncotarget. 2015;6(6):4496-504.

113.	Seo Y, Mari C, Hasegawa BH. Technological development and advances in single-photon emission computed tomography/computed tomography. Semin Nucl Med. 2008;38(3):177-98.

114.	Brandon D, Alazraki A, Halkar RK, Alazraki NP. The role of single-photon emission computed tomography and SPECT/computed tomography in oncologic imaging. Semin Oncol. 2011;38(1):87-108.

115.	Schillaci O, Filippi L, Manni C, Santoni R. Single-photon emission computed tomography/computed tomography in brain tumors. Semin Nucl Med. 2007;37(1):34-47.

116.	O'Connor MK, Kemp BJ. Single-photon emission computed tomography/computed tomography: basic instrumentation and innovations. Semin Nucl Med. 2006;36(4):258-66.

117.   Jan F. Development of a Novel Readout System for Small Animal Positron Emission Tomography. 2008.

118.   Meikle SR, Beekman FJ, Rose SE. Complementary molecular imaging technologies: High resolution SPECT, PET and MRI. Drug Discov Today Technol. 2006;3(2):187-94.

119.   Dokic DD. [Technetium-99m radiopharmaceuticals for *in vivo* diagnostics]. Med Pregl. 2005;58(3-4):180-4.

120.   Hsieh YJ, Lin LC, Tsai TH. Measurement and pharmacokinetic study of plumbagin in a conscious freely moving rat using liquid chromatography/tandem mass spectrometry. J Chromatogr B Analyt Technol Biomed Life Sci. 2006;844(1):1-5.

121.   World Nuclear Association. Radioisotopes in Medicine. London, England: World Nuclear Association; 2015 [updated Apr 2015; cited 2015 Apr 6]; Available from:http://www.world-nuclear.org/info/Non-Power-Nuclear-Applications/ Radioisotopes/Radioisotopes-in-Medicine/.

122.   Trager W, Jensen J. Human malaria parasites in continuous culture. Science ; . 1976;193:673-5.

123.   Lambros C, Vanderberg JP. Synchronization of *Plasmodium falciparum* erythrocytic stages in culture. J Parasitol. 1979 Jun;65(3):418-20.

124.   Bennett TN, Paguio M, Gligorijevic B, Seudieu C, Kosar AD, Davidson E, *et al.* Novel, rapid, and inexpensive cell-based quantification of antimalarial drug efficacy. Antimicrob Agents Chemother. 2004 May;48(5):1807-10.

125.   Smilkstein M, Sriwilaijaroen N, Kelly JX, Wilairat P, Riscoe M. Simple and inexpensive fluorescence-based technique for high-throughput antimalarial drug screening. Antimicrob Agents Chemother. 2004 May;48(5):1803-6.

126.   OECD. Test No. 420: Acute Oral Toxicity - Fixed Dose Procedure: OECD Publishing; 2001 [cited 2015 Jan 3]. Available from: /content/book/9789264070943-en http://dx.doi.org/10.1787/9789264070943-en.

127.   OECD. Test No. 407: Repeated Dose 28-day Oral Toxicity Study in Rodents: OECD Publishing; 2008 [cited 2015 Jan 3]. Available from: /content/book/9789264070684-en http://dx.doi.org/10.1787/9789264070684-en.

128.   Twaij H, Kery A, Al-Khazraji N. Some pharmacological, toxicological and phytochemical investigations on Centaurea phyllocephala. J Ethnopharmacol. 1983;9(2-3):299-314.

129.   Esume CO, Emudainohwo JOT, Opajobi AO, Osifo IM, Onyemekeih UR. An investigation into the anti-malaria property of ethanolic extract of the leaves of gongronema latifolium on artesunate sensitive *P. berghei* infected albino mice. Continental J Tropical Medicine 2011;5(1):10 - 4.

130.   Tona L, Totte J, Pieters L, Mesia K, Vlietinck AJ, Ngimbi NP, et al. *In-vivo* antimalarial activity of *Cassia occidentalis, Morinda morindoides* and *Phyllanthus niruri.* Annals of Tropical Medicine and Parasitology. 2001;95(1):47-57.

131.   Wang XD, Meng MX, Gao LB, Liu T, Xu Q, Zeng S. Permeation of astilbin and taxifolin in Caco-2 cell and their effects on the P-gp. Int J Pharm. 2009;378(1-2):1-8.

132.   Ma B, Wang J, Sun J, Li M, Xu H, Sun G, et al. Permeability of rhynchophylline across human intestinal cell *in vitro*. Int J Clin Exp Pathol. 2014;7(5):1957-66.

133.   Sun H, Pang KS. Permeability, transport, and metabolism of solutes in Caco-2 cell monolayers: a theoretical study. Drug Metab Dispos. 2008;36(1):102-23.

134.   Rodriguez A, Webster P, Ortego J, Andrews NW. Lysosomes behave as $Ca2^{+}$-regulated exocytic vesicles in fibroblasts and epithelial cells. J Cell Biol. 1997;137(1):93-104.

135.   Wang XY, Demelash A, Kim H, Jensen-Taubman S, Dakir el H, Ozbun L, et al. Matrilysin-1 mediates bronchiolization of alveoli, a potential premalignant change in lung cancer. Am J Pathol. 2009 Aug;175(2):592-604.

136.   Ferruzza S, Rossi C, Scarino ML, Sambuy Y. A protocol for differentiation of human intestinal Caco-2 cells in asymmetric serum-containing medium. Toxicol *In Vitro*. 2012;26(8):1252-5.

137.   Lee JS, Paull K, Alvarez M, Hose C, Monks A, Grever M, et al. Rhodamine efflux patterns predict P-glycoprotein substrates in the National Cancer Institute drug screen. Mol Pharmacol. 1994;46(4):627-38.

138.   Aiba T, Susa M, Fukumori S, Hashimoto Y. The effects of culture conditions on CYP3A4 and MDR1 mRNA induction by 1alpha, 25-dihydroxyvitamin D(3) in human intestinal cell lines, Caco-2 and LS180. Drug Metab Pharmacokinet. 2005;20(4):268-74.

139.   Shirasaka Y, Kawasaki M, Sakane T, Omatsu H, Moriya Y, Nakamura T, *et al*. Induction of human P-glycoprotein in Caco-2 cells: development of a highly sensitive assay system for P-glycoprotein-mediated drug transport. Drug Metab Pharmacokinet. 2006;21(5):414-23.

140.   Mahavorasirikul W, Viyanant V, Chaijaroenkul W, Itharat A, Na-Bangchang K. Cytotoxic activity of Thai medicinal plants against human cholangiocarcinoma, laryngeal and hepatocarcinoma cells *in vitro*. BMC Complement Altern Med. 2010;10(55).

141.   Plengsuriyakarn T, Viyanant V, Eursitthichai V, Picha P, Kupradinun P, Itharat A, *et al*. Anticancer activities against cholangiocarcinoma, toxicity and pharmacological activities of Thai medicinal plants in animal models. BMC Complement Altern Med. 2012a;12(23):1472-6882.

142.   Lavhekar S, Lohade A, Coutinho E, Iyer K. Estimation of microsomal CYP1A2 activity by high performance liquid chromatography. Indian Journal of Pharmaceutical Sciences. 2006;68(2):258.

143.   Patki KC, Von Moltke LL, Greenblatt DJ. *In vitro* metabolism of midazolam, triazolam, nifedipine, and testosterone by human liver microsomes and recombinant cytochromes P450: role of cyp3A4 and cyp3A5. Drug Metab Dispos. 2003;31(7):938-44.

144.   He N, Edeki T. The inhibitory effects of herbal components on CYP2C9 and CYP3A4 catalytic activities in human liver microsomes. Am J Ther. 2004;11(3):206-12.

145.   Sumsakul W, Plengsuriyakarn T, Chaijaroenkul W, Viyanant V, Karbwang J, Na-Bangchang K. Antimalarial activity of plumbagin *in vitro* and in animal models. BMC Complement Altern Med. 2014;14(15):1472-6882.

146.   Martignoni M, de Kanter R, Grossi P, Mahnke A, Saturno G, Monshouwer M. An *in vivo* and *in vitro* comparison of CYP induction in rat liver and intestine using slices and quantitative RT-PCR. Chem Biol Interact. 2004;151(1):1-11.

147.   McCune JS, Hawke RL, LeCluyse EL, Gillenwater HH, Hamilton G, Ritchie J, et al. *In vivo* and *in vitro* induction of human cytochrome P4503A4 by dexamethasone. Clin Pharmacol Ther. 2000;68(4):356-66.

148.   Bradford MM. A rapid and sensitive method for the quantitation of microgram quantities of protein utilizing the principle of protein-dye binding. Anal Biochem. 1976;72:248-54.

149.   Sumsakul W, Chaijaroenkul W, Na-Bangchang K. *In vitro* inhibitory effects of plumbagin, the promising antimalarial candidate, on human cytochrome P450 enzymes. Asian Pacific Journal of Tropical Medicine. 2015.

150.   Farah A, Nooraain N, Noriham O, Azizah A, Nurul H. Acute and Oral Subacute Toxicity Study of Ethanolic Extract of Cosmos Caudatus Leaf in Sprague Dawley Rats. IJBBB. 2013;3(4):301-5.

151.   Zhang Y, Huo M, Zhou J, Xie S. PKSolver: An add-in program for pharmacokinetic and pharmacodynamic data analysis in Microsoft Excel. Comput Methods Programs Biomed. 2010;99(3):306-14.

152.   Priyadarshani A, Chuttani K, Mittal G, Bhatnagar A. Radiolabeling, biodistribution and gamma scintigraphy of noscapine hydrochloride in normal and polycystic ovary induced rats. J Ovarian Res. 2010;3(10):1757-2215.

153.   Agashe HB, Babbar AK, Jain S, Sharma RK, Mishra AK, Asthana A, *et al*. Investigations on biodistribution of technetium-99m-labeled carbohydrate-coated poly(propylene imine) dendrimers. Nanomedicine. 2007;3(2):120-7.

154.   Yigit US, Lambrecht FY, Unak P, Biber FZ, Medine EI, Cetinkaya B. Preparation of ^{99m}Tc labeled vitamin C (ascorbic acid) and biodistribution in rats. Chem Pharm Bull. 2006;54(1):1-3.

155.   Okarvi SM, Jammaz IA. Preparation and *in vitro* and *in vivo* evaluation of technetium-99m-labeled folate and methotrexate conjugates as tumor imaging agents. Cancer Biother Radiopharm. 2006;21(1):49-60.

156. Banerjee T, Singh AK, Sharma RK, Maitra AN. Labeling efficiency and biodistribution of Technetium-99m labeled nanoparticles: interference by colloidal tin oxide particles. Int J Pharm. 2005;289(1-2):189-95.

157. Chang YJ, Chang CH, Chang TJ, Yu CY, Chen LC, Jan ML, *et al*. Biodistribution, pharmacokinetics and microSPECT/CT imaging of [188]Re-bMEDA-liposome in a C26 murine colon carcinoma solid tumor animal model. Anticancer Res. 2007;27(4B):2217-25.

158. Tsopelas C, Penglis S, Ruskiewicz A, Bartholomeusz DL. Scintigraphic imaging of experimental colitis with technetium-99m-infliximab in the rat. Hell J Nucl Med. 2006;9(2):85-9.

159. Glazer DI, Brown RK, Wong KK, Savas H, Gross MD, Avram AM. SPECT/CT evaluation of unusual physiologic radioiodine biodistributions: pearls and pitfalls in image interpretation. Radiographics. 2013;33(2):397-418.

160. Merkel OM, Librizzi D, Pfestroff A, Schurrat T, Behe M, Kissel T. *In vivo* SPECT and real-time gamma camera imaging of biodistribution and pharmacokinetics of siRNA delivery using an optimized radiolabeling and purification procedure. Bioconjug Chem. 2009;20(1):174-82.

161. Tavelin S, Grasjo J, Taipalensuu J, Ocklind G, Artursson P. Applications of epithelial cell culture in studies of drug transport. Methods Mol Biol. 2002;188:233-72.

162. Yuan J, Cheng KC, Johnson RL, Huang R, Pattaradilokrat S, Liu A, *et al*. Chemical genomic profiling for antimalarial therapies, response signatures, and molecular targets. Science. 2011;333(6043):724-9.

163. Pade V, Stavchansky S. Link between drug absorption solubility and permeability measurements in Caco-2 cells. Journal of Pharmaceutical Sciences. 1998;87(12):1604-7.

164. Kumar MR, Aithal BK, Udupa N, Reddy MS, Raakesh V, Murthy RS, *et al*. Formulation of plumbagin loaded long circulating pegylated liposomes: *in vivo* evaluation in C57BL/6J mice bearing B16F1 melanoma. Drug Deliv. 2011 2011/10/01;18(7):511-22.

165.   Wahlang B, Pawar YB, Bansal AK. Identification of permeability-related hurdles in oral delivery of curcumin using the Caco-2 cell model. Eur J Pharm Biopharm. 2011;77(2):275-82.

166.   Giacomini KM, Huang SM, Tweedie DJ, Benet LZ, Brouwer KL, Chu X, *et al*. Membrane transporters in drug development. Nat Rev Drug Discov. 2010;9(3):215-36.

167.   Kalvass JC, Maurer TS, Pollack GM. Use of plasma and brain unbound fractions to assess the extent of brain distribution of 34 drugs: comparison of unbound concentration ratios to *in vivo* p-glycoprotein efflux ratios. Drug Metab Dispos. 2007;35(4):660-6.

168.   Fenner KS, Troutman MD, Kempshall S, Cook JA, Ware JA, Smith DA, *et al*. Drug-drug interactions mediated through P-glycoprotein: clinical relevance and *in vitro-in vivo* correlation using digoxin as a probe drug. Clin Pharmacol Ther. 2009;85(2):173-81.

169.   Wu JJ, Ai CZ, Liu Y, Zhang YY, Jiang M, Fan XR, et al. Interactions between phytochemicals from traditional Chinese medicines and human cytochrome P450 enzymes. Curr Drug Metab. 2012;13(5):599-614.

170.   Zhou S, Gao Y, Jiang W, Huang M, Xu A, Paxton JW. Interactions of herbs with cytochrome P450. Drug Metab Rev. 2003;35(1):35-98.

171.   U.S. FDA. Guidance for Industry: Drug Interaction Studies-Study Design, Data Analysis, Implications for Dosing, and Labeling Recommendations.: U.S. Department of Health and Human Services Food and Drug Administration Center for Drug Evaluation and Research (CDER). ; 2012.

172.   Wrighton SA, Stevens JC. The human hepatic cytochromes P450 involved in drug metabolism. Crit Rev Toxicol. 1992;22(1):1-21.

173.   Danielson PB. The cytochrome P450 superfamily: biochemistry, evolution and drug metabolism in humans. Curr Drug Metab. 2002;3(6):561-97.

174.   Wolbold R, Klein K, Burk O, Nussler AK, Neuhaus P, Eichelbaum M, *et al*. Sex is a major determinant of CYP3A4 expression in human liver. Hepatology. 2003;38(4):978-88.

175.   Bailey DG, Malcolm J, Arnold O, David Spence J. Grapefruit juice–drug interactions. Br J Clin Pharmacol. 1998;46(2):101-10.

176.   Ho PC, Saville DJ, Wanwimolruk S. Inhibition of human CYP3A4 activity by grapefruit flavonoids, furanocoumarins and related compounds. J Pharm Pharm Sci. 2001;4(3):217-27.

177.   Greenblatt DJ, Leigh-Pemberton RA, von Moltke LL. *In vitro* interactions of water-soluble garlic components with human cytochromes p450. J Nutr. 2006;136(3 Suppl):806S-9S.

178.   Ho BE, Shen DD, McCune JS, Bui T, Risler L, Yang Z, et al. Effects of Garlic on Cytochromes P450 2C9- and 3A4-Mediated Drug Metabolism in Human Hepatocytes. Sci Pharm. 2010;78(3):473-81.

179.   Huang Y, Jiang B, Nuntanakorn P, Kennelly EJ, Shord S, Lawal TO, *et al*. Fukinolic acid derivatives and triterpene glycosides from black cohosh inhibit CYP isozymes, but are not cytotoxic to Hep-G2 cells *in vitro*. Curr Drug Saf. 2010;5(2):118-24.

180.   Tsukamoto S, Aburatani M, Ohta T. Isolation of CYP3A4 Inhibitors from the Black Cohosh (Cimicifuga racemosa). Evid Based Complement Alternat Med. 2005;2(2):223-6.

181.   Hellum BH, Nilsen OG. *In vitro* inhibition of CYP3A4 metabolism and P-glycoprotein-mediated transport by trade herbal products. Basic Clin Pharmacol Toxicol. 2008;102(5):466-75.

182.   Komoroski BJ, Zhang S, Cai H, Hutzler JM, Frye R, Tracy TS, *et al*. Induction and inhibition of cytochromes P450 by the St. John's wort constituent hyperforin in human hepatocyte cultures. Drug Metab Dispos. 2004;32(5):512-8.

183.   Thiengsusuk A, Chaijaroenkul W, Na-Bangchang K. Antimalarial activities of medicinal plants and herbal formulations used in Thai traditional medicine. Parasitol Res. 2013 2013/04/01;112(4):1475-81.

184.   Sumsakul W, Plengsuriyakarn T, Chaijaroenkul W, Viyanant V, Karbwang J, Na-Bangchang K. Antimalarial activity of plumbagin *in vitro* and in animal models. BMC Complement Altern Med. 2014;14(15).

185. Marwa K, Schmidt T, Sjogren M, Minzi O, Kamugisha E, Swedberg G. Cytochrome P450 single nucleotide polymorphisms in an indigenous Tanzanian population: a concern about the metabolism of artemisinin-based combinations. Malar J. 2014;13(420):1475-2875.

186. Desta Z, Zhao X, Shin JG, Flockhart DA. Clinical significance of the cytochrome P450 2C19 genetic polymorphism. Clin Pharmacokinet. 2002;41(12):913-58.

187. Fan L, Wang G, Wang L-s, Chen Y, Zhang W, Huang Y-f, et al. Herbal medicine Yin Zhi Huang induces CYP3A4-mediated sulfoxidation and CYP2C19-dependent hydroxylation of omeprazole. Acta Pharmacol Sin. 2007;28(10):1685-92.

188. Wang L-S, Zhou G, Zhu B, Wu J, Wang J-G, El-Aty AMA, et al. St John's wort induces both cytochrome P450 3A4–catalyzed sulfoxidation and 2C19–dependent hydroxylation of omeprazole. Clinical Pharmacology & Therapeutics. 2004;75(3):191-7.

189. Yin OQ, Tomlinson B, Waye MM, Chow AH, Chow MS. Pharmacogenetics and herb-drug interactions: experience with Ginkgo biloba and omeprazole. Pharmacogenetics. 2004;14(12):841-50.

190. Rendic S, Di Carlo FJ. Human cytochrome P450 enzymes: a status report summarizing their reactions, substrates, inducers, and inhibitors. Drug Metab Rev. 1997;29(1-2):413-580.

191. Ingelman-Sundberg M. Human drug metabolising cytochrome P450 enzymes: properties and polymorphisms. Naunyn Schmiedebergs Arch Pharmacol. 2004;369(1):89-104.

192. Izzo AA, Ernst E. Interactions between herbal medicines and prescribed drugs: a systematic review. Drugs. 2001;61(15):2163-75.

193. Tokunaga T, Takada N, Ueda M. Mechanism of antifeedant activity of plumbagin, a compound concerning the chemical defense in carnivorous plant. Tetrahedron Letters. 2004;45(38):7115-9.

194.   Sunil Kumar MR, Kiran Aithal B, Udupa N, Sreenivasulu Reddy M, Raakesh V, Murthy RSR, *et al.* Formulation of plumbagin loaded long circulating pegylated liposomes: *in vivo* evaluation in C57BL/6J mice bearing B16F1 melanoma. Drug Delivery. 2011 2011/10/01;18(7):511-22.

195.   Hommel M, Gilles HM. Malaria.   Topley & Wilson's Microbiology and Microbial Infections: John Wiley & Sons, Ltd; 2010.

196.   Sowunmi A. Disposition of oral quinine in African patients suffering from acute uncomplicated falciparum malaria. East Afr Med J. 1996;73(8):519-23.

197.   Verdier F, Pussard E, Blayo MC. [Pharmacokinetics of antimalarials: quinine and mefloquine, halofantrine, qinghaosu, amino-4-quinolines]. Med Trop. 1986;46(4):329-43.

APPENMDICES

APPENDIX A

REAGENT PREPARATION

Reagent for *in vitro* model

1. Culture medium

1.1 Incomplete RPMI 1640

The RPMI medium was prepared as a stock solution by mixing the following ingredients 1 L of distilled water (DW):

- RPMI 1640 (Invitrogen, U.S.A.)   10.43 g
- Sodium hydrogen carbonate   2.00   g

This mixture were filtrated through 0.2 μm acrylic membrane for sterilizing and then stored at 4 °C until used.

1.2 1M HEPES (*N*- 2-hydroxyethylpiperazine-*N*-2 ethanesulfonic acid)

- HEPES (M.W. = 238.31 g/mol)   23.831 g
- Distilled water   80   ml

Adjust pH to 7.4 and make volume to 100 ml. Mix well and sterile by filtration with filter pore size 0.2 μm.

1.3 Complete culture medium for HepG2 culture (100 ml)

- Incomplete RPMI   86 ml
- HEPES   2.5 ml
- Fetal bovine serum   10 ml
- 100 IU/ml Antibiotics and Antimycitics solution   1   ml

In order to check for contamination, the medium was incubated at 37°C for 24 h. If there is contamination, the medium color will change from red/pink to orange. Thereafter the medium will be stored at 4°C until use.

1.4 Complete culture medium for Caco2 cell culture (100 ml)

- Incomplete RPMI   73 ml
- HEPES   5 ml
- Fetal bovine serum   20 ml
- 100 IU/ml Antibiotics and Antimycitics solution   1 ml
- 100 mM Sodium pyruvic acid   1 ml

In order to check for contamination, the medium was incubated at 37°C for 24 h. If there is contamination, the medium color will change from red/pink to orange. Thereafter the medium will be stored at 4°C until use.

1.5 50% ethanol

This solution was preparation by diluted 25 ml 95% ethanol with 25 ml distilled water.

2. Cell retrieval and continuous culture

After took frozen cell from storage in liquid nitrogen tanks

- Thaw immediately in water bath at 37°C and transfer cell suspension to 15 ml centrifuge tube with 10 ml of complete media.

- Remove supernatant by centrifugation at 700 x g for 5 min

- Transferred the suspension into a 25 cm^2 tissue culture flask and be maintained at 37°C in a 5% CO2 atmosphere with 95% humidity.

3. Cryopreservation of parasite cultures

The cryopreservation of cell cultures were done by

- Transferred trypsinised cell to 15 ml centrifuge tube

- Spin down at 700 x g for 5 min and discard supernatant

- Add an equal volume of culture meia with 10% DMSO, then transfer the suspension to cryopreservation tubes and pluged into liquid nitrogen tank

Reagent for *in vivo*model

1. 50% ethanol

This solution was preparation by diluted 25 ml 95% ethanol with 25 ml distilled water.

2. Chloroquine diphosphate

Chloroquine diphosphate (Sigma, United states, USA) was measured 10 mg/kg of weight mouse and dissolved in distilled water.

3. 0.9% Normal saline

The solution was prepared by dissolved 4.5 g NaCl in 500 ml DW, and filtered through a sterile 0.2 μm acrylic membrane for sterilizing and then stored at 4°C until used.

4. Freezing solution

The freezing solution consisted 30 ml of 99% glycerol and 70 ml of distilled water. The solution was sterilized by filtering through a 0.45 μm Millipore membrane and keep at 4°C until used.

5. Heparin solution

Working solution concentration 200 U/ml was prepared from 5 ml 10X stock solution with 25 ml distilled water.

APPENDIX B

DNASE TREATMENT OF RNA SAMPLES AND cDNA SYNTHESIS

DNase Treatment of RNA Samples Prior to RT-PCR

1. Set up the DNase digestion reaction as follows:

RNA in water or TE buffer	1–8µl
RQ1 RNase-Free DNase 10X Reaction Buffer	1µl
RQ1 RNase-Free DNase	1u/µg RNA
Nuclease-free water to a final volume of	10µl

Note: Use 1 unit of RQ1 RNase-Free DNase per microgram of RNA. For smaller amounts of RNA, use 1 unit of RQ1 RNase-Free DNase per reaction.

2. Incubate at 37ºC for 30 min.

Note: If analyzing RNA samples by gel electrophoresis, perform a phenol:chloroform extraction and ethanol precipitation before loading the samples on the gel because salts in the RQ1 DNase Reaction Buffer and Stop Solution may cause aberrant migration or smearing of RNA on gels. Steps 3 and 4 may be omitted if a phenol:chloroform extraction is performed.

3. Add 1µl of RQ1 DNase Stop Solution to terminate the reaction.

4. Incubate at 65ºC for 10 mins to inactivate the DNase.

First-Strand cDNA Synthesis by SuperScript™ III Reverse Transcriptase

Description

SuperScript™ III Reverse Transcriptase is an engineered version of M-MLV RT with reduced RNase H activity and increased thermal stability. The enzyme can be used to synthesize first-strand cDNA at temperatures up to 55°C It can generate cDNA from 100 bp to >12 kb. Component.

The following 20-µl reaction volume can be used for 10 pg–5 µg of total RNA or 10 pg–500 ng of mRNA.

1. Add the following components to a nuclease-free microcentrifuge tube:

- 1 µl of oligo(dT)$_{20}$(50 µM); or 200–500 ng of oligo(dT)12-18; or 50–250 ng of random primers; or2 pmol of gene-specific primer

- 10 pg–5 µg total RNA or10 pg–500 ng mRNA

- 1 µl 10 mM dNTP Mix (10 mM each dATP, dGTP, dCTP and dTTP at neutral pH)

- Sterile, distilled water to 13 µl

2. Heat mixture to 65°C for 5 min and incubate on ice for at least 1 min

3. Collect the contents of the tube by brief centrifugation and add:

- 4 µl 5X First-Strand Buffer

- 1 µl 0.1 M DTT

- 1 µl RNaseOUT™ Recombinant RNase Inhibitor (40 units/µl). Note: When using less than 50 ng of starting RNA, the addition of RNaseOUT™ is essential.

- 1 µl of SuperScript™ III RT (200 units/µl)*
  *If generating cDNA longer than 5 kb at temperatures above 50°C using a gene-specific primer or oligo(dT)20, the amount of SuperScript™ III RT may be raised to 400 U (2 µl) to increase yield.

4. Mix by pipetting gently up and down. If using random primers, incubate tube at 25°C for 5 min.

5. Incubate at 50ºC for 30-60 min. Increase the reaction temperature to 55ºC for gene-specific primer. Reaction temperature may also be increased to 55ºC for difficult templates or templates with high secondary structure.

6. Inactivate the reaction by heating at 70ºC for 15 min. The cDNA can now be used as a template for amplification in PCR. However, amplification of some PCR targets (those >1 kb) may require the removal of RNA complementary to the cDNA. To remove RNA complementary to the cDNA, add 1 µl (2 units) of *E. coli* RNase H and incubate at 37ºC for 20 min.
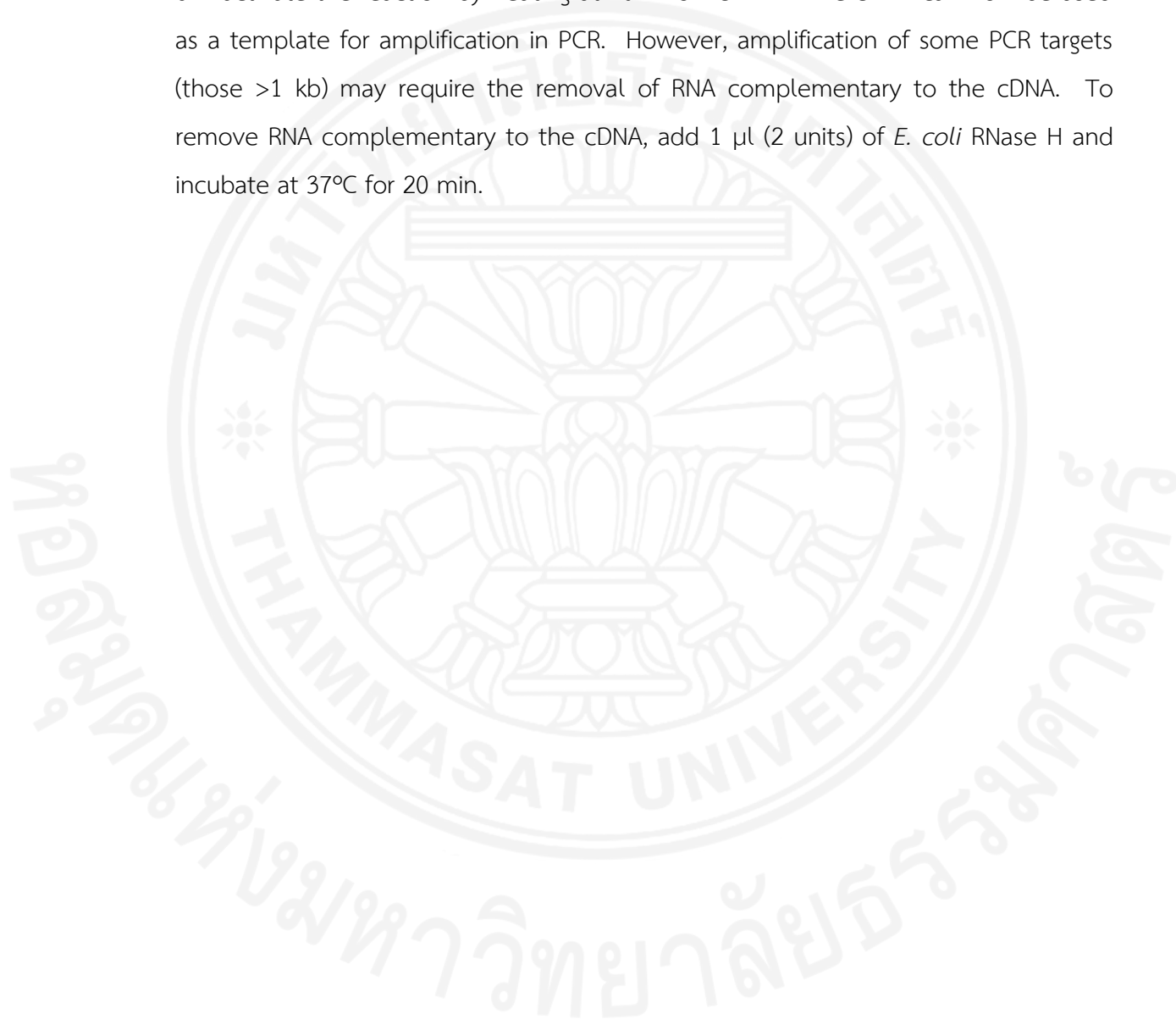
BIOGRAPHY

Name	Miss Wiriyaporn Sumsakul
Date of Birth	2nd November 1986
Educational Attainment	2005-2009: Bachelor Degree in Science, Faculty of Allied Health Sciences, Thammasat University
Work Position	Lecturer in Public health Department, Faculty of Sciences and Technology, Valaya alongkorn Rajabhat University
Scholarship	2008: Thammasat University and Thailand Research Joint Fund through a Royal Golden Jubilee Ph.D. scholarship

International research publication

1. Sumsakul W, Plengsuriyakarn T, Chaijaroenkul W, Viyanant V, Karbwang J, Na-Bangchang K. Antimalarial activity of plumbagin *in vitro* and in animal models. BMC Complement Altern Med. 2014;14(15):1472-6882.

2. Sumsakul W, Chaijaroenkul W, Na-Bangchang K. *In vitro* inhibitory effects of plumbagin, the promising antimalarial candidate, on human cytochrome P450 enzymes. Asian Pacific Journal of Tropical Medicine. 2015.

3. Sumsakul W, Mahavorasirikul W, Na-Bangchang K. Inhibitory Activities of Thai Medicinal Plants with Promising Activities Against Malaria and Cholangiocarcinoma on Human Cytochrome P450. Phytother Res. 2015;22(10).

4. Sumsakul W, Karbwang J, Na-Bangchang K. Application of SPECT/CT imaging system and radiochemical analysis for investigation of blood kinetics and tissue distribution of radiolabeled plumbagin in healthy and Plasmodium berghei-infected mice. Exp Parasitol. 2015;20(15):30065-5.

5. Sumsakul W, Na-Bangchang K. Permeability of plumbagin across human intestinal cell *in vitro*. Arch Pharm Res. 2015;30:30.

National research publications

1. Sumsakul W, Viyanant V, Mahavorasirikul, W, Cheoymong, A, Tassaneeyakul, W, and Na-Bangchang K (2012). Inhibition of Human CYP1A2 and CYP3A4 Activities by Thai Medicinal Plants with Promising Antimalarial Activity. *Thai J Pharmacol* 34(1): 66-70.

2. Sumsakul W, Chaijaroenkul W, Plengsuriyakarn T, Viyanant V, and Na-Bangchang K (2013). Toxicity evaluation of plumbagin in animal model. *Thai J Pharmacol* 35(1): 153-156.

3. Sumsakul W, Karbwang J, Na-Bangchang K (2015). Application of SPECT/CT imaging system and radiochemical analysis for investigation of blood kinetics and tissue distribution of radiolabeled plumbagin in healthy and *Plasmodium berghei*-infected mice. Proceedings of 37th Pharmacological and Therapeutic Society of Thailand Meeting

Work Experiences   2015-Present: Lecturer in Public health
                                    Department, Faculty of Sciences and
                                    Technology, Valaya alongkorn Rajabhat University